The Jet/CGC Correspondence:

A Conformal Perspective.

A dissertation presented for the degree of

Master of Science

Author: Mr J. A. Bohra

Supervisor: Prof. H. Weigert

Department of Physics,
University of Cape Town,
Rondebosch, 7700, South Africa

Abstract

This study aims to bridge, with the use of conformal transformations, two distinct applications of QCD which are encapsulated by evolution equations for associated observables. Superficially, the interjet energy flow multiplicity and the cross section of Deep Inelastic Scattering (DIS) at small-$x_{\rm bj}$ describe, as observables, entirely different phenomena. Jet evolution equations describe how soft gluons enter the final state of e^+e^- annihilation events and, accordingly, drive the energy dependence of s-channel multiplicities. On the other hand, Color Glass Condensate (CGC) evolution equations describe the change of dynamic gluon saturation effects (characteristic of DIS events at small-$x_{\rm bj}$) in terms of the change in kinematic rapidity – and, accordingly, characterize the t-channel exchange between probe and target.

Despite differences in phenomenological applications, independently derived 't Hooft large N_c limit Jet and CGC evolution equations (namely: BMS and BK, respectively) demonstrate remarkable structural similarities. These have triggered a search for tools to understand the origin and limitations of this relationship. The correspondence of Jet/CGC evolution at large N_c was key in the derivation of the BMS-W equation – which, along with JIMWLK equation, establishes an analogous correspondence at finite N_c. In parallel, a surge of $\mathcal{N} = 4$ SYM interest in relating small-$x_{\rm bj}$ DIS and interjet energy flow – based on the AdS/CFT Correspondence – provided new perspectives on associated QCD descriptions.

Foundationally, the structural similarities showcased by BMS-W/JIMWLK equations are geometric in origin: Wilson lines and the product of integration kernels and measures are tagged by transverse coordinates in the CGC case and by a sphere of directions on the Jet side. The product measures and kernels are known to be related explicitly through a Euclidean stereographic projection. Moreover, a Minkowskian conformal transformation posited by Hofman and Maldacena (HM) has been used to relate Wilson line geometry in other applications. It is this transformation (called the HM map), properly adapted to the present purpose, that is used to study the relationship of virtually all ingredients of BMS-W/JIMWLK. In particular, re-parametrization of independently established mathematical objects encountered in both Jet and CGC evolution is used to furnish a four dimensional relationship of Wilson line geometry, logarithm structure, and integration kernels.

Acknowledgements

To commence, I would like to express my gratitude and extend my acknowledgments to the funding organizations that provided financial support throughout my degree. The National Research Foundation, which honoured me with an MSc Bursary, and the Joseph Stone Bursary granted by the Postgraduate Funding Office of the University of Cape Town (UCT), have played a crucial role in facilitating my academic pursuits.

Furthermore, I extend my heartfelt appreciation to Prof. Heribert Weigert, whose dedication as a supervisor far surpasses the reasonable expectations of any student. I am especially indebted to him for his invaluable editorial suggestions that sculpted a *vastly* superior dissertation out of my initial manuscripts. It is through his unyielding standards and meticulous attention to detail that my work has attained the calibre it sits at today. I am sincerely thankful for the countless hours he has invested and the insightful perspectives he has shared during the course of my training.

I wholeheartedly thank Prof. Weigert, the Department of Physics, and SA-CERN for their support that enabled my participation in the events FIPS 2022 and eQCD 2022. Special gratitude goes to Prof. Alan Cornell, the Theory-Elect Head of SA-CERN, whose prompt email responses were instrumental in helping me navigate the tedious administrative processes. I also wish to express my gratitude to the organizing committee of eQCD 2022 for accepting my abstract for presentation at the conference. The limitations of that twenty-minute presentation significantly contributed to my ability to craft a coherent narrative and incorporate the numerous visual elements showcased in this dissertation. The proceedings of my presentation are set to be published in *Acta Physica Polonica B* under an eponymous title [1]. Additionally, I would like to extend my thanks to Mr Jason Barrella, who travelled all the way to Sicily, Giardini Naxos, to attend my presentation – *u a real one for that.*

In the sequence of appearances, I express my gratitude to my fellow officemates from Room 3.08 of the R.W. James Building: Avotra Elie, Farid Sedaria, Matthew Maddock, Daniel Weiss, and Faaris Alam. Their engaging discussions, probing questions, and insightful answers have enriched the tapestry of my comprehension even beyond the realm of physics itself.

Lastly — I thank my parents, whose largesse has provided me with food, clothing, and shelter throughout my life.

Contents

List of Figures

At last he came nearer and nearer by degrees, still observing the Brightness of the Fire and its marvellous Efficacy in consuming every thing it touch'd and changing it into its own Nature; till at last his Admiration of it and that innate Boldness and Fortitude which The Almighty had implanted in his Nature prompted him on, that he stretch'd out his Hand to take some of it.

— Abū Bakr ibn Ṭufail in *Ḥayy ibn Yaqẓān* [2]

Chapter 1

Introduction

1.1 On High Energy Quantum Chromodynamics and Conformal Transformations...

Only a fraction of the mass of the universe (as it is presently understood) is accounted for by bright matter – that is, matter described by the roster of elementary particles posited by the Standard Model (SM). Yet, virtually all of the mass of this bright matter is accounted for by nucleons like protons and neutrons – which, much like the atoms they constitute, are not elementary. Nucleons, in fact, are described as states of quarks and antiquarks bound by the strong nuclear force. Mediated by gluons, the strong force, is mathematically described by a Quantum Field Theory (QFT) known as Quantum Chromodynamics (QCD) [3–7] – which is a non-Abelian gauge theory associated with the special unitary Lie group $\mathsf{SU}(3)$. As in Electrodynamics where particles like electrons carry electric charge – quarks, antiquarks, and gluons carry color charge, and accordingly transform under representations of $\mathsf{SU}(3)$. The strong coupling quantifies the interactions between two colored objects and depending on energy or momentum scales μ^2 in such an interaction,

$$\alpha_s(\mu^2) := \frac{g^2(\mu^2)}{4\pi} \approx \frac{2\pi}{\beta_0} \frac{1}{\ln\left(\mu^2/\Lambda_{\text{QCD}}\right)}, \tag{1.1.1}$$

becomes smaller as $\mu^2 \to \infty$ since, $\beta_0 > 0$ for QCD. Conversely, the coupling becomes larger as $\mu^2 \to \Lambda_{\text{QCD}}$. The strong coupling of QCD shown in eq. (1.1.1) gives rise to many interesting properties of the strong nuclear force. In particular, the divergence of the coupling at Λ_{QCD} indicates that long distance interactions are strong. Ultimately, this leads to a phenomenon called **confinement** where colored objects cannot be directly observed at low energy scales – and must bind together into color neutral states such as hadrons and mesons.

High energy scales which correspond to small coupling constants, therefore, allow the study of internal structure of nucleons using perturbative methods. Modern collider experiments, in particular, allow for highly energetic experimental conditions needed to study the nature of the strong nuclear force. Naively, if the coupling is small then one might hope that expansion in powers of α_s yields a good approximation to QCD observables. However, in high energy

collider experiments, there are typically enhanced contributions arising from singularities in internal propagators that ultimately lead to large logarithms. Generically, kinematic variables V feature in observables through logarithms $\ln V$ – the largeness of which compensates the smallness of the coupling rendering a, naive, perturbative treatment invalid since $\alpha_s \ln V \sim \mathcal{O}(1)$. In cases of logarithmically enhanced contributions to observables, the resummation of logarithms to all orders $(\alpha_s \ln V)^m$ is necessitated to compute observables[1]. Contributions to the observable which demonstrate the highest degree of logarithmic enhancement constitute the leading logarithmic approximation of the associated observable; see appendix B.1. Most commonly, leading logarithmic contributions to observables are incorporated by solving the differential equations called renormalization group equations (RGEs).

It is worth noting that although QCD corresponds to the gauge group $\mathsf{SU}(N_c = 3)$ where N_c is the number of colors – expressions are evaluated in terms of a generic and finite N_c. This allows one direct access to a degree of freedom in computing results. It also allows one to simplify calculations in the 't Hooft large N_c limit [8] which is formally: $N_c \to \infty$ and $\alpha_s \to 0$ such that $\alpha_s N_c \ll 1$ serves as a reasonable perturbation coefficient.

The core of this dissertation will be focussed on relating two sets of RGEs which arise in seemingly unrelated contexts of high energy QCD phenomenology – namely: Jet evolution [9–12] (which models high energy particle production experiments), CGC (Color Glass Condensate) evolution [13–20] (which models high energy scattering experiments). Historically, the structural similarities of BMS (Banfi – Marchesini – Smye) [9] and BK (Balitsky – Kovchegov) [13–16] equations (which, respectively, characterize Jet and CGC evolution in the large N_c limit) motivated Weigert to derive a finite N_c generalization of the BMS equation called the BMS-W (BMS – Weigert) equation [10]. Weigert's attempts extended the correspondence of Jet and CGC physics at finite N_c with the BMS-W and JIMWLK (Jalilian-Marian – Iancu – McLerran – Weigert – Leonidov – Kovner) [17–20] frameworks.

In parallel, the study of Jet and CGC physics in $\mathcal{N} = 4$ Supersymmetric Yang-Mills theories [21, 22], based on the AdS/CFT Correspondence (Anti de Sitter / Conformal Field Theory Correspondence) [23], provided new perspectives on corresponding QCD descriptions. In particular the structural similarity, which was suggestive of a geometric correspondence, of the BK and BMS equations (first identified by Weigert [10]) was concretized by Hatta [24] through a stereographic projection. The phenomenological perspectives of this correspondence of Jet and CGC physics have been studied by Marchesini and Mueller [25]. On the mathematical side – by employing a Minkowskian conformal transformation first posited by Hofman and Maldacena (HM) [26] – Caron-Huot [27] inferred next-to-leading order (NLO) contributions for CGC evolution from known contributions on the Jet side (at finite N_c). However, a direct derivation of the JIMWLK equation at NLO by Kovner et al [28–30] does not agree with Caron-Huot's results. Therefore, a substantive study identifying the cause of such discrepancies is strongly motivated.

These developments have exposed conformal transformations as useful tools with which to formalize the correspondence of Jet and CGC phenomenology. Historically, first applications of conformal transformations pertained to uses in cartography where their 'angle-preserving'

[1] Note that resummation of $(\alpha_s \ln V)^m$ only accounts for single logarithmically contributions to observables relevant for this thesis.

qualities, for natural reasons, were used to define conformal maps. On (flat) metric spaces where notions of distances and directions give way to notions of norm and orthogonality, conformal transformations $x \mapsto y$ are defined[2] as all transformations which rescale the metric by a smooth function $\Omega : x \mapsto \mathbb{R}$ [31, 32],

$$g_{\mu'\nu'} \frac{\partial y^{\mu'}(x)}{\partial x^{\mu}} \frac{\partial y^{\nu'}(x)}{\partial x^{\nu}} \stackrel{!}{=} \Omega^2(x) g_{\mu\nu}. \tag{1.1.2}$$

As evidenced by the definition in eq. (1.1.2), among the chief motivations behind the study of conformal applications is the fact that conformal symmetry forms an extension to Poincaré symmetry of Minkowski space. In particular, $\Omega \equiv 1$ corresponds precisely to the conditions which impose Lorentz covariance and, as such, maps which respect conformal symmetry are necessarily less stringent than maps which respect Poincaré symmetry.

[2] A mathematically rigorous definition has been provided in the appendix (B.7.2).

1.2 Reading Guide

The first main Chapters 2 and 3 introduce the concepts required to discuss the rapidity evolution of the Color Glass Condensate (CGC) and the energy evolution of Jets, respectively. In particular, it is the structural similarity exhibited by the Jet and CGC evolution equations at Leading Order (LO) which suggests a formal correspondence between the physics description of Jets and CGC. Conformal transformations have demonstrated considerable success in establishing a formal correspondence between Jet and CGC physics [24, 27]. To this end, Chapter 4 provides a historical overview of the developments which suggest a formal Jet/CGC Correspondence explored through explicit conformal transformations and the substantive study thereof.

The narrative of Chapter 2, is directed toward explaining the phenomenological importance of Deep Inelastic Scattering (DIS) events which serve as vehicle to study the internal structure of hadrons. The quantum field theoretical description of a DIS event, involves a t-channel exchange of a mediating photon between a leptonic probe and hadronic target. In particular, the mediating photon, exhibiting a large (or deep) virtuality, and the interaction thereof with the hadronic target are characterized by kinematic variables Q^2 and x_{bj}, respectively. The hadronic target, when probed through DIS events, exhibits features in accordance with the kinematic limits of Q^2 and x_{bj}. In particular, the Regge-Gribov limit (where $x_{\text{bj}} \to 0$ and Q^2 is fixed) is employed to study the gluon saturation effects of the hadron – which gives rise to an effective theory known as the Color Glass Condensate.

The rapidity separation, Y, of a DIS event in the Regge-Gribov limit may be described as $Y \simeq \ln 1/x_{\text{bj}}$. Therefore, in the CGC formalism, both kinematic (high rapidity separation) and dynamic (gluon saturation) features may be discussed simultaneously by small-x_{bj} corrections to observables. Wilson line correlators which described eikonal interactions of probing colored objects with the hadronic target in CGC observables, therefore, have manifest dependence of $Y \simeq \ln 1/x_{\text{bj}}$. The JIMWLK equation, therefore, which is a renormalization group equation (RGE) that describes the rapidity evolution of CGC observables, characterizes how logarithmically enhanced $\ln 1/x_{\text{bj}}$ quantum fluctuations induced by the QCD action drive saturation effects within CGC observables.

The JIMWLK framework, which the supervisor has had a key role in developing, has received greater attention in assorted dissertations [33–35]. The theoretical background required, a skeletal derivation, and assorted features of the JIMWLK framework have been featured in appendices B.3, B.4, and B.5 respectively. The JIMWLK (finite N_c) evolution of the color dipole correlator (the simplest Wilson line correlator) will be presented. Moreover, JIMWLK evolution of a color dipole will be used to demonstrate the Balitsky hierarchy where, generically, $(n+1)$-correlators are required to compute the rapidity evolution of n-point correlator. The intractability, therefore, of the CGC evolution at finite N_c is remedied by the large N_c limit which yields the BK equation that does not feature the Balitsky hierarchy.

The narrative of Chapter 3, is concerned with explaining the phenomenological importance of the study of jets – which are observed collimated collections of final state particles in modern colliders. The creation of highly energetic colored objects generates eikonal radiation of gluons which, due to confinement, result in the high multiplicity of final state particles encountered as

ubiquitous features of high energy collisions. The study of jets, therefore, provides a window into understanding the relation between what is perturbatively calculated using QCD and what is observed in collider experiments – and is, therefore, crucial in understanding mechanisms of color neutralization due to confinement.

A dijet event characteristically features two back-to-back hard jets, in the centre-of-momentum (COM) frame, which contain most of the COM energy E associated with the underlying particle production process. Emission arising from the particle production process, therefore, are sensitive to soft singularities ($\omega_p \to 0$) everywhere and are sensitive to collinear singularities ($\theta_{pk} \to 0$) within hard jets. Therefore, the properties and behaviour of jets are largely determined by the observables that are considered. In particular, in regions away from hard jets, so-called interjet region, the angle of emissions are necessarily large and emissions are therefore not sensitive to collinear singularities. The interjet energy E_{out} (which definitively sums all final state energies in the interjet region), restricts the resummation structure of the semi-inclusive observable to single logarithmic contributions.

When the associated particle production is described through e^+e^- annihilation, the BMS equation characterizes how, under an increase of COM energy or a decrease in the interjet energy, contributions enhanced by non-global logarithms $\Delta := \ln E/E_{\text{out}}$ feature within hard jets. A derivation of the BMS equation adapted from the original source [9] has been presented in the dissertation. The BMS equation exhibits remarkable similarities to the BK equation - which, in an unrelated application, governs the rapidity evolution of a color dipole in the CGC formalism. The theoretical reasons behind the structural similarities motivate a finite N_c generalization of the Jet/CGC correspondence exhibited by the BK/BMS equations in the large N_c limit.

In Chapter 4, a motivation behind establishing a formal correspondence from the structural similarity exhibited by Jet and CGC evolution equations and the phenomenological consequences thereof is discussed. Historically, a geometric correspondence between the BK/BMS equations, suggested by Weigert [10], involved relating a transverse plane to sphere of directions. Hatta concretized the geometric correspondence of the BK/BMS equations at LO with the explicit use of a stereographic projection [24]. Caron-Huot attempted to extend the correspondence between CGC and Jet evolution at NLO [27]. However, substantive details of Caron-Huot's work remain to be verified by explicit calculation. Therefore, a Minkowski space conformal map: posited by Hofman-Maldacena [26] and used by both Hatta and Caron-Huot [24, 27] will be analysed to lay the groundwork of a substantive study. A formal Jet/CGC Correspondence will be discussed with explicit mappings to relate independently established mathematical objects through re-parametrization (with the help of Vladimirov's developments [36, 37]).

Chapter 2

Rapidity Evolution of the Color Glass Condensate

Prototypically, Deep Inelastic Scattering events serve as vehicle to study the internal structure of hadrons. Kinematic variables such as the virtuality of the mediating photon and the momentum fraction known in the literature as Bjorken-x are used to characterize different kinematic limits of Deep Inelastic Scattering. The Regge-Gribov limit, in particular, is employed to study the gluon saturation effects of the hadron which gives rise to an effective theory known as the Color Glass Condensate. Dynamic and kinematic considerations thereof manifest in Wilson line correlators which characterize eikonal interactions of probing partons with the Color Glass Condensate. The JIMWLK equation, which is a functional framework which describes the rapidity evolution of Wilson line correlators, is used to characterize the small Bjorken-x dependence of Color Glass Condensate observables.

2.1 Probing Subatomic Structures at High Energies

Ernest Rutherford, renowned for contributions to the study of radioactivity and the atomic structure, conducted the famous Gold Foil Experiment - wherein the resultant scattering of (positively charged) alpha particles, directed onto a gold foil leaf, was observed. Published results of the experiment [38] heralded a significant departure from the prevailing Plum Pudding model of the atom which posited an even distribution of positive and negative charges throughout the atomic volume. Evidence of instances of near complete backscatter of alpha particles through their interaction with the gold atoms, suggested that atomic structure consists of a small yet dense, positively charged, nucleus which is surrounded by cloud of negative charge.

Over the century of research of the structure of the atom that has precipitated since, theoretical descriptions demonstrated categorically impressive displays of accuracy and precision. For one, the Standard International (SI) unit of time, the second (s) - which is defined by the the unperturbed ground-state hyperfine transition frequency of the ^{133}Cs isotope [39] - is established with a combined fractional uncertainty to order $\times 10^{-15}$ [40]. Moreover, the electron anomalous magnetic moment g-2 is known experimentally up to 13 digits of precision [41,

42] – and it is claimed in [43] that the Quantum Electrodynamics (QED) calculation thereof is evaluated up to 1100 digits of precision. Ultimately, the understanding of atomic structure is an innate reflection of the fundamental physics of the electromagnetic force. Analogously, understanding hadronic structure reflects comprehension of the strong nuclear force.

While the theoretical description of the strong nuclear force, that is QCD, predicts through confinement the existence of color neutral bounds states such as hadrons – the exact mechanisms along which hadrons are actually formed remains inadequately understood. The blueprint of the Gold Foil Experiment demonstrates how a scattering event serves, in essence, as a microscope which is able to resolve internal structure of a target by observing a scattered probe. Therefore, to study hadronic structure, **Deep Inelastic Scattering** (DIS) events are employed – which involve, prototypically, the *scattering* of a leptonic probe off a hadronic target at high centre-of-momentum energies. The t-channel probe-target interaction, mediated by an exchange of a spacelike photon has been demonstrated in Figure 2.1.

Kinematics of DIS are described through the following Lorentz invariants:

$$s := (P + l)^2, \tag{2.1.1a}$$

$$Q := \sqrt{-q^\mu q_\mu}, \tag{2.1.1b}$$

$$x_{\mathrm{bj}} := \frac{-q^2}{2P.q}, \tag{2.1.1c}$$

$$y := \frac{P.q}{P.l}, \tag{2.1.1d}$$

which define, according to the Feynman amplitude in Figure 2.1: the Mandelstam invariant s, the hard scale $Q \in \mathbb{R}_+$, a scaleless momentum fraction called Bjorken-x (denoted as x_{bj}), and the inelasticity, y, of the DIS process.

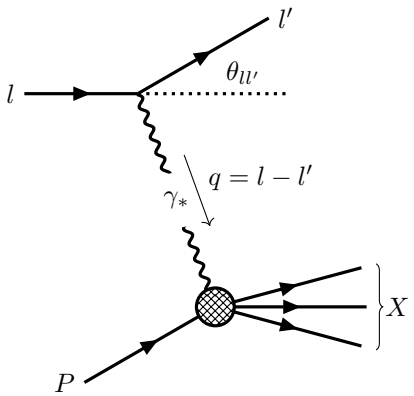

Figure 2.1: *Feynman diagram detailing the amplitude of a DIS event.*

As with most treatments of Feynman amplitudes, it is useful to break the kinematics of DIS into a leptonic part and a hadronic part. The leptonic probe carrying an initial momentum l emits a *spacelike* virtual photon γ_* and is scattered into a final momentum l'. Observing the scattering of the lepton, $\sim \theta_{ll'}$, quantifies the spacelike photon momentum $q = l - l'$. Therefore, the hard scale Q, which describes the virtuality of the mediating photon, is entirely determined by the leptonic part. Analogously, the hadronic target carrying an initial momentum P absorbs a *spacelike* virtual photon γ_* and produces the observed hadronic final states with invariant mass $X^2 = (P + q)^2$. The Bjorken-x kinematic variable,

$$x_{\mathrm{bj}} := \frac{-q^2}{2P.q} = \frac{Q^2}{Q^2 + (X^2 - P^2)} \in [0, 1), \tag{2.1.2}$$

when expressed in terms the hard scale and invariant mass of the hadronic final states, is explicitly demonstrated to lie in the interval $x_{\mathrm{bj}} \in [0, 1)$ since $Q^2 > 0$ and $X^2 > P^2$. The Bjorken-x kinematic variable is used to quantify the interaction between the spacelike photon and the hadronic target.

In the high centre-of-momentum (COM) energy limit $s := (P+l)^2 \simeq 2P.l$, the Lorentz invariants displayed in eq. (2.1.1) may be related,

$$Q^2 \simeq s x_{\rm bj} y, \tag{2.1.3}$$

such that the proportionality of s to Q^2 is readily apparent at fixed $x_{\rm bj}$ and y. As highlighted in Figure 2.2, an increase in COM energy (characterized by $\sqrt{s}$) corresponds to an access of larger Q^2 values. Since Q^2 characterizes the virtuality of the mediating spacelike photon, Q^2 is identified with the resolution scale of DIS events – and correspondingly sets the apparent transverse size of hadronic constituents, $A_\perp \sim 1/Q^2$ [45].

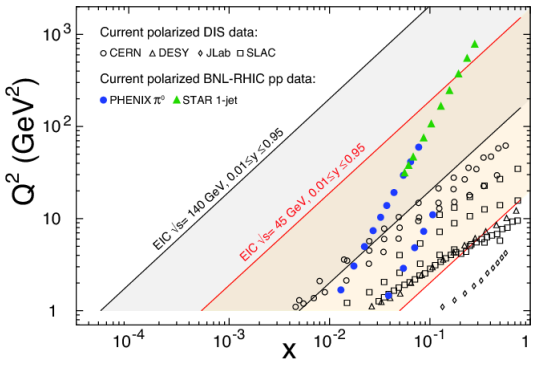

Figure 2.2: *[Colour online] Plot of Q^2 and $x_{\rm bj}$ [44] demonstrating how, at fixed y, an increase in COM energy (characterized by $\sqrt{s}$) corresponds to an access of larger Q^2 and smaller $x_{\rm bj}$.*

To resolve hadronic structure - a DIS event must be employed at high COM energies at the order of $\sqrt{s} > 10^2$GeV. For protons and neutrons with rest mass ~ 1GeV, hadronic constituents demonstrate a overwhelming probability to be liberated from their bound state - such a feature is characteristic of *inelastic* collisions. In general, there is a correlation between COM energy and the probability of inelasticity in a collision. The Figure 2.3, depicts three scattering events involving leptonic probes and hadronic target at different values of $\sqrt{s}$. Moving rightward: the first is an elastic collision which occurs at a similar energy scale as the Gold Foil Experiment, the second is a slightly inelastic collision at an intermediate energy scale which liberates a hadronic constituent, and the last is a DIS event demonstrating an overwhelming probability to liberate all hadronic constituents.

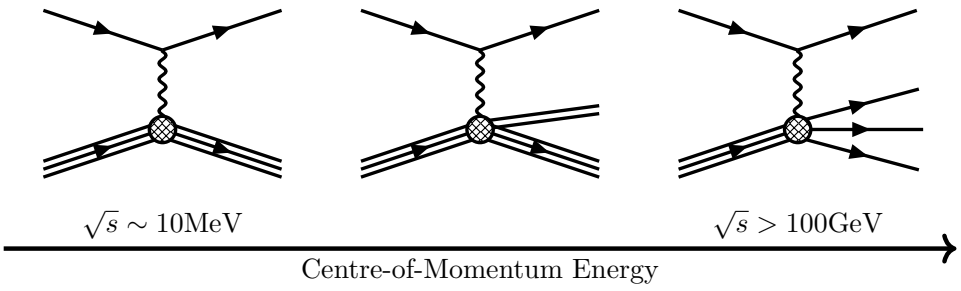

Figure 2.3: *Feynman diagrams of scattering events depicted as a function of the centre-of-momentum energy $\sim \sqrt{s}$. Detailing interaction between leptonic probe and hadronic target, from left to right: an elastic scattering event, a slightly inelastic scattering event and, a DIS event.*

In practice, the high centre-of-momentum energy, as prerequisite to a DIS event, is achieved in modern colliders by accelerating both the probe and target to speeds near the speed of light. Without loss of generality, the probe and target are taken to traverse (in instant form coordinates) along $-\underline{e}_3$ and $+\underline{e}_3$ directions respectively. Therefore, the x^3 coordinate is explicitly

identified as the longitudinal spatial component, whereas x^1 and x^2 are explicitly identified as transverse spatial components. The rest frames of the probe and target, with rapidity separation Y, are thus related by a pure Lorentz boost in the longitudinal direction,

$$\begin{bmatrix} x^0_{\text{target}} \\ x^1_{\text{target}} \\ x^2_{\text{target}} \\ x^3_{\text{target}} \end{bmatrix} = \begin{bmatrix} \cosh Y & 0 & 0 & \sinh Y \\ 0 & 1 & 0 & 0 \\ 0 & 0 & 1 & 0 \\ \sinh Y & 0 & 0 & \cosh Y \end{bmatrix} \begin{bmatrix} x^0_{\text{probe}} \\ x^1_{\text{probe}} \\ x^2_{\text{probe}} \\ x^3_{\text{probe}} \end{bmatrix}. \tag{2.1.4}$$

Adopting lightcone or front form coordinates, shown in Figure 2.4, in the Kogut-Soper convention [46],

$$x^{\pm} := \frac{1}{\sqrt{2}}(x^0 \pm x^3), \tag{2.1.5}$$

defines new lightlike directions n and $\bar{n}$ such that,

$$x = x^+\bar{n} + x_\perp + x^- n. \tag{2.1.6}$$

Note that, in matrix form, square and round brackets denote instant and front form coordinates respectively – see appendix (A.1). As eigendirections of the boost matrix in the longitudinal direction, n and $\bar{n}$, the boost matrix in front form coordinates is diagonal,

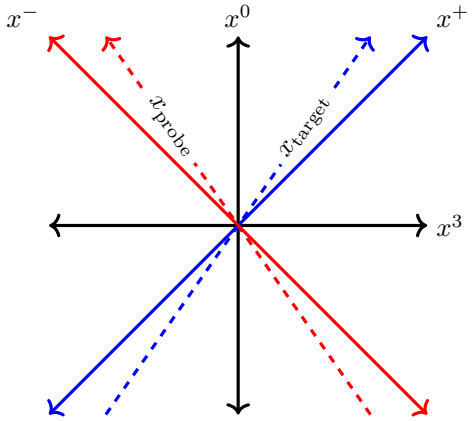

Figure 2.4: *A spacetime diagram detailing probe and target trajectories and motivating use of lightcone coordinates*

$$\begin{pmatrix} x^+_{\text{target}} \\ x^1_{\text{target}} \\ x^2_{\text{target}} \\ x^-_{\text{target}} \end{pmatrix} = \begin{pmatrix} e^{+Y} & 0 & 0 & 0 \\ 0 & 1 & 0 & 0 \\ 0 & 0 & 1 & 0 \\ 0 & 0 & 0 & e^{-Y} \end{pmatrix} \begin{pmatrix} x^+_{\text{probe}} \\ x^1_{\text{probe}} \\ x^2_{\text{probe}} \\ x^-_{\text{probe}} \end{pmatrix}. \tag{2.1.7}$$

Note that the DIS amplitude displayed in Figure 2.1 cannot be perturbatively calculated using QCD. Applications of QCD are restricted to colored objects such as quarks, antiquarks, and gluons and not color neutral configurations such as hadrons. To explore the connection between perturbative QCD and hadronic physics, therefore, one must rely on the parton model - which is a theoretical framework that describes the structure of the hadron in terms of constituent fundamental building blocks called **partons**. The parton model [47] predates QCD, and describes partons as point-like and essentially free within the hadron. With the advent of QCD, however, which describes the hadron as a bound state of colored objects – quarks, antiquarks, and gluons are collectively referred to as partons (for a textbook exposition see [48, Chapter 32]).

Kinematic variables x_{bj} and Q^2 demonstrated in eqs (2.1.2) and (2.1.3) will be used to identify the kinematic limits of DIS events which highlight key features of hadronic structure.

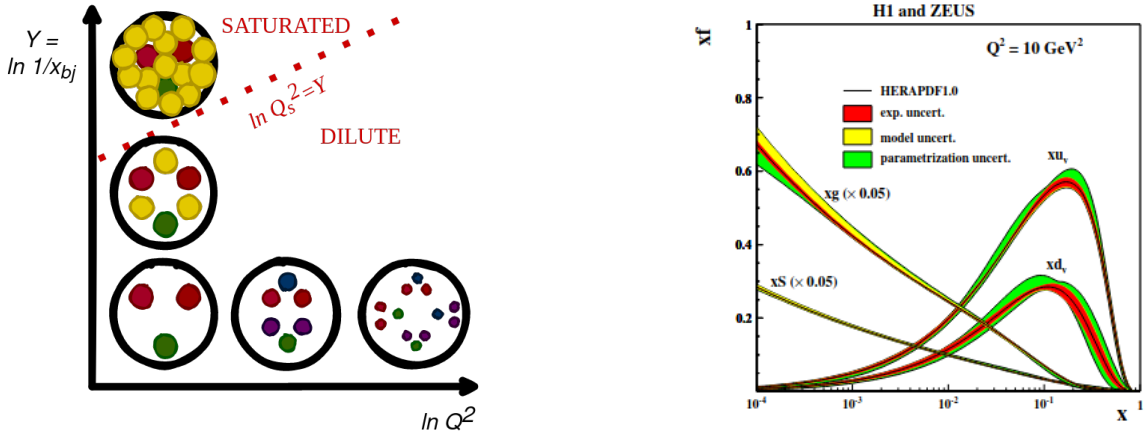

(a) **(b)**

Figure 2.5: *[Colour online] Behaviour of partons of the hadronic target characterized in terms of* $\ln 1/x_{\rm bj}$ *and* $\ln Q^2$ *in a QCD Phase Space diagram in Figure 2.5a. Plot of parton distribution functions, featuring HERA data [50], that demonstrates hadronic occupation as a function of* $x_{\rm bj}$ *at fixed* $Q^2 = 10\text{GeV}^2$ *in Figure 2.5b.*

In Figure 2.5a, the QCD phase space diagram demonstrates the features that the hadronic target exhibits when probed in different kinematic limits of DIS in terms of $x_{\rm bj}$ and Q^2. For one, to probe hadronic structure such that the resolution of hadronic constituents is prioritized, the Bjorken Limit of DIS events is invoked where photon virtuality is increased at fixed Bjorken-x [49],

$$\textbf{Bjorken Limit}: \Big\{x_{\rm bj} \text{ fixed}, Q^2 \to \infty\Big\}. \tag{2.1.8}$$

Dependence of the observed density of partons inside a hadron on the kinematic variable Q^2 is described by the DGLAP[1] equation. As a renormalization group equation, DGLAP equation describes, at fixed $x_{\rm bj}$, the observed density of partons increases logarithmically $\ln Q^2$. The combined effect of probing the hadron, in the Bjorken limit, is demonstrated in Figure 2.5a moving rightward; increasing the photon virtuality Q^2 (which characterizes the resolution of the DIS event and sets the apparent size of probed partons) increases hadronic occupation by partons observed at finer resolutions so that hadron is probed as a dilute collection of partons.

In Figure 2.5b, experimental results from the HERA experiment, interpreted in terms of the parton model, demonstrates hadronic occupation by the different species of partons as a function of the Bjorken-x kinematic variable at fixed $Q^2 = 10\text{GeV}^2$. The parton distribution functions (PDFs) depicted in Figure 2.5b, demonstrate how at large-$x_{\rm bj}$, the hadron is comprised of (on average) twice as many valence up quarks as down quarks. In particular, at $x_{\rm bj} = 10^{-1}$, where the sum of valence (up and down) quark PDFs is approximately one, the notion of a proton being comprised of two up quarks and one down quark is established.

However, at small-$x_{\rm bj}$, there is a simultaneous fall of valence quark PDFS and sharp rise of gluon and sea quark PDFs (which are scaled down by a factor of 20). Sea quarks, which

[1] Dokshitzer–Gribov–Lipatov–Altarelli–Parisi

collectively refer to (anti)quarks other than the valence quarks, are dominantly strange quarks due to the relatively low mass of strange quarks relative to heavier quarks such as charm, top, and bottom quarks. The presence of sea quarks, therefore, naturally alludes to presence of quantum fluctuations which are mediated by gluons and establishes that the small-$x_{\rm bj}$ part of the hadronic target is largely dominated by gluonic dynamics.

To further investigate the small-$x_{\rm bj}$ behaviour of the hadronic target, the **Regge-Gribov Limit** of DIS events is invoked,

$$\textbf{Regge-Gribov Limit}: \Big\{ x_{\rm bj} \to 0, Q^2 \text{ fixed} \Big\}. \tag{2.1.9}$$

where the Bjorken-x is decreased at fixed photon virtuality – the hadronic is increasingly occupied by partons (mainly gluons) of the same apparent size, as demonstrated in Figure 2.5a moving upwards. Beyond the saturation scale $\ln 1/x_{\rm bj} = \ln Q_s^2$, gluons of the same apparent size set by the transverse resolution Q^2 occupy, entirely, the transverse area of the hadronic target – consequently, instead of using individual degrees of freedom for each parton (in accordance with the parton model), it is more efficient to use collective degrees of freedom to describe the gluon saturated behaviour of the hadronic target at small-$x_{\rm bj}$.

In addition, at small-$x_{\rm bj}$, there exists a definite kinematic interpretation of the rapidity separation Y encountered in eq. (2.1.7) in terms of the Bjorken-x - that is, $Y \simeq \ln 1/x_{\rm bj}$, and details of the interpretation have been sketched in the appendix (B.2). The kinematic effects of DIS, characterized by high rapidity separation, manifest as length contraction and time dilation effects on the hadronic target,

$$j^{\mu a}(\boldsymbol{x}, x^-) := \bar{n}^\mu \delta(x^-) \rho^a(\boldsymbol{x}), \tag{2.1.10}$$

which possesses no coordinate dependence on x^+ and demonstrates its infinitesimal support in x^- due to respective kinematic enhancement and suppression through the Lorentz matrix in eq. (2.1.7). All transverse coordinate dependence, is encapsulated in the color charge density $\rho^a(\boldsymbol{x})$ where the $\mathsf{SU}(N_c)$ adjoint color index takes values $a \in \{1, \dots, N_c^2 - 1\}$.

The hadronic target, in eq. (2.1.10), is modelled as a color current [51] that arises from bound state configurations of valence quarks and kinematically enhanced quantum fluctuations mediated by gluons. The presence of the bound state and emission processes induced by the QCD action, give a statistical interpretation of the color current $j^{\mu a}(\boldsymbol{x}, x^-)$ as a member in an ensemble of configurations. A single color current, is therefore unable to characterize all quantum effects mediated by gluons. A given color current $j^{\mu a}(x)$ gives rise to gluonic effects described by some non-Abelian gauge field $b^{\mu a}(x)$ through the classical Yang-Mills equation [52],

$$\big[D_\mu^x[b], F^{\mu\nu}[b](x) \big] = j^\nu(x). \tag{2.1.11}$$

Since the gluon field strength tensor, $F^{\mu\nu}[b](x)$, is Lorentz covariant – the action of the boost in eq. (2.1.7) allows the inference of the kinematically enhanced components thereof,

$$F^{i+} \overset{e^Y}{\gg} F^{ij}, F^{-+} \overset{e^Y}{\gg} F^{i-}. \tag{2.1.12}$$

Moreover, the coordinate dependence of the the gluon field strength tensor may be inferred through eq. (2.1.10). All in all, $F^{\mu\nu}[b]$ may be characterized solely in terms of the kinematically enhanced components $F^{i+}[b]$ which showcase coordinate dependence like eq. (2.1.10),

$$F^{\mu\nu}[b](x) := \frac{i}{g}\big[D^{\mu}_{x}[b], D^{\nu}_{x}[b]\big] \xrightarrow{\text{kinematics}} F^{i+}[b](\boldsymbol{x}, x^-) = \partial^{i}_{x} b^{+}(\boldsymbol{x}, x^-). \tag{2.1.13}$$

Effects of the kinematics of DIS events characterized in the gauge covariant expression in eq. (2.1.13) trickle down into defining the classical **background field**,

$$b^{\mu a}(\boldsymbol{x}, x^-) = \bar{n}^{\mu}\delta(x^-)\beta^{a}(\boldsymbol{x}), \tag{2.1.14}$$

where $\beta(\boldsymbol{x})$, called the color field, demonstrates a dependence on the transverse coordinates of the target. $\beta(\boldsymbol{x}) = \beta^{a}(\boldsymbol{x})t^{a}$ is an element of the Lie algebra of $\mathsf{SU}(N_c)$.

In the Regge-Gribov limit the hadronic target is probed in a manner that exposes gluon saturation effects at small-x_{bj}. Both dynamics and kinematics of gluons are encoded in the background field in eq. (2.1.14) - which manifestly carries *color* through representation of the Lie algebra of $\mathsf{SU}(N_c)$. Kinematically, in the rest frame of the probe, where the target is 'length contracted' along the x^- coordinate and 'time dilated' along the x^+ coordinate - gluons of hadronic target are effectively frozen. On the short time scales during which the target is probed, the gluons appear frozen - however, generically, the gluons undergo inter-parton interaction; much like *glass* which is "on short time scales a solid and on long time scales a liquid" to quote from personal communication [53]. Lastly, gluons as massless bosons, are expected to arrange in a new form of matter akin to a *condensate*, with characteristically high occupation of gluons at order $1/\alpha_s$, in the saturation regime [17]. Ultimately, what arises is a universal state of matter that describes the high gluon density part of the hadronic wavefunction at small x_{bj} - namely, the **Color Glass Condensate** (CGC).

Interaction of the leptonic probe (traversing along the x^- coordinate) and hadronic target (traversing along the x^+ coordinate) occurs through the exchange of a spacelike virtual photon. A spacetime diagram of the interaction between the spacelike virtual photon and the hadronic target is shown in Figure 2.6. Kinematic effects on the hadron - such as the contraction along the x^- coordinate and the dilation along the x^+ coordinate - are depicted. Dynamic effects on the hadron - such as gluon saturation giving rise to collective degrees of freedom are also depicted.

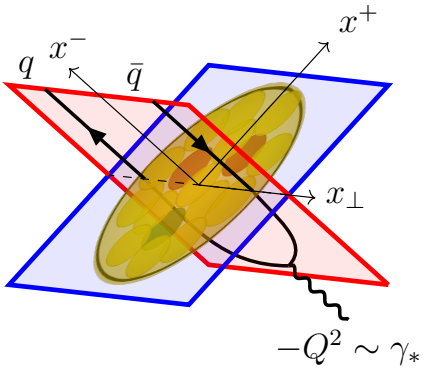

Figure 2.6: *[Colour online] Graphical depiction of the interaction between photon and hadron in the Regge-Gribov limit of DIS. Photon splits into quark-antiquark pair and traverses along x^- on the (red) lightsheet. Hadron exhibiting Lorentz contraction and gluon saturation traverses along x^+ on (blue) lightsheet.*

Moreover, the QCD interaction between the mediating photon and target involves the spacelike virtual photon splitting into a color neutral combination of probing partons. Fig-

ure 2.6, only shows the zeroth order color neutral combination, a hard $\bar{q}q$ pair. At higher order more partons will appear, always in global color singlet since the photon is a global color singlet. The highly energetic nature of the probing partons motivate the use of the **eikonal approximation**, where the partons pierce the hadronic target without being displaced from their trajectories. Nonetheless, soft gluon interactions of the probing partons with the background field, when resummed to all orders (for a textbook exposition see [54, Chapter 5]), give rise to Wilson lines,

$$U^{(\text{rep.})}_{\boldsymbol{x};f,i}[b] := P \exp\left[(-ig)\int_i^f dx^- n_\mu b^{\mu a}(x) t^a_{(\text{rep.})}\right]; \tag{2.1.15}$$

which are path ordered exponentials of the gauge field $b^{\mu a}(x)t^a_{(\text{rep.})}$ and consequently elements of representations of the $\mathsf{SU}(N_c)$ gauge group. Generically, the species of parton involved in the interaction with hadronic target determines the representation of the associated Wilson line, - more specifically - quark, antiquark, and gluon interactions involve Wilson lines in the fundamental, anti-fundamental, and adjoint representations respectively. In essence, Wilson lines account for finite local (position dependent) color rotations to the partonic wavefunctions due to resummed interactions with the background field. CGC Wilson lines are taken to traverse along x^- and have an explicit dependence on the transverse position of the interaction with hadronic target $\boldsymbol{x}$. Due to the nature of the gauge field $b^{\mu a}(x) = \bar{n}^\mu \delta(x^-)\beta^a(\boldsymbol{x})$ which is localized at $x^- = 0$, interactions with the hadronic target are instantaneous. It, therefore, suffices to use Wilson line along a straight path. This motivates the use of,

$$U^{(\text{rep.})}_{\boldsymbol{x}} := U^{(\text{rep.})}_{\boldsymbol{x};+\infty,-\infty}[b]. \tag{2.1.16}$$

as a given shorthand for CGC Wilson lines.

The total cross section of a DIS process in Regge-Gribov limit may be derived using the optical theorem. In the review, [20], the total DIS cross section is given as,

$$\sigma_{\text{DIS}}\left(x_{\text{bj}}, Q^2\right) = \sum_{\lambda=T,L}\int d^2\boldsymbol{r}\int_0^1 d\alpha \left|\psi_\lambda(\alpha, \boldsymbol{r}^2, Q^2)\right|^2 \int d^2\boldsymbol{b} N_{\boldsymbol{xy}}(x_{\text{bj}}). \tag{2.1.17}$$

Note the manifest dependence of the total cross section on the rapidity separation $Y \simeq \ln 1/x_{\text{bj}}$ and the hard scale Q^2. On the right hand side in eq. (2.1.17), there is a sum over the transverse $\lambda = T$ and longitudinal $\lambda = L$ polarizations of the spacelike virtual photon. The transition probability of the spacelike virtual photon $\gamma_* \sim -Q^2$ splitting into a quark-antiquark pair of transverse size $\boldsymbol{r} := \boldsymbol{x} - \boldsymbol{y}$ where the quark carries the fraction α of the incoming photon momentum q and the antiquark carries the remainder $(1-\alpha)$ is given by the normalized square amplitude of the wavefunction $\left|\psi_\lambda(\alpha, \boldsymbol{r}^2, Q^2)\right|^2$.

All rapidity separation dependence is carried by the **color dipole correlator** integrated

over the impact parameter of the color dipole relative to the target $\boldsymbol{b} := (\boldsymbol{x} + \boldsymbol{y})/2$,‘

$$\begin{aligned} N_{\boldsymbol{xy}}(x_{\mathrm{bj}}) &:= \frac{1}{N_c}\left\langle \mathrm{tr}\Big(\big(U_{\boldsymbol{x}}[b]U^{\dagger}_{\boldsymbol{y}}[b]-1\big)^{\dagger}\big(U_{\boldsymbol{x}}[b]U^{\dagger}_{\boldsymbol{y}}[b]-1\big)\Big)\right\rangle_b(x_{\mathrm{bj}}) \\ &= 2\left(1-\frac{\mathrm{Re}\big\langle \mathrm{tr}\big(U_{\boldsymbol{x}}[b]U^{\dagger}_{\boldsymbol{y}}[b]\big)\big\rangle_b(x_{\mathrm{bj}})}{N_c}\right). \end{aligned} \tag{2.1.18}$$

The color dipole correlator in eq. (2.1.18) demonstrates structural similarities with the transfer matrix $\mathcal{T} := \mathcal{S} - 1$ encountered in QFT. The non-trivial part of the color dipole correlator,

$$S_{\boldsymbol{xy}} := \frac{\big\langle \mathrm{tr}\big(U^{\dagger}_{\boldsymbol{x}}[b]U_{\boldsymbol{y}}[b]\big)\big\rangle_b(x_{\mathrm{bj}})}{N_c}, \tag{2.1.19}$$

describes the eikonal interaction of the quark and antiquark pair, shown in Figure 2.6, with the hadronic target. Moreover, the background field dependent averaging procedure $\langle\ldots\rangle_b(x_{\mathrm{bj}})$ which characterizes the Bjorken-x or rapidity separation dependence of Wilson line correlators represents an average over the ensemble of color configurations alluded to in the discussion of the color current $j(x)$.

Note that, for future reference, the background field dependence of Wilson lines and the averaging procedure will be suppressed unless explicitly required.

2.2 Resummation of Gluonic Fluctuations in the CGC

The relation between rapidity separation and Bjorken-x, $Y \simeq \ln 1/x_{\rm bj}$, allows the classical background gauge field $b^{\mu a}(x) = \bar{n}^\mu \delta(x^-)\beta^a(\boldsymbol{x})$ to simultaneously characterize the kinematics (due to high rapidity separation) and the dynamics (due to gluon saturation effects) of DIS events in the Regge-Gribov limit. In particular, the classical treatment of the background field is further motivated since saturation is expected at gluon phase space density of order $1/\alpha_s$ [17]. For small α_s, the background field is considered too large for a perturbative treatment. Nevertheless, fluctuations arising from the vacuum which characterize changes to the background field are amenable to perturbative expansions. The Large Background Field (LBF) formalism will be employed to describe changes to the classical background field $b^{\mu a}(x)$ in terms of a quantum **fluctuation field** $\alpha^{\mu a}(x)$. A Lagrangian $\mathcal{L}_{\rm gluons}[A, j](x)$ is employed such that total gauge field is decomposed into a background field and fluctuation field,

$$A^{\mu a}(x) = b^{\mu a}(x) + \alpha^{\mu a}(x). \tag{2.2.1}$$

The gluonic dynamics of the CGC will be described through a Yang-Mills term, and a gauge-fixing term, and a source term ,

$$\begin{aligned}\mathcal{L}_{\rm gluons}[A, j](x) := &-\frac{1}{4}F^a_{\mu\nu}[A](x)F^{a\mu\nu}[A](x) - \frac{1}{2\xi}\left(\bar{n}_\mu A^{a\mu}(x)\right)\left(\bar{n}_\nu A^{a\nu}(x)\right) \\ &- A^{a\mu}(x)j_{a\mu}(x).\end{aligned} \tag{2.2.2}$$

A finite value of ξ regularizes the gluon propagator resulting from the gauge field $A^{\mu a}(x) = b^{\mu a}(x) + \alpha^{\mu a}(x)$. Taking the limit $\xi \to 0$ within a path integral strictly enforces the axial gauge-fixing prescription, in which $\bar{n}.A = A^- = 0$ for all field configurations. The choice of gauge reflects lightcone gauge-fixing condition $\bar{n}_\mu(b+\alpha)^\mu = (b+\alpha)^- = 0$ which encapsulates the kinematic suppression of the minus components of the background field; transverse components of the fluctuation field are not considered suppressed. All in all, the components of the background and fluctuation gluonic interactions to be considered,

$$A^a(x) = b^a(x) + \alpha^a(x) = \begin{pmatrix} b^{+a}(x) \\ 0 \\ 0 \\ 0 \end{pmatrix} + \begin{pmatrix} \alpha^{+a}(x) \\ \alpha^{1a}(x) \\ \alpha^{2a}(x) \\ 0 \end{pmatrix}. \tag{2.2.3}$$

Explicitly, in accordance with the LBF formalism, $\mathcal{L}_{\rm gluons}[A = b + \alpha, j]$ is expanded in terms of the fluctuation field where $\mathcal{L}^{(n)}_{\rm gluons}[b + \alpha, j]$ denotes the n-th order in α - see appendix (B.4.2). Quantum fluctuations are typically characterized by $\alpha^{+a}_x := \alpha^{+a}(x)$ modes of the Lagrangian $\mathcal{L}_{\rm gluons}[b + \alpha]$ which couple to kinematically enhanced component of the background field $b^{+a}_x := b^{+a}(x)$. The coupling of the fluctuation field to the background field motivates an averaging procedure $\langle \dots \rangle_\alpha[b]$ akin to the target averaging procedure encountered in Wilson line correlators. The expectation value of the first order fluctuation is taken to be zero,

$$\langle \alpha^\nu_x \rangle_\alpha[b] = 0 \iff [D^\mu_x[b], F_{\mu\nu}[b](x)] = j_\nu(x), \tag{2.2.4}$$

due to the manifestation of the Classical Yang-Mills (CYM) equation [55] in $\mathcal{L}^{(1)}_{\text{gluons}}[b+\alpha, j]$ which is the Euler-Lagrange equation of motion of the non-abelian background gauge field. The CYM equation is used to define the background field $b^{\mu a}(x)$ in terms of the color current $j^{\mu a}(x)$.

Wilson line correlators which are used to characterize eikonal partonic interactions with CGC are entirely determined by the background field. Additionally, in CGC observables, such as the DIS cross section in the Regge-Gribov limit showcased in eq. (2.1.17), all rapidity or, equivalently, all Bjorken-x dependence is encapsulated by Wilson line correlators which may arbitrarily be constructed through a generating functional,

$$\left\langle \bigotimes_{i=1}^{m} U_{\boldsymbol{x}_i}[b] \bigotimes_{j=1}^{\bar{m}} U^{\dagger}_{\boldsymbol{y}_j}[b] \right\rangle_b (Y) = \bigotimes_{i=1}^{m} \frac{\delta}{\delta J^{\dagger}_{\boldsymbol{x}_i}} \bigotimes_{j=1}^{\bar{m}} \frac{\delta}{\delta J_{\boldsymbol{y}_j}} \Bigg|_{J^{(\dagger)}\equiv 0} \left\langle \exp S[b, J^{(\dagger)}] \right\rangle_b (Y), \tag{2.2.5}$$

where both Wilson lines $U^{(\dagger)}[b]$ and the correlation function $\langle \dots \rangle_b$ are defined by the specification of $b^{\mu a}(x)$. Products of Wilson lines are, specifically, constructed by evaluating functional derivatives with respect to sources $J^{(\dagger)}$. The exponent of the generating functional is,

$$S[b, J^{(\dagger)}] := \int_{\boldsymbol{x}} \big[J^{\dagger}_{\boldsymbol{x}}\big]_{ij} \big[U_{\boldsymbol{x}}[b]\big]_{ij} + \big[J_{\boldsymbol{x}}\big]_{kl} \big[U^{\dagger}_{\boldsymbol{x}}[b]\big]_{kl}. \tag{2.2.6}$$

Wilson line correlators in eq. (2.2.5), therefore, establish the definition of the kinematically enhanced component of the background field, in accordance with eq. (2.2.4), as an innately rapidity dependent statement. That is, if the background field $b^{\mu a}(x)$ corresponds to the target probed at rapidity Y, then a fluctuation induced upon the background field $(b+\alpha)^{\mu a}(x)$ appropriately corresponds to a change in the rapidity $Y + \delta Y$ at which the target is probed. Using Lagrangian dynamics dictated by eq. (2.2.2), loop corrections induced by the fluctuation allow the inference of the explicit rapidity dependence of Wilson line correlators and consequently of CGC observables like $\sigma_{\text{DIS}}(x_{\text{bj}} = e^{-Y}, Q^2)$ in eq. (2.1.17). To proceed, the Taylor expansion of the generating functional encapsulates changes induced by fluctuations to arbitrary Wilson line correlators in eq. (2.2.5),

$$\exp\big(S[b+\alpha]\big) = \Big(1 + \int_u \alpha^{+a}_u \frac{\delta}{\delta b^{+a}_u} + \frac{1}{2}\int_{uv} \alpha^{+a}_u \frac{\delta}{\delta b^{+a}_u} \alpha^{+b}_v \frac{\delta}{\delta b^{+b}_v} + \mathcal{O}(\alpha^3)\Big) \exp\big(S[b]\big). \tag{2.2.7}$$

where $\int d^4u =: \int_u$ et cetera. The Taylor expansion of the generating functional $\exp S[b+\alpha]$ sets up a finite difference equation which characterize how, under a change of rapidity $Y \to Y + \delta Y$, modes which were previously considered quantum fluctuations $\alpha^{\mu a}(x)$ atop the background field $b^{\mu a}(x)$ are re-incorporated into a re-definition of the background field $b \to b + \alpha$ [33]. Quantum fluctuations will be incorporated with the **fluctuation gluon propagator** $\big\langle \alpha^{+a}_u \alpha^{+b}_v \big\rangle_\alpha [b]$.

All in all, the LBF formalism allows calculation of 1-loop soft gluon corrections to the Wilson line correlators through a finite difference equation,

$$\begin{aligned} &\left\langle \exp\big(S[b+\alpha]\big) \right\rangle_{b+\alpha} (Y+\delta Y) - \left\langle \exp\big(S[b]\big) \right\rangle_b (Y) \\ &= + \frac{1}{2}\int_{uv} \left\langle \big\langle \alpha^{+a}_u \alpha^{+b}_v \big\rangle_\alpha [b] \Big\{ \frac{\delta S[b]}{\delta b^{+a}_u} \frac{\delta S[b]}{\delta b^{+b}_v} + \frac{\delta^2 S[b]}{\delta b^{+a}_u \delta b^{+b}_v} \Big\} \exp\big(S[b]\big) \right\rangle_b + \mathcal{O}(\alpha^3). \end{aligned} \tag{2.2.8}$$

The right hand side of the finite difference equation (2.2.8) features a sum of two terms arising from background field derivatives of the generating functional. The product of the background field derivatives and the fluctuation propagator (whose structures are respectively elucidated in appendices (B.4.1) and (B.4.2)) give rise to gluon exhange diagrams and gluon self-energy diagrams. The gluon exchange diagrams,

$$+\frac{1}{2}\int_{uv}\left\langle \alpha_u^{+a}\alpha_v^{+b}\right\rangle_\alpha[b]\frac{\delta S[b]}{\delta b_u^{+a}}\frac{\delta S[b]}{\delta b_v^{+b}} =: \delta Y\cdot\int_{\boldsymbol{u},\boldsymbol{v}}\frac{1}{2}J^\alpha_{\boldsymbol{u}}J^\beta_{\boldsymbol{v}}\chi^{\alpha\beta}_{\boldsymbol{u},\boldsymbol{v}}[\vec{U}], \tag{2.2.9}$$

involve a color transfer between two distinct partons which is mediated by a soft gluon. Evaluating the momentum integrals of the fluctuation propagator give rise to the factorized structure demonstrated in eq. (2.2.9). Rapidity separation δY is inferred by regulating the ultraviolet and infrared divergent lightcone momentum integral $\int_0^\infty dk^-/k^-$ since canonically $Y := (1/2)\ln k^+/k^-$. The contracted indices on the sources J and the Wilson line products $\chi_{\boldsymbol{u},\boldsymbol{v}}[\vec{U}]$ are employed as short-hand for $\alpha,\beta\in\{q,\bar{q}\}$ so that $\vec{U} := [U^q, U^{\bar{q}}] = [U, U^\dagger]$ and $\vec{J} := [J^q, J^{\bar{q}}] = [J^\dagger, J]$. For the Wilson line products, the term $\chi^{q\bar{q}}_{\boldsymbol{u},\boldsymbol{v}}$ denotes lightcone coordinate x^--ordered color exchanges which are diagrammatically,

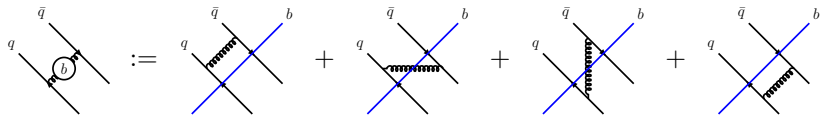

(2.2.10)

note that the hadronic target is localized at $x^- = 0$. Only soft gluons emitted at $x^- < 0$ and absorbed at $x^- > 0$ undergo interactions with hadronic target. In cases of non-interaction the soft gluon does not undergo color rotation.

Quite analogously, gluon self-energy diagrams,

$$+\frac{1}{2}\int_{uv}\left\langle \alpha_u^{+a}\alpha_v^{+b}\right\rangle_\alpha[b]\frac{\delta^2 S[b]}{\delta b_u^{+a}\delta b_v^{+b}} =: \delta Y\cdot\int_{\boldsymbol{u}} J^\alpha_{\boldsymbol{u}}\sigma^\alpha_{\boldsymbol{u}}, \tag{2.2.11}$$

involve color transfer from a parton with itself which is mediated by a soft gluon.

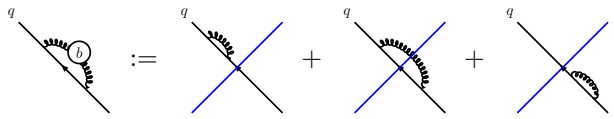

(2.2.12)

note that the hadronic target is localized at $x^- = 0$. Only soft gluons emitted at $x^- < 0$ and absorbed at $x^- > 0$ undergo interactions with hadronic target. In cases of non-interaction the soft gluon does not undergo color rotation.

Using the terms in eqs (2.2.9) and (2.2.11), in the finite difference eq. (2.2.8) sets up a functional differential equation (known as a group renormalization equation) which explicitly

demonstrates the rapidity dependence of Wilson line correlators,

$$\begin{aligned}&\frac{d}{dY}\Big\langle \exp\big(S[b,\vec{J}]\big)\Big\rangle_b(Y)\\&=\Big\langle\Big\{\frac{1}{2}\int_{\boldsymbol{uv}}J^\alpha_{\boldsymbol{u}}J^\beta_{\boldsymbol{v}}\bar{\chi}^{\alpha\beta}_{\boldsymbol{u},\boldsymbol{v}}[\vec{U}]+\int_{\boldsymbol{u}}J^\alpha_{\boldsymbol{u}}\bar{\sigma}^\alpha_{\boldsymbol{u}}[\vec{U}]\Big\}\exp\big(S[b,\vec{J}\big)\Big\rangle_b(Y)+\mathcal{O}(\alpha^3).\end{aligned}\tag{2.2.13}$$

Gluon exchange and gluon self-energy effects which manifest in the functional differential equation eq. (2.2.13), may be recast in terms of the differential operator called the JIMWLK Hamiltonian,

$$H^{(\mathrm{LL})}_{\mathrm{JIMWLK}}=-\frac{\alpha_s}{2\pi}\int_{\boldsymbol{uzv}}\mathcal{K}_{\boldsymbol{uzv}}\big[\tilde{U}^{ab}_{\boldsymbol{z}}\big(i\bar{\nabla}^a_{\boldsymbol{u}}i\nabla^b_{\boldsymbol{v}}+i\bar{\nabla}^a_{\boldsymbol{v}}i\nabla^b_{\boldsymbol{u}}\big)+i\nabla^a_{\boldsymbol{u}}i\nabla^a_{\boldsymbol{v}}+i\bar{\nabla}^a_{\boldsymbol{u}}i\bar{\nabla}^a_{\boldsymbol{v}}\big],\tag{2.2.14}$$

where ∇^a and $\bar{\nabla}^a$ are left and right invariant vector fields; their operational definition is given below,

$$\begin{aligned}i\nabla^a_{\boldsymbol{x}}U_{\boldsymbol{y}}&=-U_{\boldsymbol{x}}t^a\delta^{(2)}_{\boldsymbol{x},\boldsymbol{y}},\quad i\nabla^a_{\boldsymbol{x}}U^\dagger_{\boldsymbol{y}}=+t^aU^\dagger_{\boldsymbol{x}}\delta^{(2)}_{\boldsymbol{x},\boldsymbol{y}},\\i\bar{\nabla}^a_{\boldsymbol{x}}U_{\boldsymbol{y}}&=+t^aU_{\boldsymbol{x}}\delta^{(2)}_{\boldsymbol{x},\boldsymbol{y}},\quad i\bar{\nabla}^a_{\boldsymbol{x}}U^\dagger_{\boldsymbol{y}}=-U^\dagger_{\boldsymbol{x}}t^a\delta^{(2)}_{\boldsymbol{x},\boldsymbol{y}},\end{aligned}\tag{2.2.15}$$

and $\mathcal{K}_{\boldsymbol{uzv}}$ is a **gluon emission kernel** which arises from the transverse momentum integrals in the fluctuation propagator,

$$\mathcal{K}_{\boldsymbol{uzv}}:=\frac{(\boldsymbol{u}-\boldsymbol{z})\cdot(\boldsymbol{z}-\boldsymbol{v})}{(\boldsymbol{u}-\boldsymbol{z})^2(\boldsymbol{z}-\boldsymbol{v})^2}.\tag{2.2.16}$$

The evolution of an arbitrary CGC Wilson line correlators manifests as a diffusion equation known as the JIMWLK[2] equation which is a framework that tracks the rapidity evolution of CGC observables,

$$\frac{d}{dY}\Big\langle\bigotimes_{i=1}^{m}U_{\boldsymbol{x}_i}\bigotimes_{j=1}^{\bar{m}}U^\dagger_{\boldsymbol{y}_j}\Big\rangle_b(Y)=\Big\langle-H^{(\mathrm{LL})}_{\mathrm{JIMWLK}}\bigotimes_{i=1}^{m}U_{\boldsymbol{x}_i}\bigotimes_{j=1}^{\bar{m}}U^\dagger_{\boldsymbol{y}_j}\Big\rangle_b(Y).\tag{2.2.17}$$

Which characterizes how logarithmically enhanced $Y\simeq\ln 1/x_{\mathrm{bj}}$ quantum fluctuations induced by the QCD action drive saturation effects within CGC observables. Solving the equation in eq. (2.2.17) provides a resummation structure for the leading logarithmic approximation to CGC observables.

[2] Jalilian-Marian–Iancu–McLerran–Weigert–Leonidov–Kovner

2.3 JIMWLK Evolution of a Color Dipole

Consider the non-trivial part of the color dipole correlator in eq. (2.1.18),

$$S_{\boldsymbol{xy}}(x_{\rm bj}) := \frac{\big\langle \mathrm{tr}\big(U^\dagger_{\boldsymbol{x}} U_{\boldsymbol{y}}\big)\big\rangle(x_{\rm bj})}{N_c}. \tag{2.3.1}$$

The trace of Wilson line product $\mathrm{tr}\big(U_{\boldsymbol{x}}U^\dagger_{\boldsymbol{y}}\big)$ when expressed in terms of graphical notation called birdtracks [56] highlights how initial color singlet is color rotated by Wilson lines into a final color singlet. To elaborate, consider the birdtrack notation for Kronecker deltas and Hermitian generators of the Lie algebra of $\mathsf{SU}(N_c)$:

$\delta^i{}_j =$ 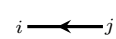 , (2.3.2a)

$\delta_i{}^j =$ 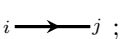 ; (2.3.2a)

$[t^a]^i{}_j =$ 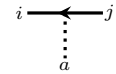 , (2.3.2b)

$[t^{a*}]^i{}_j =$ 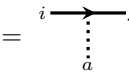 $= [t^a]_j{}^i$. (2.3.2b)

Position dependent fundamentally and anti-fundamentally represented Wilson lines may also be expressed in birdtrack notation (as in [57]):

$[U_{\boldsymbol{x}}]^i{}_j =:$  , (2.3.3a)

$[U^\dagger_{\boldsymbol{y}}]^j{}_i =:$ 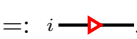 $= [U^*_{\boldsymbol{y}}]_i{}^j$. (2.3.3b)

The trace of the Wilson line product $\mathrm{tr}\big(U_{\boldsymbol{x}}U^\dagger_{\boldsymbol{y}}\big)$,

$$\mathrm{tr}\big(U_{\boldsymbol{x}}U^\dagger_{\boldsymbol{y}}\big) = \delta^{\bar i}{}_i \big[U_{\boldsymbol{x}}\big]^i{}_j \big[U^\dagger_{\boldsymbol{y}}\big]^{\bar j}{}_{\bar i} \delta^j{}_{\bar j}, \tag{2.3.4}$$

is expressed in birdtrack notation in Figure 2.7.

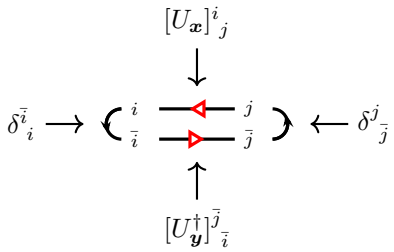

Figure 2.7: $\mathrm{tr}\big(U_{\boldsymbol{x}}U^\dagger_{\boldsymbol{y}}\big)$ *expressed in birdtrack notation reveals how an initial singlet* $\delta^j{}_{\bar j}$ *is color rotated by the Wilson lines* $\big[U_{\boldsymbol{x}}\big]^i{}_j \big[U^\dagger_{\boldsymbol{y}}\big]^{\bar j}{}_{\bar i}$ *into a final singlet* $\delta^{\bar i}{}_i$.

To evaluate the rapidity $Y \simeq \ln 1/x_{\rm bj}$ evolution of the Wilson line correlator $S_{\boldsymbol{xy}}(x_{\rm bj})$ - one evaluates the action of the JIMWLK Hamiltonian,

$$H^{(\rm LL)}_{\rm JIMWLK} = -\frac{\alpha_s}{2\pi^2}\int_{\boldsymbol{uzv}} \mathcal{K}_{\boldsymbol{uzv}}\big[\tilde U^{ab}_{\boldsymbol{z}}\big(i\bar\nabla^a_{\boldsymbol{u}} i\nabla^b_{\boldsymbol{v}} + i\bar\nabla^a_{\boldsymbol{v}} i\nabla^b_{\boldsymbol{u}}\big) + i\nabla^a_{\boldsymbol{u}} i\nabla^a_{\boldsymbol{v}} + i\bar\nabla^a_{\boldsymbol{u}} i\bar\nabla^a_{\boldsymbol{v}}\big]. \tag{2.2.14}$$

However, note that the numerator of the JIMWLK kernel $\mathcal{K}_{\boldsymbol{uzv}}$ defined in eq. (2.2.16), may be written in terms of the sum of squared distances between transverse coordinates,

$$(\boldsymbol{u}-\boldsymbol{z})\cdot(\boldsymbol{z}-\boldsymbol{v}) = \frac{1}{2}\big[(\boldsymbol{u}-\boldsymbol{v})^2 - (\boldsymbol{u}-\boldsymbol{z})^2 - (\boldsymbol{z}-\boldsymbol{v})^2\big], \tag{2.3.5}$$

using which the CGC gluon emission kernel $\mathcal{K}_{\boldsymbol{uzv}}$ may thus be expressed in terms of CGC **dipole kernel** $\tilde{\mathcal{K}}_{\boldsymbol{uzv}}$ and two additional contributions,

$$\mathcal{K}_{\boldsymbol{uzv}} = \frac{\tilde{\mathcal{K}}_{\boldsymbol{uzv}}}{2} - \frac{1}{2(\boldsymbol{z}-\boldsymbol{v})^2} - \frac{1}{2(\boldsymbol{u}-\boldsymbol{z})^2}, \tag{2.3.6}$$

$$\tilde{\mathcal{K}}_{\boldsymbol{uzv}} := \frac{(\boldsymbol{u}-\boldsymbol{v})^2}{(\boldsymbol{u}-\boldsymbol{z})^2(\boldsymbol{z}-\boldsymbol{v})^2}. \tag{2.3.7}$$

Only the dipole kernel carries dependence on all three transverse coordinates $\boldsymbol{u}, \boldsymbol{z}, \boldsymbol{v}$ in eq. (2.3.6); the remainder, that is $\mathcal{K}_{\boldsymbol{uzv}} - \tilde{\mathcal{K}}_{\boldsymbol{uzv}}/2$, necessarily injects terms such as:

$$\int_{\boldsymbol{u}} i\nabla^a_{\boldsymbol{u}} \quad \text{and} \quad \int_{\boldsymbol{v}} i\nabla^a_{\boldsymbol{v}}; \tag{2.3.8a}$$

$$\int_{\boldsymbol{u}} i\bar{\nabla}^a_{\boldsymbol{u}} \quad \text{and} \quad \int_{\boldsymbol{v}} i\bar{\nabla}^a_{\boldsymbol{v}}. \tag{2.3.8b}$$

The action of terms such as $\int_{\boldsymbol{u}} i\nabla^a_{\boldsymbol{u}}$ and $\int_{\boldsymbol{v}} i\bar{\nabla}^a_{\boldsymbol{v}}$ (which are considered without loss of generality) on the Wilson line product showcased in eq. (2.3.4),

$$\int_{\boldsymbol{u}} i\nabla^a_{\boldsymbol{u}} \mathrm{tr}\big(U_{\boldsymbol{x}} U^\dagger_{\boldsymbol{y}}\big) = -\mathrm{tr}\big(U_{\boldsymbol{x}} t^a U^\dagger_{\boldsymbol{y}}\big) + \mathrm{tr}\big(U_{\boldsymbol{x}} t^a U^\dagger_{\boldsymbol{y}}\big) = 0, \tag{2.3.9a}$$

$$\int_{\boldsymbol{v}} i\bar{\nabla}^a_{\boldsymbol{v}} \mathrm{tr}\big(U_{\boldsymbol{x}} U^\dagger_{\boldsymbol{y}}\big) = +\mathrm{tr}\big(t^a U_{\boldsymbol{x}} U^\dagger_{\boldsymbol{y}}\big) - \mathrm{tr}\big(U_{\boldsymbol{x}} U^\dagger_{\boldsymbol{y}} t^a\big) = 0, \tag{2.3.9b}$$

is seen to annihilate the Wilson line products. However, in birdtrack notation,

$\int_{\boldsymbol{u}} i\nabla^a_{\boldsymbol{u}}$ 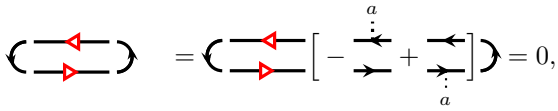 (2.3.10a)

$\int_{\boldsymbol{v}} i\bar{\nabla}^a_{\boldsymbol{v}}$ 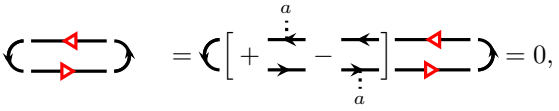 (2.3.10b)

the action of $\int_{\boldsymbol{u}} i\nabla^a_{\boldsymbol{u}}$ and $\int_{\boldsymbol{v}} i\bar{\nabla}^a_{\boldsymbol{v}}$ is explicitly seen to generate infinitesimal global (that is, coordinate independent) color rotations,

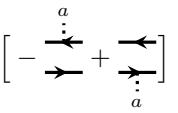 $\overset{!}{=}$ generator of $\mathsf{SU}(N_c)$ in a $q\bar{q}$ product representation. (2.3.11)

Color singlets such as $\delta^{\bar{i}}_{\ i}$ and $\delta^{j}_{\ \bar{j}}$, which are by definition, invariant under finite global color rotations – are accordingly annihilated by generators of the type highlighted in eq. (2.3.11),

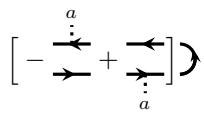 $= 0,$ (2.3.12a)

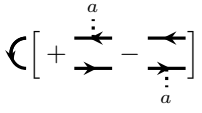 $= 0.$ (2.3.12b)

In the expansion of the gluon emission kernel $\mathcal{K}_{\boldsymbol{uzv}}$ it is only the dipole kernel $\tilde{\mathcal{K}}_{\boldsymbol{uzv}}/2$ which drives the evolution of color singlet Wilson line correlators; the remainder $\mathcal{K}_{\boldsymbol{uzv}} - \tilde{\mathcal{K}}_{\boldsymbol{uzv}}/2$ only

activates for color non-singlet Wilson line correlators.

The action of $H^{(\mathrm{LL})}_{\mathrm{JIMWLK}}$ on eq. (2.3.1), when re-arranged, yields the JIMWLK evolution of the color dipole [19],

$$\begin{aligned}&\frac{d}{d\ln(1/x_{\mathrm{bj}})}\frac{\big\langle \mathrm{tr}(U_{\boldsymbol{x}}U^{\dagger}_{\boldsymbol{y}})\big\rangle(x_{\mathrm{bj}})}{N_c}\\&\quad=\frac{\alpha_s C_f}{\pi}\int\frac{d^2\boldsymbol{z}}{2\pi}\tilde{\mathcal{K}}_{\boldsymbol{xzy}}\left\{\frac{\big\langle \tilde{U}^{ab}_{\boldsymbol{z}}2\mathrm{tr}(t^aU_{\boldsymbol{x}}t^bU^{\dagger}_{\boldsymbol{y}})\big\rangle(x_{\mathrm{bj}})}{N_c^2-1}-\frac{\big\langle \mathrm{tr}(U_{\boldsymbol{x}}U^{\dagger}_{\boldsymbol{y}})\big\rangle(x_{\mathrm{bj}})}{N_c}\right\},\end{aligned}\tag{2.3.13}$$

where the Wilson line correlators have been pre-emptively normalized according to the different representations of the gauge group $\mathsf{SU}(N_c)$: the dimensionality of the fundamental representation $d_f = N_c$, the dimensionality of the adjoint representation $d_A = N_c^2 - 1$, and the Casimir in the fundamental rep. $C_f = (N_c^2-1)/2N_c$.

Note that the JIMWLK evolution of a 2-point correlator features a 3-point correlator; inductively, the evolution of an n-point correlator will feature an $(n+1)$-correlator. Consequently, the JIMWLK evolution of the color dipole $S_{\boldsymbol{xy}}(x_{\mathrm{bj}})$ features an infinite tower of coupled differential equations known as the Balitsky hierarchy.

The Wilson line product featured in the 3-point correlator, may be rewritten using the Fierz identity,

$$2\tilde{U}^{ab}_{\boldsymbol{z}}\mathrm{tr}(t^aU_{\boldsymbol{x}}t^bU^{\dagger}_{\boldsymbol{y}})=\mathrm{tr}(U_{\boldsymbol{x}}U^{\dagger}_{\boldsymbol{z}})\mathrm{tr}(U_{\boldsymbol{z}}U^{\dagger}_{\boldsymbol{y}})-\frac{1}{N_c}\mathrm{tr}(U_{\boldsymbol{x}}U^{\dagger}_{\boldsymbol{y}}),\tag{2.3.14}$$

which removes all terms of $\mathcal{O}(1/N_c)$ in the JIMWLK evolution of a color dipole in eq. (2.3.13),

$$\begin{aligned}&\frac{d}{d\ln(1/x_{\mathrm{bj}})}\frac{\big\langle \mathrm{tr}(U_{\boldsymbol{x}}U^{\dagger}_{\boldsymbol{y}})\big\rangle(x_{\mathrm{bj}})}{N_c}\\&\quad=\frac{\alpha_s N_c}{\pi}\int\frac{d^2\boldsymbol{z}}{2\pi}\tilde{\mathcal{K}}_{\boldsymbol{xzy}}\left\{\frac{\big\langle \mathrm{tr}(U_{\boldsymbol{x}}U^{\dagger}_{\boldsymbol{z}})\mathrm{tr}(U_{\boldsymbol{z}}U^{\dagger}_{\boldsymbol{y}})\big\rangle(x_{\mathrm{bj}})}{N_c^2}-\frac{\big\langle \mathrm{tr}(U_{\boldsymbol{x}}U^{\dagger}_{\boldsymbol{y}})\big\rangle(x_{\mathrm{bj}})}{N_c}\right\}.\end{aligned}\tag{2.3.15}$$

To make calculations more tractable, the large N_c limit of the JIMWLK equation known as the BK[3] equation is considered [13–16]. In the BK equation, the Balitsky hierarchy is absent due to the factorization assumption (which is thought to hold up in the large N_c limit),

$$\big\langle \mathrm{tr}(U_{\boldsymbol{x}}U^{\dagger}_{\boldsymbol{z}})\times\mathrm{tr}(U_{\boldsymbol{z}}U^{\dagger}_{\boldsymbol{y}})\big\rangle(x_{\mathrm{bj}})\xrightarrow{\text{'t Hooft large } N_c}\big\langle \mathrm{tr}(U_{\boldsymbol{x}}U^{\dagger}_{\boldsymbol{z}})\big\rangle(x_{\mathrm{bj}})\times\big\langle \mathrm{tr}(U_{\boldsymbol{z}}U^{\dagger}_{\boldsymbol{y}})\big\rangle(x_{\mathrm{bj}}).\tag{2.3.16}$$

In the BK equation, the evolution of a 2-point correlator is characteristically closed unlike in the JIMWLK equation,

$$\frac{d}{d\ln(1/x_{\mathrm{bj}})}S_{\boldsymbol{xy}}(x_{\mathrm{bj}})=\frac{\alpha_s N_c}{\pi}\int\frac{d^2\boldsymbol{z}}{2\pi}\tilde{\mathcal{K}}_{\boldsymbol{xzy}}\Big\{S_{\boldsymbol{xz}}(x_{\mathrm{bj}})S_{\boldsymbol{zy}}(x_{\mathrm{bj}})-S_{\boldsymbol{xy}}(x_{\mathrm{bj}})\Big\}.\tag{2.3.17}$$

[3] Balitsky–Kovchegov

Chapter 3

Energy Evolution of Jets

Collimated collections of particles observed in the final state of a high energy collision are called jets. These are ubiquitous features of experiments in modern particle colliders. Traits of jets, which reflect underlying particle production processes, are typically studied through specific observables. Among these are thrust (a measure of how collimated a jet event is) and interjet energy loss (a measure of how much energy is deposited in regions away from hard jets). In particular, the energy evolution of jet observables under kinematic constraints imposed by interjet energy vetoes is governed by the BMS equation which exhibits remarkable similarities to the BK equation. The similarities persist for the finite N_c generalizations characterized by BMS-W and JIMWLK equations.

3.1 Multiplicities of Semi-Inclusive Jet Observables

Jets – which are collimated collections of particles observed in the final state of high energy collision – are ubiquitous features of experiments in modern particle colliders. Jets are typically studied from underlying particle production processes (such as electron-positron, proton-proton or heavy ion collisions) which create hard partons near the collision point that radiate soft gluons while traversing near lightlike trajectories. The emitted soft gluons subsequently emit softer gluons giving rise to a cascade of soft objects such as quark-antiquark pairs et cetera. In a collection, colored objects hadronize, due to the manifest confinement effects of the strong force, into color-neutral bound states composed of quarks and gluons. The resultant hadrons, subsequently decay into metastable particles such as π mesons which are ultimately observed by detectors of collider experiments (for a textbook exposition see Chapter 36 in [48]).

However, the QCD description of the exact mechanisms of hadronization - which, essentially, is the relation between what is, perturbatively, calculated (involving partons) and what is, in a high energy collision, observed (involving hadrons and mesons) [58] - remains, by and large, inadequately understood. The ability to characterize the behaviour of jets, therefore, provides a window into understanding (among other things) the mechanisms of color neutralization processes involved in hadronization.

Accordingly, information encoded by QCD amplitudes in the cross section $\sigma_{\text{total}}(Q)$ at a given hard scale Q and the constraints imposed by kinematic variable V may be used to derive

a distribution which characterizes the multiplicity of the underlying event,

$$\Sigma(Q,V) = \sum_n \int \frac{d\sigma^{(n)}(Q)}{\sigma_{\text{total}}(Q)} \cdot \Theta\Big(V - \sum_{j=1}^{m} v_j\Big), \tag{3.1.1}$$

where $d\sigma^{(n)}(Q)$ is the n-loop contribution to the differential cross section. All constraints imposed by the kinematic variable are encapsulated in the Heaviside function where v_j is a single particle's contribution to the kinematic variable V.

Generically, singularities of the collinear and the infrared type manifest due to the underlying cross sections and the kinematic constraints imposed by the Jet observables. Nonetheless, for a broad class of observables logarithmically enhanced contributions exponentiate to yield a perturbative expansion of the form [59],

$$\ln \Sigma(Q,V) = \sum_{n=1}^{\infty} \frac{\alpha_s^n(Q^2)}{\pi^n} \big(A_n \ln V^{n+1} + B_n \ln V^n + \dots\big), \tag{3.1.2}$$

where the A_n series is referred to as double logarithmic and the B_n series is referred to as single logarithmic. The remaining contributions are all sub-leading logarithms which are not enhanced to the same degree as double or single logarithmic contributions. The structure of the resummation presented in eq. (3.1.2) is highly non-trivial [59] - as it states that only of the 'exponentiated gluons' may carry both collinear and infrared singularities, or equivalently terms such as $\alpha_s^n(Q^2) \ln^m V$ are limited to $m = n$ or $m = n + 1$.

Kinematic variables play a crucial role in determining the structure of multiplicity in eq. (3.1.1) and subsequently the structure of logarithmic resummation in eq. (3.1.2) of jet observables - which are broadly classified into two groups, namely: global/inclusive observables, and non-global/semi-inclusive observables. Observables of the **inclusive** type account for *all* final state particles in a jet measurement - and are, typically, employed to characterize properties such as *event shapes*. The manner in which event shapes are defined varies from text to text, the **thrust**, as defined in [60] is,

$$T := \sum_j t_j(\hat{\underline{\eta}}_{\text{thrust}}), \text{ where } \quad t_j(\hat{\underline{\eta}}) = \frac{|\underline{p}_j \cdot \hat{\underline{\eta}}|}{\sum_i |\underline{p}_i|}. \tag{3.1.3}$$

Note that the sums are defined over the spatial momenta of *all* particles in an event. The direction which maximizes the thrust observable is called the **thrust axis** - denoted $\hat{\underline{\eta}}_{\text{thrust}}$. A dijet event in the centre-of-momentum (COM) frame, characteristically features two back-to-back hard jets. The thrust, as presented in eq. (3.1.3), quantifies the degree of collimation exhibited by the event: in a highly collimated (pencil-like) dijet event, the thrust tends to $T \to 1$ – whereas, in a highly isotropic (ball-like) event, the thrust tends to $T \to 1/2$ (as discussed in [61]).

Explicitly, in eq. (3.1.1) when the kinematic variable of choice is thrust, that is $V = T$, the single hadron contribution is $v_j = t_j(\hat{\underline{\eta}}_{\text{thrust}})$. However, in evaluating power corrections to the distribution in eq. (3.1.1), it is more convenient to expand around the collimated hard jet limit $V = 1 - T$ [62] and kinematics of the thrust observable are typically enacted through integral

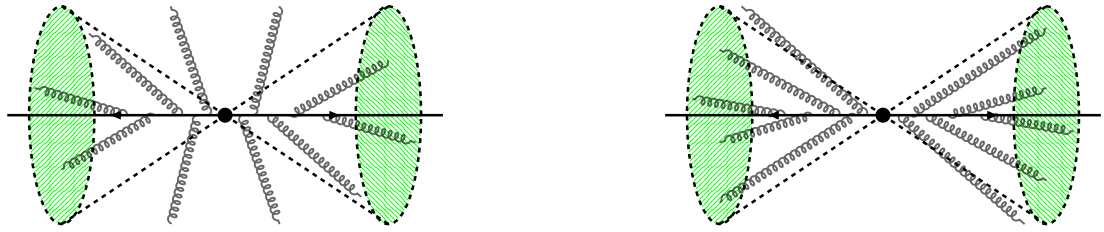

(a) (b)

Figure 3.1: *Figure depicting dijet events with different thrust values (T). Lower thrust events correspond to more final state particles in the interjet region in Figure 3.1a and vice versa in Figure 3.1b.*

transforms of the Heaviside function [63]. In general, soft singularities which arise from soft emission cascades and collinear singularities which arise from emissions from highly collimated events produce characteristic double logarithmic resummation structures in eq. (3.1.2) for inclusive observables (as discussed in [24]).

In Figure 3.1, dijet events with two different thrust values are depicted. Higher thrust events are more susceptible to collinear singularities as most of the emissions arise from the hard jet regions. In contrast, for lower thrust events emissions necessarily occur at large angles and thus emitted particles are not sensitive to collinear singularities. Therefore, in regions away from hard jets the structure of resummation is restricted to single logarithmic contributions arising from soft emissions. However, to study emissions in the interjet region (away from all hard jets) - one naturally invites consideration of observables of the **semi-inclusive** type, in which only a subset of events are accepted according to some selection criterion. Semi-inclusive observables, however, are not without pitfalls - as any semi-inclusive accounting of final state particles will demonstrate an incomplete cancellation of Sudakov logarithms generated through real emission and virtual correction processes (for a textbook exposition see [48, 64]). In general, coefficients in the QCD perturbation expansion can be parametrically large [65].

Consider the **interjet energy**,

$$E_{\text{out}} = \sum_{h \in \mathcal{C}_{\text{out}}} \omega_h, \tag{3.1.4}$$

which quantifies the total energy E_{out} of hadrons emitted in the region between two jets. Note that, ω_h is the energy of single final state particle. Figure 3.2, shows the geometry of back-to-back dijet event with a clearly labelled jet region $\mathcal{C}_{\text{in}}$ and away-from-jet region ($\mathcal{C}_{\text{out}}$). Note that choosing θ_{in} defines a pair of back-to-back cones that comprise the jet region $\mathcal{C}_{\text{in}}$ as shown in Figure 3.2. The complement $\mathcal{C}_{\text{out}}$, the interjet region, is then used to define E_{out} in eq. (3.1.4). This can then be used to impose an event selection criterion: only events with a total interjet energy less than the veto $E_{\text{out}} < E_{\text{veto}}$ are accepted and all others are rejected. Employing the interjet energy veto introduces a bias toward high thrust events as showcased in Figure 3.1. To elaborate, when

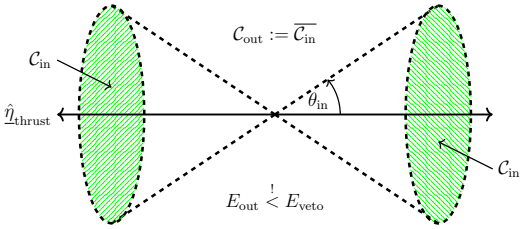

Figure 3.2: *Schematic of the associated geometry of E_{out} for a dijet event.*

$E_{\text{out}}/E \ll 1$ most of the hard scale energy is found in the jet region.

3.2 BMS Evolution of a Dijet Event

The first treatment of interjet energy loss was presented by Banfi, Marchesini, and Smye in [9]. This section gives an abbreviated account of their derivation of what is today known as the BMS equation. The result is a renormalization group equation for the associated cross section of particle production resulting from an e^+e^- annihilation process at leading logarithmic accuracy. In particular, eikonalized emissions considered in a strongly ordered setting (to be elaborated below) allow one to collect the leading logarithmic contributions. Moreover, to obtain a closed equation for a single quantity, the large N_c limit is imposed in a spirit very much reminiscent of the BK equation presented in [13–16].

To proceed, consider an electron and positron annihilating and creating a virtual timelike photon γ^* at a high centre-of-mass energy. The hard scale is set by the annihilation process, $\sqrt{s} =: Q$. From the decay of the virtual photon γ^*, a hard quark-antiquark pair and n accompanying soft gluons are produced. As with most QCD calculations, it is useful to view the lepton annihilation and parton production processes separately,

$$e^+e^- \to \gamma^* \to (q\bar{q})_{\text{hard}} g^n_{\text{soft}}. \tag{3.2.1}$$

At parton level, the amplitude in eq. (3.2.1) characterizes a dijet event wherein the thrust axis is defined by the trajectories of the hard quark-antiquark pair $(q\bar{q})_{\text{hard}}$ in the COM frame. Additionally, the cascade of soft final state particles observed in jet events, analogously, is described at parton level by the softly emitted gluons g^n_{soft}.

The produced partons in the $(q\bar{q})_{\text{hard}} g^n_{\text{soft}}$ amplitude are all assumed to possess lightlike trajectories. The momenta of the hard quark, hard antiquark, and soft gluons will be denoted by p, q, and k_i for $i \in \{1, 2, \ldots, n\}$. Lightlike momenta admit the following structure,

$$p^\mu = \omega_p \hat{p}^\mu, \tag{3.2.2}$$

where $\omega_p := p^0$ is the energy of the parton in the COM frame.

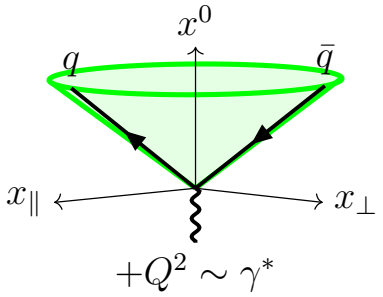

Figure 3.3: *[Colour online] Spacetime diagram demonstrating the lightlike trajectories of the hard quark-antiquark pair.*

Eikonalized soft emission is characterized by a parent particle which possesses energy ω_p that emits a particle with a much smaller energy ω_k such that their respective energies observe $\omega_k \ll \omega_p$. Given the manifest relation of energy scales during soft emission, the trajectories of parent particles remain unchanged. The leading logarithmic contributions emerge if, throughout the entirety of the soft emission chain, emission remain strongly ordered in energy:

$$\omega_n \ll \omega_{n-1} \ll \ldots \omega_1 \ll \omega_q \sim \omega_p. \tag{3.2.3}$$

To leading logarithmic accuracy, therefore, the cross section generated by the squared am-

plitude $(q\bar{q})_{\text{hard}} g^n_{\text{soft}}$, is given by the nested expression [9, 66, 67],

$$M_n^2\big(pk_1\dots k_nq\big) = M_0^2\big(pq\big)\cdot S_{pq}\big(k_1\dots k_n\big), \tag{3.2.4a}$$

$$S_{pq}\big(k_1\dots k_n\big) := \frac{1}{n!}\prod_i \frac{\bar{\alpha}_{\text{s}}}{\omega_i^2}\sum_{\pi_n} W_n\big(pk_{i_1}\dots k_{i_n}q\big), \quad \bar{\alpha}_{\text{s}} := \frac{\alpha_{\text{s}}N_c}{\pi} \tag{3.2.4b}$$

$$W_n\big(pk_1\dots k_nq\big) := \frac{(pq)}{(pk_1)\,(k_1k_2)\dots(k_nq)}, \quad \big(qq'\big) := \hat{q}.\hat{q}' =: 1-\cos\theta_{qq'} \tag{3.2.4c}$$

To unpack, the cross section is factorized into a hard part $M_0^2(pq)$ and a corresponding soft part $S_{pq}(k_1,\dots,k_n)$. The appearance of $\bar{\alpha}_s$ is typical of the large N_c limit. The definition of $S_{pq}\big(k_1\dots k_n\big)$ features a combinatorial factor $1/n!$, a product over the energies of the emitted particles, and a sum over the permutations of $W_n\big(pk_1\dots k_nq\big)$. The ingredients of the $W_n\big(pk_1\dots k_nq\big)$, like $\big(qq'\big)$ are defined in terms lightlike vectors $\hat{q}^\mu = q^\mu/\omega_q$ featured in eq. (3.2.2). Generically, the distribution in eq. (3.2.4a) features both soft ($\omega_i \to 0$) and collinear ($\theta_{qq'} \to 0$) singularities and is valid in any strongly energy-ordered region. No collinear approximations are involved in the derivation, so it is valid even at large angles as needed for the study [9] of the interjet energy variable showcased in eq. (3.1.4).

From eq. (3.1.1), the multiplicity distribution of the e^+e^- annihilation process may be computed for the interjet energy $V = E_{\text{out}}$ where, additionally, the total jet energy $E \sim Q$ approximates the hard scale and is treated as a kinematic variable,

$$\Sigma_{e^+e^-}\big(E, E_{\text{out}}\big) = \sum_n \int \frac{d\sigma^{(n)}(E)}{\sigma_{\text{total}}(E)}\cdot\Theta\Big(E_{\text{out}} - \sum_{h\in\mathcal{C}_{\text{out}}}\omega_h\Big). \tag{3.2.5}$$

In eq. (3.2.5), the kinematic constraints imposed by the interjet energy on the final states may be expressed in terms of a Mellin transform to simplify combinatorics,

$$\Theta\Big(E_{\text{out}} - \sum_{h\in\mathcal{C}_{\text{out}}}\omega_h\Big) = \int d\nu \frac{e^{\nu E_{\text{out}}}}{2\pi i\nu}\Big[\prod_i u(k_i)\Big]; \tag{3.2.6a}$$

$$u(k) = \Theta_{\text{in}}(k) + e^{-\nu\omega_k}\Theta_{\text{out}}(k) \tag{3.2.6b}$$

where the Heaviside functions $\Theta_{\text{out}}(k)$ and $\Theta_{\text{in}}(k)$ are defined such that their supports correspond to the interjet and jet regions $\mathcal{C}_{\text{out}}$ and $\mathcal{C}_{\text{in}}$ respectively. The geometry of the interjet region $\mathcal{C}_{\text{out}}$, that is, the θ_{in} dependence, is totally contained in the factor $u(k)$. Note that the coefficient of the $\Theta_{\text{out}}(k)$ is a decaying exponential which implements the veto demonstrated in fig. (3.1). Highly energetic particles are kinematically suppressed by the function $u(k)$. Nevertheless, the interjet energy distribution may be re-expressed as the Mellin transform of the quantity $G_{pq}\big(E,\nu^{-1}\big)$,

$$\Sigma_{e^+e^-}\big(E, E_{\text{out}}\big) = \int \frac{d\nu e^{\nu E_{\text{out}}}}{2\pi i\nu} G_{pq}\big(E,\nu^{-1}\big); \tag{3.2.7a}$$

$$G_{pq}(E,\nu^{-1}) := \sum_{n=1}^{\infty}\int \frac{d\sigma^{(n)}(E)}{\sigma_{\text{total}}(E)}\Big[\prod_i^n u(k_i)\Big]. \tag{3.2.7b}$$

Note that Mellin integration is implemented by steepest descent to give $\nu = E_{\text{out}}^{-1}$ [9].

Comparatively, the interjet energy is considered to be significantly smaller than the total jet energy $E_{\text{out}} \ll E \sim Q$. To leading logarithmic accuracy, for small interjet energy E_{out}, the purely real emission part of the interjet energy distribution $\Sigma_{e^+e^-}(E_{\text{out}})$ is obtained [9] by using,

$$\frac{d\sigma^{(n)}_{\text{real}}(E)}{\sigma_{\text{total}}(E)} = S_{pq}(k_1 \dots k_n) \cdot d\Phi_n; \tag{3.2.8a}$$

$$d\Phi_n = \prod_{i=1}^{n} d\omega_i \omega_i \frac{d^2\Omega_i}{4\pi} \Theta(E - \omega_i). \tag{3.2.8b}$$

The phase space measure employed is an on-shell momentum integral expressed in spherical coordinates. In particular, the surface measure is defined as $d^2\Omega_i := \sin\theta_i d\theta_i d\phi_i$. Moreover, a limit on the total energy on final state particles is imposed with $\Theta(E - \omega_i)$. Using both the eqs (3.2.8a) and (3.2.8b), the purely real part of interjet energy distribution in eq. (3.2.7b) is explicitly,

$$G^{(\text{real})}_{pq}\,(E, E_{\text{out}}\,) = 1 + \sum_{n=1}^{\infty} \int \prod_{i=1}^{n} \left\{ \bar{\alpha}_{\text{s}} \frac{d\omega_i}{\omega_i} \frac{d^2\Omega_i}{4\pi} u\,(k_i)\,\Theta\,(E - \omega_i) \right\} W_n\,(pk_1 \dots k_n q)\,. \tag{3.2.9}$$

A differential equation in E may be used to characterize changes to $G^{(\text{real})}_{pq}\,(E, E_{\text{out}}\,)$ in terms of the 1-loop contribution from the hardest soft gluon to the total jet energy. While it is not generically feasible to complement virtual contributions as a whole in accordance with eq. (3.2.9), by requiring appropriate cancellations in the differential equation, the structure of the virtual contributions may be inferred. Moreover, anticipating logarithmic enhancement in terms of the total jet energy, logarithmic derivatives $E\partial_E$ of the E-dependent parts of $G^{(\text{real})}_{pq}\,(E, E_{\text{out}}\,)$ is evaluated,

$$\begin{aligned} E\partial_E \Big\{ W(pk_1 \dots k_n q) \prod_{i=1}^{n} \Theta(E - \omega_i) \Big\} &= \sum_{\ell=1}^{n} E\delta\,(E - \omega_\ell)\, w_{pq}\,(k_\ell) \\ &\cdot \Big\{ W\,(pk_1 \dots k_\ell) \prod_{i=1}^{\ell-1} \Theta\,(E - \omega_i) \Big\} \cdot \Big\{ W\,(k_\ell \dots k_n q) \prod_{i=\ell+1}^{n} \Theta\,(E - \omega_i) \Big\}, \end{aligned} \tag{3.2.10}$$

which is seen to gives rise to the BMS kernel, $w_{pq}(k)$ has the structure of a dipole kernel,

$$w_{pq}(k) := \frac{(1 - \cos\theta_{pq})}{(1 - \cos\theta_{pk})(1 - \cos\theta_{kq})}. \tag{3.2.11}$$

All of which implies,

$$E\partial_E G_{pq}(E, E_{\text{out}}\,)\Big|_{(\text{real})} = \frac{\alpha_s N_c}{\pi} \int \frac{d^2\Omega_k}{4\pi} w_{pq}(k) u(k) G_{pk}(E, E_{\text{out}}\,) G_{kq}(E, E_{\text{out}}\,), \tag{3.2.12}$$

that the evolution of $G_{pq}(E, E_{\text{out}}\,)$ is non-linear (or quadratic) - and, much like the BK equation, reflects the fact that an additional gluon appears in the final state. The dipole kernel $w_{pq}(k)$ clearly diverges when k is aligned with either p or q (under manifestations of collinear

singularities, that is $\theta_{pk} \to 0$ et cetera). The collinear singularities of the dipole kernel must be cancelled by appropriate virtual corrections to the energy dependence of $G_{pq}(E, E_{\rm out}\,)$ as a whole. Moreover, since purely virtual contributions do not feature additional particles in the final state, their contribution must be linear and, furthermore, cannot be affected by the factor $u(k)$,

$$E\partial_E G_{pq}(E, E_{\rm out}\,)\Big|_{\rm (virtual)} = -\frac{\alpha_s N_c}{\pi}\int \frac{d^2\Omega_k}{4\pi} w_{pq}(k) G_{pq}(E, E_{\rm out}\,). \tag{3.2.13}$$

The logarithmic derivative structures above allow the inference of the evolution of a general interjet energy distribution $G_{pq}(E, E_{\rm out}\,)$ which is given by the BMS equation,

$$E\partial_E G_{pq}(E) = \frac{\alpha_s N_c}{\pi}\int \frac{d^2\Omega_k}{4\pi} w_{pq}(k)\Big\{u(k)G_{pk}(E)G_{kq}(E) - G_{pq}(E)\Big\}. \tag{3.2.14}$$

Naturally, the virtual contribution piece may be expanded $1 = u(k) + [1 - u(k)]$ so that like terms may then be collected into $u(k)$ and $[1 - u(k)]$ dependent pieces.

$$\begin{aligned} E\partial_E G_{pq}(E) =& \frac{\alpha_s N_c}{\pi}\int \frac{d^2\Omega_k}{4\pi} w_{pq}(k)u(k)\Big\{G_{pk}(E)G_{kq}(E) - G_{pq}(E)\Big\} \\ &- \frac{\alpha_s N_c}{\pi} E\partial_E \int_0^E \frac{d\omega}{\omega}\int \frac{d^2\Omega_k}{4\pi} w_{ab}(k)[1-u(k)]G_{pq}(E). \end{aligned} \tag{3.2.15}$$

Note that $1-u(k) = [1-e^{-\omega/E_{\rm out}}]\Theta_{\rm out}(k)$. Note that for small $E_{\rm out}$, $[1-e^{-\omega/E_{\rm out}}] \simeq \Theta(\omega - E_{\rm out})$. Uncancelled virtual contributions in the interjet region $\mathcal{C}_{\rm out}$ demonstrate the $E_{\rm out}$ dependence on the logarithmic enhancements through non-global logarithms,

$$\Delta := \int_0^E \frac{d\omega}{\omega}\Big[1 - e^{-\omega/E_{\rm out}}\Big] \simeq \int_{E_{\rm out}}^E \frac{d\omega}{\omega} = \ln\frac{E}{E_{\rm out}}. \tag{3.2.16}$$

For small $E_{\rm out}$, the approximation $[1-u(k)] \simeq \Theta(\omega - E_{\rm out})\Theta_{\rm out}(k)$ implies that $[u(k)] \simeq \Theta_{\rm in}(k)$. The BMS equation in terms of the non-global logarithms,

$$\begin{aligned} \frac{d}{d\ln(E/E_{\rm out})} G_{pq}(E) =& \frac{\alpha_s N_c}{\pi}\int_{\mathcal{C}_{\rm in}} \frac{d^2\Omega_k}{4\pi} w_{pq}(k)\Big\{G_{pk}(E)G_{kq}(E) - G_{pq}(E)\Big\} \\ &- \frac{\alpha_s N_c}{\pi}\int_{\mathcal{C}_{\rm out}} \frac{d^2\Omega_k}{4\pi} w_{pq}(k) G_{pq}(E). \end{aligned} \tag{3.2.17}$$

Solving the evolution equation provides recourse to resum single logarithmic contributions due to the interjet energy variable. All non-global logs are resummed in the jet region $\mathcal{C}_{\rm in}$ and $\mathcal{C}_{\rm out}$ separately.

3.3 Generalizing to finite N_c: The BMS-W Equation

The BMS equation, which describes the energy evolution of semi-inclusive jet measurements from dijet events, shares many characteristics the BK equation, which - in a seemingly unrelated application - describes the rapidity evolution of an eikonal interaction between a color dipole and the CGC. Compare the BK evolution of $S_{\boldsymbol{xy}}(x_{\rm bj})$ and the BMS evolution of $G_{pq}(E)$:

$$\frac{d}{d\ln(1/x_{\rm bj})}S_{\boldsymbol{xy}}(x_{\rm bj}) = \frac{\alpha_s N_c}{\pi}\int\frac{d^2\boldsymbol{z}}{2\pi}\tilde{\mathcal{K}}_{\boldsymbol{xzy}}\Big\{S_{\boldsymbol{xz}}(x_{\rm bj})S_{\boldsymbol{zy}}(x_{\rm bj}) - S_{\boldsymbol{xy}}(x_{\rm bj})\Big\}, \tag{2.3.17}$$

$$\begin{aligned}\frac{d}{d\ln(E/E_{\rm out})}G_{pq}(E) =& \frac{\alpha_s N_c}{\pi}\int_{\mathcal{C}_{\rm in}}\frac{d^2\Omega_k}{4\pi}w_{pq}(k)\Big\{G_{pk}(E)G_{kq}(E) - G_{pq}(E)\Big\}\\ &- \frac{\alpha_s N_c}{\pi}\int_{\mathcal{C}_{\rm out}}\frac{d^2\Omega_k}{4\pi}w_{pq}(k)G_{pq}(E).\end{aligned} \tag{3.2.17}$$

The structural similarities between the hard jet region $\mathcal{C}_{\rm in}$ evolution described by the BMS equation and the color dipole evolution described by the BK equation are readily apparent. For one, where the BMS equation provides recourse to resum non-global logarithms $\Delta := \ln E/E_{\rm out}$ in Jet evolution, the BK equation provides recourse to resum rapidity logarithms $Y \simeq \ln 1/x_{\rm bj}$ in CGC evolution. Furthermore, note that $\boldsymbol{x}$ and $\boldsymbol{y}$ (p and q) respectively denote the transverse position (momenta) of the hard quark and antiquark produced by the deeply spacelike (timelike) decay of the virtual photon $\gamma_* \to (q\bar{q})_{\rm hard}$ ($\gamma^* \to (q\bar{q})_{\rm hard}$). Moreover, note that $\boldsymbol{z}$ (k) denotes the transverse coordinate (momentum) of the emitted soft gluon used to track the 1-loop correction to $S_{\boldsymbol{xy}}(x_{\rm bj})$ ($G_{pq}(E)$). Additionally, the transverse coordinate (momentum direction) of the *hardest* soft gluon - which drives CGC (Jet) evolution - is integrated over by the transverse coordinate measure $\int d^2\boldsymbol{z}$ (surface measure $\int d^2\Omega_k = \int \sin\theta_k d\theta d\phi_k$). Lastly, both BK and BMS equations feature a dipole kernel, respectively denoted as $\tilde{\mathcal{K}}_{\boldsymbol{uzv}}$ and $w_{pq}(k)$.

The structural similarities of the BK and BMS equations, is not entirely surprising. The derivations of the BK and BMS equations share a host of technical similarities: both are derived in the large N_c limit, both employ eikonalized soft emission techniques in a strongly ordered setting [20], and both track 1-loop contributions through the *hardest* soft gluon.

The phenomenological implications of the structural similarities of Jet and CGC evolution equations, however, are wholly non-trivial due to the suggested equivalence in their respective theoretical descriptions. The proclivity toward hard jet events (with high thrust T) when studying interjet energy flow has already been discussed in fig. (3.1). However, hard jets do not, in general, demonstrate saturation type behaviour like the CGC as indicated by the structural similarities of the BK and BMS equations. To encounter any such indication is therefore wholly surprising - especially, if the observed jets are created through e^+e^- annihilation where the density is of little significance (as opposed to heavy ion collisions where density effects are significant). Although it is conceivable to expect saturation type physics to manifest in extremely collimated jets - most would relegate such highly focussed jet events to be rare enough to carry minimal experimental relevance [20].

Noting the theoretical causes of the myriad structural similarities between the BK and BMS equations and considering the phenomenological implications thereof - Weigert derived a finite N_c generalization of the BMS equation [10] which will appropriately be referred to as the

BMS-W[1] equation [53]. The step beyond the large N_c limit in both cases produces functional differential equations, both of them characterized by their respective 'Hamiltonians' [10],

$$H_{\text{JIMWLK}} := -\frac{\alpha_s}{\pi}\int\frac{d^2\boldsymbol{z}}{2\pi}\mathcal{K}_{\boldsymbol{uzv}}\Big[\tilde{U}^{ab}_{\boldsymbol{z}}\left(i\bar{\nabla}^a_{\boldsymbol{u}}i\nabla^b_{\boldsymbol{v}}+i\bar{\nabla}^a_{\boldsymbol{v}}i\nabla^b_{\boldsymbol{u}}\right) + \left(i\nabla^a_{\boldsymbol{u}}i\nabla^a_{\boldsymbol{v}}+i\bar{\nabla}^a_{\boldsymbol{u}}i\bar{\nabla}^a_{\boldsymbol{v}}\right)\Big] \tag{3.3.2a}$$

$$H_{\text{BMS-W}} := -\frac{\alpha_s}{\pi}\int\frac{d^2\Omega_k}{4\pi}w_{pq}(k)\Big[\tilde{\mathcal{V}}^{ab}_{k}\left(i\bar{\nabla}^a_{p}i\nabla^b_{q}+i\bar{\nabla}^a_{q}i\nabla^b_{p}\right)u(k) + \left(i\nabla^a_{p}i\nabla^a_{q}+i\bar{\nabla}^a_{p}i\bar{\nabla}^a_{q}\right)\Big] \tag{3.3.2b}$$

Note that the similarities of the large N_c equations map onto similarities of the Hamiltonians in eq. (3.3.2). In the JIMWLK framework, the $S_{\boldsymbol{xy}}(x_{\text{bj}})$ functions of the BK equation are replaced by Wilson line correlators which are transverse position dependent and characterize the eikonal interactions of a probing color dipole with the CGC,

$$S_{\boldsymbol{xy}}(x_{\text{bj}}) = \frac{\left\langle \text{tr}(U_{\boldsymbol{x}}U^\dagger_{\boldsymbol{y}})\right\rangle(x_{\text{bj}})}{N_c}. \tag{3.3.3}$$

Quite analogously, the $G_{pq}(E)$ functions of the BMS equation which model a hard quark-antiquark pair with lightlike momenta p and q, is described by a statistical average of product of half-infinite Wilson lines,

$$G_{pq}(E) \overset{!}{=} \frac{\left\langle \text{tr}(\mathcal{V}_p\mathcal{V}^\dagger_q)\right\rangle(E)}{N_c};\ \text{where}\ \mathcal{V}_p := (VV')_p. \tag{3.3.4}$$

It is understood in eq. (3.3.4) that the half-infinite Wilson lines V and V' arise from the amplitude and complex conjugate amplitude (respectively) in the cross section. Moreover, path ordering of the Wilson lines prevents a cancellation of the product $\mathcal{V}_p$. The Lie derivative $i\bar{\nabla}_p$ and ∇_p act on the product $\mathcal{V}_p$ - details are given in [10].

Acting on the BMS observable $G_{pq}(E)$, expressed as a Wilson line correlator in eq. (3.3.4), with the functional differential operator in eq. (3.3.2b) yields the correspondent BMS-W equation to the JIMWLK equation (which are both the first set of equations arising from the Balitsky hierarchy),

$$\begin{aligned}&\frac{d}{d\ln(1/x_{\text{bj}})}\frac{\left\langle \text{tr}(U_{\boldsymbol{x}}U^\dagger_{\boldsymbol{y}})\right\rangle(x_{\text{bj}})}{N_c}\\ &\quad=\frac{\alpha_s C_f}{\pi}\int\frac{d^2\boldsymbol{z}}{2\pi}\tilde{\mathcal{K}}_{\boldsymbol{xzy}}\left\{\frac{\left\langle \tilde{U}^{ab}_{\boldsymbol{z}}2\text{tr}(t^aU_{\boldsymbol{x}}t^bU^\dagger_{\boldsymbol{y}})\right\rangle(x_{\text{bj}})}{N_c^2-1}-\frac{\left\langle \text{tr}(U_{\boldsymbol{x}}U^\dagger_{\boldsymbol{y}})\right\rangle(x_{\text{bj}})}{N_c}\right\},\end{aligned} \tag{3.3.5a}$$

$$\begin{aligned}&\frac{d}{d\ln(E/E_{\text{out}})}\frac{\left\langle \text{tr}(\mathcal{V}_p\mathcal{V}^\dagger_q)\right\rangle(E)}{N_c}\\ &\quad=\frac{\alpha_s C_f}{\pi}\int\frac{d^2\Omega_k}{4\pi}w_{pq}(k)\left\{\frac{u(k)\left\langle \tilde{\mathcal{V}}^{ab}_{k}2\text{tr}(t^a\mathcal{V}_pt^b\mathcal{V}^\dagger_q)\right\rangle(E)}{N_c^2-1}-\frac{\left\langle \text{tr}(\mathcal{V}_p\mathcal{V}^\dagger_q)\right\rangle(E)}{N_c}\right\}.\end{aligned} \tag{3.3.5b}$$

where the final state gluons are suppressed by the factor $u(k)$. Virtual corrections are not suppressed. Although the CGC evolution equations involve observables in a coordinate space

[1] (Banfi–Marchesini–Smye)–(Weigert)

representation and the jet evolution equations involve observables in a momentum space representation - structurally, however, a correspondence between the dipole kernels and the respective measures of integration is apparent.

Chapter 4

Conformal Transformations

The structural similarities between Jet and CGC evolution are striking. Wilson lines and soft logarithms appear in both BMS-W and JIMWLK descriptions. The variable dependence of the Wilson lines at fixed energies is two dimensional in both cases: the transverse plane in one case and a sphere of directions in the other. This has triggered a number of earlier studies that attempt to formalize the connection, beginning with work by Hatta et al [11, 24] that relates the transverse plane with the sphere of directions using a two dimensional stereographic projection. Independently, Vladimirov [36, 37] has used a four dimensional conformal map, originally introduced by Hofman and Maldacena [26] in the context of a supersymmetric Yang-Mills theory, to simplify calculations of Drell-Yan and other QCD processes.

This chapter summarizes this history of insights which attempt to formalize the correspondence of Jet and CGC physics. The Hofman-Maldacena map can be applied to extend Hatta's work to furnish a full four dimensional relationship between Jet and CGC observables. This chapter accordingly provides a relationship of Wilson line geometry, dipole kernels and logarithm structure – which has been investigated through the re-parametrization of independently established mathematical objects encountered in both Jet and CGC evolution.

4.1 Toward a Formal Jet/CGC Correspondence with Conformal Transformations

The structural similarities between Jet and CGC evolutions equations has been discussed at length in Chapter 3. The most interesting result motivated by these similarities is arguably Weigert's generalization of the large N_c BMS equation to its finite N_c counterpart, the BMS-W equation. This setting informally relates the sphere of directions that appear in Jet evolution with the transverse plane in CGC evolution which suggests a relationship of dipole kernels and integral measures,

$$d^2\Omega_k w_{pq}(k) = d^2\Omega_k \frac{(1-\cos\theta_{pq})}{(1-\cos\theta_{pk})(1-\cos\theta_{kq})} \overset{?}{\leftrightarrow} d^2\boldsymbol{z}\frac{(\boldsymbol{x}-\boldsymbol{y})^2}{(\boldsymbol{x}-\boldsymbol{z})^2(\boldsymbol{z}-\boldsymbol{y})^2} = d^2\boldsymbol{z}\tilde{\mathcal{K}}_{\boldsymbol{xzy}}. \quad (4.1.1)$$

The suggested identification, of the transverse plane and sphere of directions was concretized by Hatta through the use of a stereographic projection [24]. Details of Hatta's work are sketched in section 4.2 and general constructions of stereographic projections have been included in the appendix (B.6). Hatta [24] explicitly established an equality between the product of measures and kernels featured in Jet and CGC evolution when related by a stereographic projection in Euclidean space,

$$\frac{d^2\Omega_k}{4\pi}w_{pq}(k)=\frac{d^2\Omega_k}{4\pi}\frac{(1-\cos\theta_{pq})}{(1-\cos\theta_{pk})(1-\cos\theta_{kq})}=\frac{d^2\boldsymbol{z}}{2\pi}\frac{(\boldsymbol{x}-\boldsymbol{y})^2}{(\boldsymbol{x}-\boldsymbol{z})^2(\boldsymbol{z}-\boldsymbol{y})^2}=\frac{d^2\boldsymbol{z}}{2\pi}\tilde{\mathcal{K}}_{\boldsymbol{xzy}}. \quad (4.1.2)$$

In a series of parallel developments, a surging interest in DIS and e^+e^--annihilation processes considered in $\mathcal{N}=4$ supersymmetric Yang–Mills (SYM) theory (based on the AdS/CFT duality [23]) which provided new perspectives on corresponding QCD problems. In particular, work presented by Hatta [24] builds upon a conformal map provided by Hofman and Maldacena [26]. Their map is presented below up to a change in front form convention[1],

$$\mathcal{C}: x^+\bar{n}^\mu+x_\perp^\mu+x^-n^\mu\mapsto-\frac{1}{2x^+}\Big(\bar{n}^\mu+\sqrt{2}x_\perp^\mu-x_\perp^2n^\mu\Big)+x^-n^\mu. \quad (4.1.3)$$

The lack of units/scale in eq. (4.1.3) is addressed in eq. (4.1.7). Applications of the map posited by Hofman and Maldacena (HM) have demonstrated success most notably by Caron-Huot in [27] where it was used to provide NLO contributions for JIMWLK evolution from known results on the Jet side. Explicit details on the nature of HM's map remained largely unexplored until Vladimirov [36, 37] highlighted a prescription for constructing HM's map in eq. (4.1.3). In particular: translations,

$$T_a^\mu(x):=x^\mu+a^\mu, \quad (4.1.4)$$

and special conformal transformations,

$$\Sigma^\mu_{a/\varrho^2}(x):=(I_\varrho\circ T_a\circ I_\varrho)^\mu(x)=\frac{x^\mu+x^2(a^\mu/\varrho^2)}{1+2x.(a/\varrho^2)+x^2(a/\varrho^2)^2}, \quad (4.1.5)$$

were used in Vladimirov's prescription. Note that in the definition of special conformal transformations, the explicit use of an inversion radius ϱ and a translation coordinate α (where $a^\mu=\alpha n^\mu$ or $a^\mu=\alpha\bar{n}^\mu$) are used to describe a combined characteristic scale $\zeta:=\varrho^2/2\alpha$. Therefore, where HM's map in eq. (4.1.3) makes no reference to the units involved in the conformal transformation - Vladimirov's prescription may be implemented to construct HM's map with manifest scale dependence (unit-tracking mechanisms) intact,

$$\mathcal{C}: T_{[+\bar{n}\zeta]}\circ\Sigma_{[-n(1/2\zeta)]}\circ T_{[+\bar{n}\zeta]}, \quad (4.1.6)$$

such that,

$$\mathcal{C}: x^+\bar{n}^\mu+x_\perp^\mu+x^-n^\mu\mapsto-\frac{\zeta^2}{x^+}\Big(\bar{n}^\mu+x_\perp^\mu/\zeta-\frac{x_\perp^2/\zeta^2}{2}n^\mu\Big)+x^-n^\mu. \quad (4.1.7)$$

[1] The original Hofman–Maldacena paper uses the Lepage–Brodksy lightcone convention, $x^\pm:=(x^0\pm x^3)$. Eq. (4.1.3) uses the Kogut–Soper lightcone convention, $x^\pm:=(x^0\pm x^3)/\sqrt{2}$.

Conformal maps are, in general, defined as maps that, up to a position dependent rescaling factor, preserve the inner product of the space at hand:

$$g_{\mu'\nu'}\frac{\partial y^{\mu'}(x)}{\partial x^{\mu}}\frac{\partial y^{\nu'}(x)}{\partial x^{\nu}} \stackrel{!}{=} \Omega^2(x) g_{\mu\nu}. \tag{1.1.2}$$

Conformal transformations form a group that contains Poincaré transformations ($\Omega \equiv 1$) as a subgroup. Since Poincaré symmetry is the largest that respects causality in Minkowski space, the consideration of (a less stringent) conformal symmetry immediately raises the question if a more general transformation can yield physically relevant insights. Eq. (4.1.7), for example, maps spacelike hypersurfaces onto lightlike ones, which immediately raises concerns about how causality relationships will be distorted by the procedure. Note, however that, gluon saturation effects in the CGC description arise through t-channel exchanges (and thus are spacelike) while the jet obervables are necessarily s-channel (and thus timelike). This immediately highlights that some degree of change in causality relations must occur.

The map in eq. (4.1.7), does not globally preserve time direction on Minkowski space. The situation improves if one restricts oneself to certain subsets of Minkowski space. With minimal adaption of the HM map in eq. (4.1.7) to the present purpose these coincide to the subsets playing a privileged role in JIMWLK and BMS-W equations. The first adaptation is achieved by exchanging the lightlike directions $n \leftrightarrow \bar{n}$ so that the x^- coordinate undergoes an inversion instead of x^+ as in eq. (4.1.3). The **lightsheet**,

$$\mathrm{T} := \left\{ x \in \mathbb{R}^{1,3} \middle| x.n \stackrel{!}{=} 0 \right\}, \tag{4.1.8}$$

contains the support of the Wilson lines of the JIMWLK equation. The HM map takes this onto the **lightcone**,

$$\mathrm{L} := \left\{ y \in \mathbb{R}^{1,3} \middle| y.y \stackrel{!}{=} 0 \right\}, \tag{4.1.9}$$

(see Figure 4.1a), but not in a continuous way. The discontinuity occurs at $x^- = 0$ where a factor $1/x^-$ implements an inversion in the adapted HM map. Note that this is precisely where the CGC background field has its support. One can stay entirely within one of the regular regions, by either shifting the support of the background field infinitesimally back in time or by extending the locus of inversion infinitesimally forward in time. From this discussion, it becomes obvious that the sequence,

$$\mathrm{c} : T_{[+n\zeta]} \circ \Sigma_{[-\bar{n}(1/2\zeta)]} \circ T_{[+n(\zeta-\lambda)]}, \tag{4.1.10}$$

continuously maps the past lightsheet,

$$\mathrm{T}_{\mathrm{past}} := \left\{ x \in \mathbb{R}^{1,3} \middle| x^+ = 0 \text{ and } x^- \leq \lambda \right\}, \tag{4.1.11}$$

onto the future lightcone,

$$\mathrm{L}_{\mathrm{future}} := \left\{ y \in \mathbb{R}^{1,3} \middle| y.y \stackrel{!}{=} 0 \text{ and } y^0 \geq 0 \right\}, \tag{4.1.12}$$

as shown in Figure 4.1b. In eq. (4.1.10), λ serves as regulator that infinitesimally shifts the inversion point forward. When relating these two subsets, time direction is preserved, i.e. an x^--ordered trajectory defined on the lightsheet, when restricted on the interval $(-\infty, \lambda)$, corresponds to a y^0-ordered trajectory on the future lightcone. This feature cannot be maintained if one attempts to extend the regions beyond the inversion point since c takes the complement $\mathrm{T}_{\mathrm{future}}$ to the complement $\mathrm{L}_{\mathrm{past}}$ again preserving time direction – see Figure 4.1c. This is the manifestation of the discontinuity mentioned above.

For future reference within this thesis, the sequence elaborated eq. (4.1.10) which defines the map c will be referred to as the **Hofman-Maldacena** (HM) map. The image of an arbitrary $x \in \mathbb{R}^{1,3}$ under the HM map presented in eq. (4.1.10),

$$\mathrm{c}^\mu(x) = \zeta \Omega_{\mathrm{c}} n_{\mathrm{c}}^\mu + x^+ \bar{n}_{\mathrm{c}}^\mu := \zeta\Big(\frac{\zeta}{\lambda - x^-}\Big)\Big(\frac{-x_\perp^2/\zeta^2}{2}\bar{n}^\mu + x_\perp^\mu/\zeta + n^\mu\Big) + x^+\Big(\bar{n}^\mu\Big), \tag{4.1.13}$$

where terms have bracketed which highlight the definition of quantities Ω_{c}, n_{c}, and $\bar{n}_{\mathrm{c}}$. In eq. (4.1.13), the coordinate dependence of the *conformal factor* $\Omega_{\mathrm{c}}(x) = \Omega_{\mathrm{c}}(x^-)$ and the lightcone element $n_{\mathrm{c}}(x) = n_{\mathrm{c}}(x_\perp)$ have been suppressed. Note that n_{c} and $\bar{n}_{\mathrm{c}}$ are both lightlike $n_{\mathrm{c}}^2 = \bar{n}_{\mathrm{c}}^2 = 0$ and mutually reciprocal $\bar{n}_{\mathrm{c}}.n_{\mathrm{c}} = 1$.

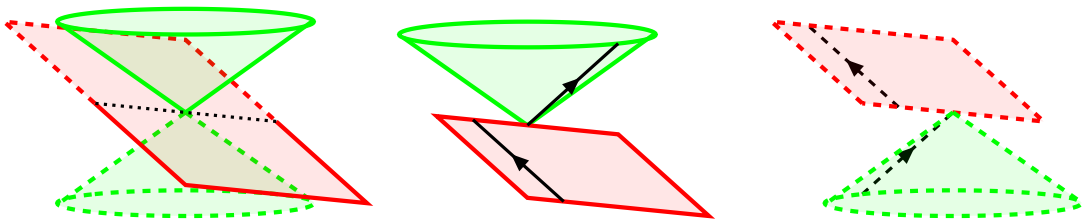

(a) **(b)** **(c)**

Figure 4.1: *[Colour online] Figure 4.1a: Graphical depiction of the relation between the (red) lightsheet and (green) lightcone geometries established by the HM map* $\mathrm{c} : \mathrm{T} \to \mathrm{L}$. *When restricted on* $\mathrm{T}_{\mathrm{past}}$ *(*$\mathrm{T}_{\mathrm{future}}$*), the transformation* c *maps on* $\mathrm{L}_{\mathrm{future}}$ *(*$\mathrm{L}_{\mathrm{past}}$*) in a manner that preserves time direction as showcased by Figure 4.1b (4.1c).*

The correspondence of Jet and CGC Wilson lines, which summarize soft emission processes in either case, must be restricted to half-infinite trajectories where the direction of time, and with it, notions of sequence of emissions and thus causality are faithfully mapped into each other. A full quantitative re-parametrization of CGC Wilson lines is discussed in section 4.4,

$$V_p^{(\mathrm{rep})} \overset{?}{\leftrightarrow} U_{\boldsymbol{x}}^{(\mathrm{rep})} = P \exp\Big[-ig\int_i^f dx^- n_\mu b^{\mu a}(x) t^a_{(\mathrm{rep})}\Big]. \tag{4.1.14}$$

Vladimirov's application uses similar features to relate ultraviolet singularities of Jet Wilson lines and rapidity singularities of parton scattering (Drell-Yan) Wilson lines [36, 37]. These applications require a more complicated combinations of HM maps that will not be explored here.

Therefore, conformal transformations in Minkowski space provide recourse to study a more general correspondence than the one posited by Hatta through a stereographic projection in

eq. (4.1.2). This will be the focus of section 4.5.

4.2 The Euclidean Correspondence of Kernels and Measures

In [24] the use of a stereographic projection was employed to relate transverse plane to the sphere of directions featured in CGC and Jet evolution, respectively. The stereographic projection, therefore, concretizes the identification prescription first posited by [10],

$$\frac{d^2\Omega_k}{4\pi}w_{pq}(k) = \frac{d^2\Omega_k}{4\pi}\frac{(1-\cos\theta_{pq})}{(1-\cos\theta_{pk})(1-\cos\theta_{kq})} = \frac{d^2\boldsymbol{z}}{2\pi}\frac{(\boldsymbol{x}-\boldsymbol{y})^2}{(\boldsymbol{x}-\boldsymbol{z})^2(\boldsymbol{z}-\boldsymbol{y})^2} = \frac{d^2\boldsymbol{z}}{2\pi}\tilde{\mathcal{K}}_{\boldsymbol{xzy}}. \quad (4.1.2)$$

The kernel and measure featured in the BMS equation (3.2.17), implicitly employs use of unit vectors $\hat{\underline{k}} := [\sin\theta_k\cos\phi_k, \sin\theta_k\sin\phi_k, \cos\theta_k]$ parametrized in terms of spherical coordinates. The surface measure is explicitly,

$$\frac{d^2\Omega_k}{4\pi} := \frac{1}{4\pi}\left|\frac{\partial\hat{\underline{k}}}{\partial\theta_k}\times\frac{\partial\hat{\underline{k}}}{\partial\phi_k}\right| d\theta_k d\phi_k = \sin\theta_k d\theta_k d\phi_k. \quad (4.2.1)$$

Similarly, the ingredients of the dipole kernel featured in the BMS kernel may be re-expressed in terms of the unit vectors, $1-\cos\theta_{pq} := 1-\hat{\underline{p}}\cdot\hat{\underline{q}}$ et cetera. The notation presented in [9] will be abandoned in favour of describing quantities through spatial unit vectors $\{\hat{\underline{p}},\hat{\underline{q}},\hat{\underline{k}}\}$ (which carry no scale).

The transverse coordinates featured in the BK equation (2.3.17), however, do carry scale. Any attempt in relating a transverse spatial coordinate to a unit vector must taking into account the effect of scales. Therefore, a construction of stereographic projections (which account for scales) has been detailed in the appendix (B.6). Using eqs (B.6.5), a scaleless spatial direction vector $\hat{\underline{k}}$ may be expressed in terms of transverse spatial coordinate $\boldsymbol{z}$,

$$\hat{\underline{k}}(\boldsymbol{z}) = \frac{2z^1/(r\mp h)}{1+\boldsymbol{z}^2/(r\mp h)^2}\underline{e}_1 + \frac{2z^2/(r\mp h)}{1+\boldsymbol{z}^2/(r\mp h)^2}\underline{e}_2 \mp \frac{1-\boldsymbol{z}^2/(r\mp h)^2}{1+\boldsymbol{z}^2/(r\mp h)^2}\underline{e}_3, \quad (4.2.2)$$

where explicitly $\hat{\underline{k}} = \underline{\sigma}_\pm(\underline{z})/r$ for $\underline{z} = [\boldsymbol{z}, h]^T$. Note that the north pole and south pole inverse stereographic projections are to be considered simultaneously. Both are, respectively, denoted by the plus and minus subscript in $\underline{\sigma}_\pm$. Moreover, the inverse stereographic projection maps points from a 2-plane at longitudinal height h onto a 2-sphere of radius h $\underline{\sigma}_\pm : \mathrm{P}^2(h) \to \mathrm{S}^2(r)$. Since stereographic projections are bijective when restricted to local neighbourhood of points, the overall effect of relating the transverse plane to the sphere of directions is equivalently described by the inverse.

Through the re-parametrization of the unit spatial vector $\hat{\underline{k}}(\boldsymbol{z})$ highlighted in eq. (4.2.2), the surface measure detailed in eq. (4.2.1) may be re-parametrized such that $\int d^2\Omega_k = \int d^2\hat{\underline{k}} = 4\pi$. In the new notation,

$$\frac{d^2\hat{\underline{k}}}{4\pi} = \frac{1}{4\pi}\left|\frac{\partial\hat{\underline{k}}}{\partial z^1}\times\frac{\partial\hat{\underline{k}}}{\partial z^2}\right| dz^1 dz^2 = \frac{d^2\boldsymbol{z}}{2\pi}\frac{1}{(r\mp h)^2}\frac{2}{\left(1+\boldsymbol{z}^2/(r\mp h)^2\right)^2}. \quad (4.2.3)$$

The surface measure $d^2\hat{\underline{k}}$ and the transverse measure $d^2\boldsymbol{z}$ - which, respectively, integrate over

all directions $\hat{\underline{k}}$ and transverse position of the hardest soft gluon in Jet and CGC evolution equation - are shown to be related in eq. (4.2.3). Note that all length scales associated with the $\boldsymbol{z}$ are appropriately cancelled by the scale term $(r \mp h)$ which is a relic of the stereographic projection employed in eq. (4.2.2).

In a similar fashion, therefore, the map $\underline{\sigma}_{\pm}/r$ - which is bijective on a local neighbourhood - may be used to relate quark, antiquark and gluon transverse coordinates in CGC evolution equations to directions in Jet evolution equations,

$$\frac{\underline{\sigma}_{\pm}}{r} : \{\boldsymbol{x}, \boldsymbol{y}, \boldsymbol{z}\} \mapsto \{\hat{\underline{p}}, \hat{\underline{q}}, \hat{\underline{k}}\}. \tag{4.2.4}$$

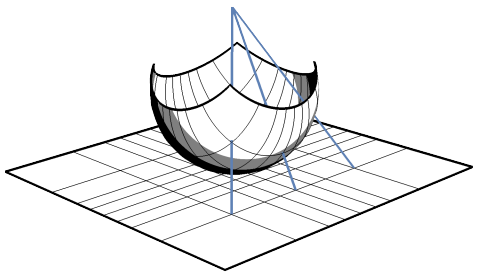

Figure 4.2: *Parametric mesh plot demonstrating an inverse north pole stereographic projection,* $\mathrm{P}^2(-1) \ni \underline{\rho} \mapsto \underline{\sigma}_{+}(\underline{\rho}) \in \mathrm{S}^2(+1)$ *for* $\boldsymbol{\rho} \in [-2, +2]^2$. *Projection lines from the north pole to three different transverse coordinates plotted.*

In Figure (4.2), a parametric mesh plot demonstrates the nature of inverse north pole stereographic projection; a patch on a transverse plane corresponds to a patch on the unit sphere. Moreover, the projection lines of three different transverse coordinates demonstrate, that unique transverse coordinates $\{\boldsymbol{x}, \boldsymbol{y}, \boldsymbol{z}\}$ map onto three unique directions $\{\hat{\underline{p}}, \hat{\underline{q}}, \hat{\underline{k}}\}$ in accordance with eq. (4.2.4).

The dipole kernel in the BMS equation $w_{pq}(k)$ is a rational fraction constructed entirely out of the Minkowski inner product of lightlike vectors $\hat{p}.\hat{q} = 1 - \hat{\underline{p}} \cdot \hat{\underline{q}}$. The spatial direction vectors may be re-expressed according to eq. (4.2.4). For example, the term with quark and antiquark coordinates are related by,

$$1 - \hat{\underline{p}} \cdot \hat{\underline{q}} = \frac{(\boldsymbol{x} - \boldsymbol{y})^2}{(r \mp h)^2} \frac{2}{\big(1 + \boldsymbol{x}^2/(r \mp h)^2\big)\big(1 + \boldsymbol{y}^2/(r \mp h)^2\big)}. \tag{4.2.5}$$

Re-expressing each scaleless direction $\{\hat{\underline{p}}, \hat{\underline{q}}, \hat{\underline{k}}\}$ in terms of transverse coordinates $\{\boldsymbol{x}, \boldsymbol{y}, \boldsymbol{z}\}$ reveals the equivalence of measures and dipole kernels featured in the Jet and CGC evolution equations respectively,

$$\frac{d^2\hat{\underline{k}}}{4\pi} \frac{(1 - \hat{\underline{p}} \cdot \hat{\underline{q}})}{(1 - \hat{\underline{p}} \cdot \hat{\underline{k}})(1 - \hat{\underline{k}} \cdot \hat{\underline{q}})} = \frac{d^2\boldsymbol{z}}{2\pi} \frac{(\boldsymbol{x} - \boldsymbol{y})^2}{(\boldsymbol{x} - \boldsymbol{z})^2(\boldsymbol{y} - \boldsymbol{z})^2}. \tag{4.2.6}$$

The Jet kernel and measure along with the CGC kernel and measure are overall scaleless and hence the equalities in eqs (4.1.2) and (4.2.6) are justified.

4.3 Features of the Hofman-Maldacena Map

This section details an analysis of the HM map used to relate the Wilson line geometries encountered in Jet and CGC evolution equations. To proceed, recall the HM map defined in accordance with the sequence in eq. (4.1.10),

$$\mathrm{c}^\mu(x) = \zeta\Omega_{\mathrm{c}} n_{\mathrm{c}}^\mu + x^+\bar{n}_{\mathrm{c}}^\mu := \zeta\Big(\frac{\zeta}{\lambda - x^-}\Big)\Big(\frac{-x_\perp^2/\zeta^2}{2}\bar{n}^\mu + x_\perp^\mu/\zeta + n^\mu\Big) + x^+\Big(\bar{n}^\mu\Big). \tag{4.1.13}$$

where terms have been bracketed in a way which highlights Ω_{c}, n_{c}, and $\bar{n}_{\mathrm{c}}$. In eq. (4.1.13), the coordinate dependence of the *conformal factor* $\Omega_{\mathrm{c}}(x) = \Omega_{\mathrm{c}}(x^-)$ and the lightcone element $n_{\mathrm{c}}(x) = n_{\mathrm{c}}(x_\perp)$ have been suppressed. Note that n_{c} and $\bar{n}_{\mathrm{c}}$ are both lightlike $n_{\mathrm{c}}^2 = \bar{n}_{\mathrm{c}}^2 = 0$ and mutually reciprocal $\bar{n}_{\mathrm{c}}.n_{\mathrm{c}} = 1$.

Eq. (4.1.13) will be analyzed in terms of three ingredients:

1. $\zeta\Omega_{\mathrm{c}}(x^-)$,
2. $n_{\mathrm{c}}(\boldsymbol{x})$,
3. $x^+\bar{n}_{\mathrm{c}}$.

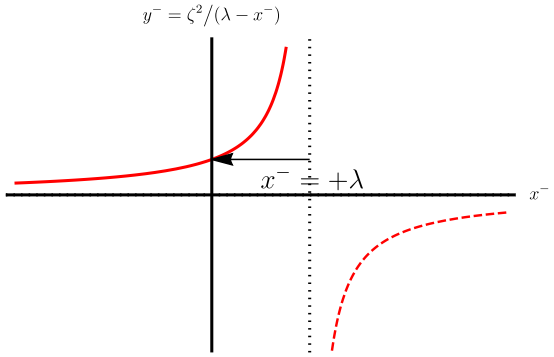

Figure 4.3: *[Colour online] Plot of conformal factor $y^- = \zeta\Omega_{\mathrm{c}}(x^-)$. Dotted black line denotes the singularity $x^- = +\lambda$. Dashed red line denotes strictly negative part of y^-. Solid red line denotes the strictly positive part of y^-.*

The first ingredient of $\mathrm{c}^\mu(x)$, in eq. (4.1.13), is the combination of the scale and the conformal factor $\zeta\Omega_{\mathrm{c}}(x^-) = \zeta^2/(\lambda - x^-)$. Setting $\mathrm{c}^\mu(x) = y^\mu$, the aforementioned combination is the lightcone coordinate of the image vector $\zeta\Omega_{\mathrm{c}} = y^-$. Analytically, therefore, y^- inherits the structure of a hyperbola through an inversion of the lightcone coordinate x^-. In Figure (4.3), a strictly positive part, and a strictly negative part are separated by the singularity of the inversion which sits at $x^- = +\lambda$. In Figure (4.3), it is assumed that $\zeta > 0$ and $\lambda > 0$. In anticipating a relation between the large background field (featured in CGC evolution) and the final state radiation (featured in Jet evolution), a one-sided limit $\lim_{\lambda\to 0^+}\lambda$ is taken to shift the singularity which sits at $x^- = +\lambda$ leftward in Figure (4.3) as annotated by the arrow. As a consequence, the location of the large background field $x^- = 0$ is mapped to $+\infty$, that is $\Omega_{\mathrm{c}}(x) \to +\infty$ as $\lambda \to 0^+$.

The second ingredient of $\mathrm{c}^\mu(x)$, is the scaleless lightlike vector n_{c} which is expressed in terms of the front form basis vectors

$$n_{\mathrm{c}}^\mu = \frac{\boldsymbol{x}^2/\zeta^2}{2}\bar{n}^\mu + (x^1/\zeta)e_1^\mu + (x^2/\zeta)e_2^\mu + n^\mu, \tag{4.3.1}$$

in eq. (4.1.13). The vector n_{c} may be expressed in terms of instant form coordinates. The resultant temporal coordinate may be factored out so that $n_{\mathrm{c}}^\mu = n_{\mathrm{c}}^0\hat{n}_{\mathrm{c}}^\mu$ and the scale $\zeta' = \sqrt{2}\zeta$ to yield,

$$n_{\mathrm{c}}^0 := \frac{1 + \boldsymbol{x}^2/\zeta'^2}{\sqrt{2}},\ \hat{n}_{\mathrm{c}}^\mu := \Big[1e_0^\mu + \frac{2x^1/\zeta'}{1 + \boldsymbol{x}^2/\zeta'^2}e_1^\mu + \frac{2x^2/\zeta'}{1 + \boldsymbol{x}^2/\zeta'^2}e_2^\mu - \frac{1 - \boldsymbol{x}^2/\zeta'^2}{1 + \boldsymbol{x}^2/\zeta'^2}e_3^\mu\Big]. \tag{4.3.2}$$

Above in eq. (4.3.2), the temporal coordinate has a transverse coordinate dependence $n_{\mathrm{c}}^{0}(\boldsymbol{x})$, as a parabola in $|\boldsymbol{x}|/\zeta'$ with an intercept at $1/\sqrt{2}$. The spatial part,

$$\underline{\hat{n}}_{\mathrm{c}} = +\frac{2x^1/\zeta'}{1+\boldsymbol{x}^2/\zeta'^2}\underline{e}_1 + \frac{2x^2/\zeta'}{1+\boldsymbol{x}^2/\zeta'^2}\underline{e}_2 - \frac{1-\boldsymbol{x}^2/\zeta'^2}{1+\boldsymbol{x}^2/\zeta'^2}\underline{e}_3, \tag{4.3.3}$$

is nothing but an inverse north pole stereographic projection $\underline{\sigma}_{+} : \mathrm{P}^2(1-\zeta') \to \mathrm{S}^2(1)$. A brief comparison with eq. (4.2.2) reveals that the map is specifically from a 2-plane at height $h = 1-\zeta'$ onto a 2-sphere with radius $r = +1$; therefore $(r-h) = \zeta'$.

The third and final ingredient, in eq. (4.1.13), is a translation of the lightcone element $\zeta\Omega_{\mathrm{c}}n_{\mathrm{c}}$ by the coordinate x^+ in the direction $\bar{n}_{\mathrm{c}}^{\mu} = \bar{n}^{\mu}$. When the domain is restricted to Minkowski space vectors such that $x^+ = 0$, the image lies on the lightcone $\mathrm{c}^{\mu}(x)|_{x^+=0} = \zeta\Omega_{\mathrm{c}}n_{\mathrm{c}} \in \mathrm{L}$. Collecting the three aforementioned ingredients of the action of $\mathrm{c}^{\mu}(x) = \zeta\Omega_{\mathrm{c}}n_{\mathrm{c}}^{\mu} + x^+\bar{n}_{\mathrm{c}}^{\mu}$ and evaluating for $x^+ = 0$,

$$\begin{aligned}\frac{\zeta'}{\sqrt{2}}\Omega_{\mathrm{c}}(x^-)n_{\mathrm{c}}^{\mu}(\boldsymbol{x}) =& \frac{\zeta'^2/2}{\lambda - x^-}\frac{1+\boldsymbol{x}^2/\zeta'^2}{\sqrt{2}} \\ &\times \left[1e_0^{\mu} + \frac{2x^1/\zeta'}{1+\boldsymbol{x}^2/\zeta'^2}e_1^{\mu} + \frac{2x^2/\zeta'}{1+\boldsymbol{x}^2/\zeta'^2}e_2^{\mu} - \frac{1-\boldsymbol{x}^2/\zeta'^2}{1+\boldsymbol{x}^2/\zeta'^2}e_3^{\mu}\right],\end{aligned} \tag{4.3.4}$$

which explicitly highlights $\mathrm{c} : \mathrm{T} \to \mathrm{L}$ since $n_{\mathrm{c}} \in \mathrm{L}$. Moreover, the expression in instant form coordinates in eq. (4.3.4) in comparison to eq. (4.2.2) immediately allows the identification of an inverse north pole stereographic projection (like the one employed by Hatta in [24]). Note that the temporal coordinate $n_{\mathrm{c}}^{0}(\boldsymbol{x})$ is positive for all $\boldsymbol{x} \in \mathbb{R}^2$. The conformal factor, however, is positive only for $x^- \in (-\infty, \lambda)$ and negative otherwise as showcased in Figure 4.3. Therefore, eq. (4.3.4) explicitly highlights $\mathrm{c} : \mathrm{T}_{\mathrm{past}} \to \mathrm{L}_{\mathrm{future}}$ and $\mathrm{c} : \mathrm{T}_{\mathrm{future}} \to \mathrm{L}_{\mathrm{past}}$.

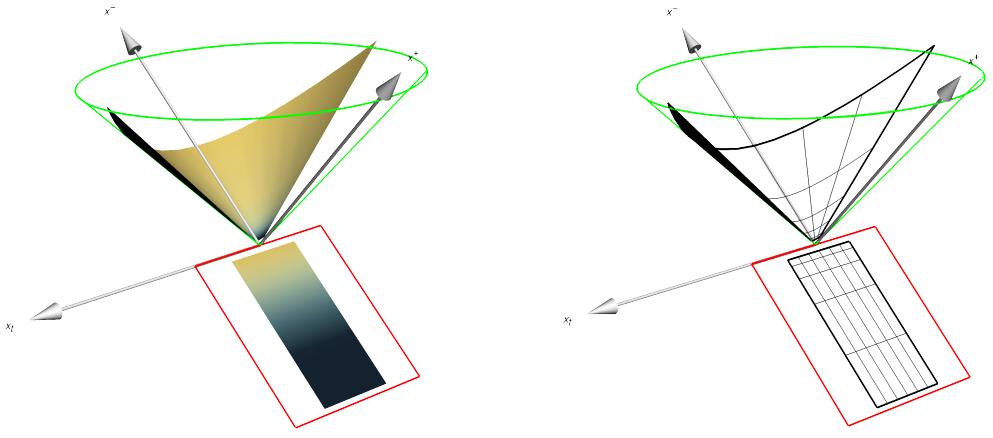

(a) **(b)**

Figure 4.4: *[Colour online] Parametric plots of eq. (4.3.4) detailing the map* $\mathrm{c} : \mathrm{T}_{\mathrm{past}} \mapsto \mathrm{L}_{\mathrm{future}}$. *Bounds of the parametric plots are* $x_{\perp} \times x^- \in [-2,+2] \times [-3,-0.18]$. *Figure 4.4a is a colour plot where* x^-*-dependence is color coded (darker colours correspond to smaller* x^- *values and vice versa). Figure 4.4b is mesh plot where lines of constant* $x_{\perp}$ *and* x^- *are shown.*

The colour plot in Figure (4.4a) demonstrates how the transformation c maps the past

lightsheet onto the future lightcone in a manner that preserves path-ordering. Note that darker colours correspond to smaller values of x^- and vice versa. an x^--ordered trajectory defined on the interval $(-\infty, \lambda)$ corresponds to a y^0-ordered trajectory for $\mathrm{c}(x) = y$.

The mesh plot in Figure (4.4b) shows lines of constant $x_\perp$ and x^-. Lines of constant $x_\perp$ on the lightsheet are to be considered as trajectories of CGC Wilson lines. Lines of constant $x_\perp$ on the lightcone are to be considered as trajectories of Jet Wilson lines since the direction of Jet Wilson lines depends only on the transverse coordinates $\hat{n}_\mathrm{c}(x_\perp)$. Lines of constant x^- on the tangent plane are straight lines. Lines of constant x^- on the lightcone are paraboloids since the temporal coordinate $n^0_\mathrm{c}(x_\perp)$ depends on the transverse coordinates.

4.4 Re-parametrization of CGC Wilson Lines

The correspondence of soft factors V_p and $U_{\boldsymbol{x}}$, respectively, featured in Jet and CGC evolution may be investigated,

$$V_p^{(\text{rep})} \overset{?}{\leftrightarrow} U_{\boldsymbol{x}}^{(\text{rep})} = P\exp\Big[-ig\int_i^f dx^- n_\mu b^{\mu a}(x) t^a_{(\text{rep})}\Big], \tag{4.1.14}$$

through the re-parametrization of CGC Wilson lines - which are defined as path-ordered exponentials of the CGC background field. When expanded in terms of constituent pieces, the Wilson line is expressed[2] as,

$$U_{x;f,i} = P\exp\left[-ig\int_i^f dx^- n^\mu g_{\mu\nu}\bar{n}^\nu \delta\big(x^-\big)\beta^a(\boldsymbol{x}) t^a_{(\text{rep.})}\right]. \tag{4.4.1}$$

The trajectory of the CGC Wilson line $\gamma^\mu(x) = x^- n^\mu + x^\mu_\perp + 0\bar{n}^\mu$ manifestly lies on the x^+ tangent of the lightcone, that is $\gamma(x) \in \mathrm{T}$. Re-parametrization of the lightsheet geometry T will employ the construction of the inverse transformation $\mathrm{d} := \mathrm{c}^{-1}$. By using $T_a^{-1} = T_{-a}$ and $\Sigma^{-1}_{a/\varrho^2} = \Sigma_{-a/\varrho^2}$, and reversing the sequence employed in eq. (4.1.10) - the inverse $\mathrm{d} := \mathrm{c}^{-1}$ is constructed,

$$\mathrm{d} := \mathrm{c}^{-1} = T_{[-n(\zeta-\lambda)]} \circ \Sigma_{[+\bar{n}(1/2\zeta)]} \circ T_{[-n\zeta]}. \tag{4.4.2}$$

Once again, the action of the map d defined in eq. (4.4.2) may be evaluated on an arbitrary $y \in \mathbb{R}^{1,3}$ such that the re-parametrization of coordinates $(x^+, x_\perp, x^-)$ takes the form,

$$\mathrm{d}^\mu(y) = y^2\bar{n}^\mu + \frac{\zeta y^\mu_\perp}{y^-} + \big(\lambda - \frac{\zeta^2}{y^-}\big)n^\mu \overset{!}{=} x^+\bar{n} + x^\mu_\perp + x^- n^\mu, \tag{4.4.3}$$

where the associated conformal factor is $\Omega_{\mathrm{d}}(y) = \Omega_{\mathrm{d}}(y^-) := \zeta/y^-$. Note that $y^2 = 0$ in eq. (4.4.3) corresponds to $x^+ = 0$ and therefore $\mathrm{d} : \mathrm{L} \to \mathrm{T}$. All coordinates in the Wilson line will be re-parametrized according to the finite transformation, eq. (4.4.3). Re-parametrization of the integral measure, Dirac delta, and the color function manifest as,

$$\int_i^f dx^- = \int_{\zeta^2/(\lambda-i)}^{\zeta^2/(\lambda-f)} dy^- \Omega_{\mathrm{d}}(y)^2 \tag{4.4.4a}$$

$$\delta\big(x^-\big) = \frac{\delta\big(y^- - \zeta^2/\lambda\big)}{\Omega^2_{\mathrm{d}}(y)} \tag{4.4.4b}$$

$$\beta^a\big(\boldsymbol{x}\big) = \beta^a\big(\boldsymbol{y}\Omega_{\mathrm{d}}(y)\big) \tag{4.4.4c}$$

Note that while the argument of any quantity in eq. (4.4.1) is subjected to a finite conformal transformation, the differential of the trajectory $\frac{d}{dx^-}\gamma^\mu(x) = n^\mu$ and the background field $b^\mu(x)$ are defined on the tangent space of $\mathbb{R}^{1,3}$. Re-parametrization of tangent space elements is,

[2] Notice that the transverse position dependence $\boldsymbol{x}$ of CGC Wilson lines in eq. (2.1.15) is, in this section, implied by the subscript x

accordingly, enacted through the differential,

$$\frac{\partial \mathrm{d}^\mu}{\partial y^\nu} = \Omega_{\mathrm{d}}(y)\Lambda_{\mathrm{d}}{}^{\mu}{}_{\nu}(y), \tag{4.4.5}$$

which factorizes into a conformal factor $\Omega_{\mathrm{d}}(y)$ and a Lorentz transformation $\Lambda_{\mathrm{d}}{}^{\mu}{}_{\nu}(y)$,

$$\Omega_{\mathrm{d}}(y) = \frac{\zeta}{y^-}, \quad \Lambda_{\mathrm{d}}(y) = \begin{pmatrix} \Omega_{\mathrm{d}}^{-1}1 & -y^1/\zeta & -y^2/\zeta & \Omega_{\mathrm{d}}^{+1}(\boldsymbol{y}^2/\zeta^2)/2 \\ 0 & 1 & 0 & \Omega_{\mathrm{d}}^{+1}y^1/\zeta \\ 0 & 0 & 1 & \Omega_{\mathrm{d}}^{+1}y^2/\zeta \\ 0 & 0 & 0 & \Omega_{\mathrm{d}}^{+1}1 \end{pmatrix}. \tag{4.4.6}$$

Note that in front form coordinates the Lorentz matrix, $(\Lambda_{\mathrm{d}}{}^{\circ}{}_{\circ}(x))$, has an upper triangular structure and, therefore it may be verified that $\det(\Lambda_{\mathrm{d}}) = 1$ by multiplying the diagonal entries. Transformation of the front form basis vectors $\{\bar{n}, e_1, e_2, n\}$ of tangent space by the differential yields,

$$\frac{\partial \mathrm{d}^\mu}{\partial y^\nu}\bar{n}^\nu = \bar{n}^\mu_{\mathrm{d}}, \quad \frac{\partial \mathrm{d}^\mu}{\partial y^\nu}e_1^\nu = \Omega_{\mathrm{d}}(y)e^\mu_{\mathrm{d}1}, \quad \frac{\partial \mathrm{d}^\mu}{\partial y^\nu}e_2^\nu = \Omega_{\mathrm{d}}(y)e^\mu_{\mathrm{d}2}, \quad \frac{\partial \mathrm{d}^\mu}{\partial y^\nu}n^\nu = \Omega^2_{\mathrm{d}}(y)n^\mu_{\mathrm{d}}, \tag{4.4.7}$$

or equivalently,

$$\bar{n}_{\mathrm{d}} := \begin{pmatrix} 1 \\ 0 \\ 0 \\ 0 \end{pmatrix}, e_{\mathrm{d}1} := \begin{pmatrix} -y^1/\zeta \\ 1 \\ 0 \\ 0 \end{pmatrix}, e_{\mathrm{d}2} := \begin{pmatrix} -y^2/\zeta \\ 0 \\ 1 \\ 0 \end{pmatrix}, n_{\mathrm{d}} := \begin{pmatrix} (\boldsymbol{y}^2/\zeta^2)/2 \\ -y^1/\zeta \\ -y^2/\zeta \\ 1 \end{pmatrix}. \tag{4.4.8}$$

$\bar{n}_{\mathrm{d}}$ and n_{d} are mutually reciprocal $\bar{n}_{\mathrm{d}}.n_{\mathrm{d}} = 1$ and lightlike. The equations in eq. (4.4.7) may be inverted to yield a re-parametrization of the tangent space basis vectors,

$$\bar{n}^\nu = \frac{1}{\Omega_{\mathrm{d}}(y)}\Lambda_{\mathrm{d}}^{-1}{}^{\nu}{}_{\mu}(y)\bar{n}^\mu_{\mathrm{d}}, \quad e_i^\nu = \Lambda_{\mathrm{d}}^{-1}{}^{\nu}{}_{\mu}(y)e^\mu_{\mathrm{d}i}, \quad n^\nu = \frac{\Omega_{\mathrm{d}}(x)}{1}\Lambda_{\mathrm{d}}^{-1}{}^{\nu}{}_{\mu}(y)n^\mu_{\mathrm{d}}, \tag{4.4.9}$$

The Lorentz invariant product of the tangent of the trajectory $n^\mu = \partial_+\gamma(x)$ and the Lorentz enhanced part of the CGC background field $\bar{n}^\mu$ may be re-parametrized in terms of n^μ_{d} and $\bar{n}^\mu_{\mathrm{d}}$ in accordance with eq. (4.4.9),

$$n^\mu g_{\mu\nu}\bar{n}^\nu = \Big(n_{\mathrm{d}}\big(\Lambda_{\mathrm{d}}^{-1}(x)\big)^T\Omega_{\mathrm{d}}^{+1}(x)\Big)^\mu g_{\mu\nu}\Big(\Omega_{\mathrm{d}}^{-1}(x)\Lambda_{\mathrm{d}}^{-1}(x)\bar{n}_{\mathrm{d}}\Big)^\nu = n^\mu_{\mathrm{d}}g_{\mu\nu}\bar{n}^\nu_{\mathrm{d}} \tag{4.4.10}$$

Using eqs (4.4.4) and (4.4.10) CGC Wilson line $U_{x;f,i}$ may be entirely re-parametrized,

$$U_{\mathrm{d}(y);f,i} = P\exp\left[-ig\int_{\zeta^2/(\lambda-i)}^{\zeta^2/(\lambda-f)} dy^- n_{\mathrm{d}}.\bar{n}_{\mathrm{d}}\delta\big(y^- - \zeta^2/\lambda\big)\beta\big(\zeta\boldsymbol{y}/y^-\big)\right] \tag{4.4.11}$$

For $y \in \mathrm{L}$ which implies that $y^2 = 0$, the vector admits a factorization of the temporal coordinate $y^\mu = y^0\hat{y}^\mu$.

$$y^\pm = \frac{y^0(1 \pm \hat{y}^3)}{\sqrt{2}}, \quad \boldsymbol{y} = y^0\hat{\boldsymbol{y}} \tag{4.4.12}$$

The Wilson line may be re-parametrized in terms of y^0,

$$U_{\mathrm{d}(y);f,i} = P\exp\Bigg[-ig\int_{\sqrt{2}\zeta^2/(\lambda-i)(1-\hat{y}^3)}^{\sqrt{2}\zeta^2/(\lambda-f)(1-\hat{y}^3)} dy^0 n_{\mathrm{d}}.\bar{n}_{\mathrm{d}} \times \delta\Big(y^0 - \frac{\sqrt{2}\zeta^2}{\lambda(1-\hat{y}^3)}\Big)\beta\Big(\frac{\zeta\hat{\boldsymbol{y}}}{(1-\hat{y}^3)}\Big)\Bigg] \tag{4.4.13}$$

which ultimately allows a correspondence to be drawn between CGC Wilson lines U_x and Jet Wilson lines V_p. Moving from right to left, in eq. (4.4.13): the transverse coordinate dependence of the color function is expressed as a stereographic projection,

$$\beta(\boldsymbol{x}) \leftrightarrow \beta\Big(\frac{\zeta\hat{\boldsymbol{y}}}{(1-\hat{y}^3)}\Big), \tag{4.4.14a}$$

the trigger denoting interaction with the CGC is transformed into a trigger on a surface which under the limit $\lambda \to 0^+$ corresponds to the asymptotic future lightcone,

$$\delta(x^-) \leftrightarrow \delta\Big(y^0 - \frac{\sqrt{2}\zeta^2}{\lambda(1-\hat{y}^3)}\Big), \tag{4.4.14b}$$

the Lorentz part of the background field in CGC corresponds to Lorentz part of the gauge field in Jet formalism (moreover, $\bar{n}_{\mathrm{d}} = \bar{n}$),

$$b^{\mu a}(x) \sim \bar{n} \leftrightarrow \bar{n}_{\mathrm{d}} = \bar{n}, \tag{4.4.14c}$$

the lightlike trajectory n transforms into lightlike trajectory n_{d},

$$\frac{d}{dx^-}\gamma(x) = n \leftrightarrow n_{\mathrm{d}}, \tag{4.4.14d}$$

and the integrands correspond with bounds $\{i, f\} \leftrightarrow \{\sqrt{2}\zeta^2/(\lambda-i)(1-\hat{y}^3), \sqrt{2}\zeta^2/(\lambda-f)(1-\hat{y}^3)\}$ for the measures dx^- and dy^0 respectively,

$$\int_i^f dx^- \leftrightarrow \int_{\sqrt{2}\zeta^2/(\lambda-i)(1-\hat{y}^3)}^{\sqrt{2}\zeta^2/(\lambda-f)(1-\hat{y}^3)} dy^0. \tag{4.4.14e}$$

Explicitly, a half-infinite Wilson line on the past lightsheet $\mathrm{T}_{\mathrm{past}}$ may be re-parametrized by a half-infinite Wilson line on the future lightcone $\mathrm{L}_{\mathrm{future}}$ by the transformation $\mathrm{d}(y) = x$,

$$\begin{aligned} U_{x;\lambda,-\infty} &= \lim_{f\to\lambda}\lim_{i\to-\infty} U_{\mathrm{d}(y);f,i} \\ &= P\exp\Bigg[-ig\int_0^{+\infty} dy^0 n_{\mathrm{d}}.\bar{n}_{\mathrm{d}}\delta\Big(y^0 - \frac{\sqrt{2}\zeta^2}{\lambda(1-\hat{y}^3)}\Big)\beta\Big(\frac{\zeta\hat{\boldsymbol{y}}}{(1-\hat{y}^3)}\Big)\Bigg]. \end{aligned} \tag{4.4.15}$$

4.5 Re-parametrization of Jet Phase Space

The explicit use of the scale ($r \mp h$, as an artefact of the map $\underline{\sigma}_{\pm}$) was used to relate scale carrying transverse positions $\{\boldsymbol{x}, \boldsymbol{y}, \boldsymbol{z}\}$ to scaleless directions $\{\underline{\hat{p}}, \underline{\hat{q}}, \underline{\hat{k}}\}$. The product of kernels and measures were scale invariant. Ultimately, the use of stereographic projection demonstrated a Euclidean correspondence of geometries. Similarly, Hatta's work provides a blueprint to investigate a Minkowskian correspondence through the HM map in eq. (4.1.13). More specifically, four-vectors denoting the momenta (positions) of quark, antiquark, and the hardest soft gluon featured in Jet (CGC) evolution equations - that is $\{p, q, k\}$ ($\{x, y, z\}$) will explicitly be related by the HM map in accordance with eq. (4.2.4),

$$\mathrm{c} : \{x, y, z\} \mapsto \{p, q, k\}. \tag{4.5.1}$$

The HM map strictly is a map either from space-time to space-time, or from energy-momentum space to energy-momentum space - since positions and momenta carry entirely different units. The HM map, however, allows one to re-parametrize logarithms (which are also scale invariant).

The relation in eq. (4.5.1) may be used to explicitly re-parametrize elements of the phase space in the BMS equation formulation - namely: the surface measure $d^2\underline{\hat{k}}$, the dipole kernel $w_{pq}(k)$, and the non-global logarithms $\ln E/E_{\text{out}}$- may be expressed in terms of the four-momenta $\{p, q, k\}$,

$$\ln \frac{E}{E_{\text{out}}} \int \frac{d^2\underline{\hat{k}}}{4\pi} \frac{(1 - \underline{\hat{p}} \cdot \underline{\hat{q}})}{(1 - \underline{\hat{p}} \cdot \underline{\hat{k}})(1 - \underline{\hat{k}} \cdot \underline{\hat{q}})} = \int \frac{d^4k}{2\pi} \delta(k^2) \tilde{W}_{pq}(k) \Theta(E \geq \omega_k \geq E_{\text{out}}), \tag{4.5.2}$$

where the on-shell four-momentum measure,

$$\begin{aligned} \int \frac{d^4k}{2\pi} \delta(k^2) \Theta(E > \omega_k > E_{\text{out}}) &= \int d\omega_k d|\underline{k}||\underline{k}|^2 \frac{d^2\underline{\hat{k}}}{2\pi} \frac{\delta(\omega_k - |\underline{k}|)}{2|\underline{k}|} \Theta(E \geq \omega_k \geq E_{\text{out}}) \\ &= \int d\omega_k \omega_k \frac{d^2\underline{\hat{k}}}{4\pi} \Theta(E \geq \omega_k \geq E_{\text{out}}), \end{aligned} \tag{4.5.3}$$

gives rise to the normalized surface measure $d^2\underline{\hat{k}}/4\pi$ and when integrated with the quantity $\tilde{W}_{pq}(k)$ will give rise to the non-global logarithms $\Delta := \ln E/E_{\text{out}} = \int_{E_{\text{out}}}^{E} d\omega_k/\omega_k$. The quantity $\tilde{W}_{pq}(k)$ possesses a structure of a dipole kernel expressed in terms of four-momenta p, q, k. Note that when the momenta are restricted onto the lightcone $p, q, k \in \mathrm{L}$ - the squared distance between two momenta $(p-q)^2$ simplifies to $(p-q)^2 = -2p.q = -\omega_p\omega_q\hat{p}.\hat{q}$. The quantity $\tilde{W}_{pq}(k)$, therefore, may be interpreted as the four-dimensional invariant squares or *covariantized* version of the Jet dipole kernel $w_{pq}(k)$,

$$\tilde{W}_{pq}(k) := -\frac{2(p-q)^2}{(p-k)^2(q-k)^2} \xrightarrow{p,q,k \in \mathrm{L}} \frac{1}{\omega_k^2} \frac{(1 - \underline{\hat{p}} \cdot \underline{\hat{q}})}{(1 - \underline{\hat{p}} \cdot \underline{\hat{k}})(1 - \underline{\hat{k}} \cdot \underline{\hat{q}})} = \frac{w_{pq}(k)}{\omega_k^2}. \tag{4.5.4}$$

In a manner analogous to eq. (4.5.4), a covariantized version of the CGC dipole kernel may be formulated. Note that when the positions x, y, z are restricted onto the lightsheet $x, y, z \in \mathrm{T}$ - the squared distance between two spacetime points $(x-y)^2$ simplifies to $(x-y)^2 = -(\boldsymbol{x}-\boldsymbol{y})^2$

- and, therefore,

$$\tilde{K}_{xy}(z) := -\frac{(x-y)^2}{(x-z)^2(y-z)^2} \xrightarrow{x,y,z\in\mathrm{T}} \frac{(\boldsymbol{x}-\boldsymbol{y})^2}{(\boldsymbol{x}-\boldsymbol{z})^2(\boldsymbol{y}-\boldsymbol{z})^2} = \tilde{\mathcal{K}}_{\boldsymbol{xzy}}. \tag{4.5.5}$$

The covariantized Jet and CGC dipole kernels, respectively, denoted $\tilde{W}_{pq}(k)$ and $\tilde{K}_{xy}(z)$ - yield conformal applications more amenable than the canonically defined $w_{pq}(k)$ and $\tilde{\mathcal{K}}_{\boldsymbol{xzy}}$. To elaborate, under the action of the HM map as showcased in eq. (4.5.1), the quantity $(p-q)^2$, for example, may be expressed in terms of $(x-y)^2$ since,

$$(p-q)^2 \overset{\mathrm{c}}{=} \Omega_{\mathrm{c}}(x)\Omega_{\mathrm{c}}(y)(x-y)^2. \tag{4.5.6}$$

The building blocks of the Jet evolution equation showcased in eq. (4.5.2), namely: the measure d^4k, the on-shell constraint $\delta(k^2)$, the dipole kernel $\tilde{W}_{pq}(k)$, and bounds of the energy integral $\Theta(E > \omega_k > E_{\mathrm{out}})$ may entirely be re-parametrized with the prescription in eq. (4.5.1). The measure, when re-parametrized, gains a Jacobian determinant,

$$\frac{d^4k}{2\pi} \overset{\mathrm{c}}{=} \frac{d^4z}{2\pi}\Omega_{\mathrm{c}}^4(z). \tag{4.5.7a}$$

Note that $k = \mathrm{c}(z) = \zeta\Omega_{\mathrm{c}}(z^-)n_{\mathrm{c}}(\boldsymbol{z}) + z^+\bar{n}_{\mathrm{c}}$, where n_{c} and $\bar{n}_{\mathrm{c}}$ are mutually reciprocal lightlike vectors. All of which implies that $k^2 = (\mathrm{c}(z))^2 = 2\zeta\Omega(z)z^+$. Therefore, when re-parametrized, the on-shell constraint of momenta in Jet evolution translates into a planar constraint positions in CGC evolution,

$$\delta\big(k^2\big) \overset{\mathrm{c}}{=} \delta\big(2\zeta\Omega(z)z^+\big) = \frac{\delta\big(z^+\big)}{2\zeta\Omega_{\mathrm{c}}(z)}. \tag{4.5.7b}$$

Using the general relation highlighted by eq. (4.5.6) for all momenta p, q, k and positions x, y, z the covariantized dipole kernel $\tilde{W}_{pq}(k)$ may be expressed in terms of $\tilde{K}_{xy}(z)$,

$$\tilde{W}_{pq}(k) \overset{\mathrm{c}}{=} \frac{2}{\Omega_{\mathrm{c}}^2(z)}\bigg[-\frac{(x-y)^2}{(x-z)^2(y-z)^2}\bigg] = \frac{2}{\Omega_{\mathrm{c}}^2(z)}\tilde{K}_{xy}(z). \tag{4.5.7c}$$

Eq. (4.5.7b) firmly establishes that the on-shell momentum corresponds to the condition $z^+ = 0$. Therefore, by eq. (4.3.4), the energy may be re-parametrized through $\omega_k = \zeta\Omega_{\mathrm{c}}(z^-)n_{\mathrm{c}}^0(\boldsymbol{z}) = \zeta^2 n_{\mathrm{c}}^0(\boldsymbol{z})/(\lambda - z^-)$. A energy bound B corresponds to a lightcone coordinate bound $\upsilon(B)$,

$$\Theta\big(E \geq \omega_k \geq E_{\mathrm{out}}\big) \overset{\mathrm{c}}{=} \Theta\big(\upsilon(E) \geq z^- \geq \upsilon(E_{\mathrm{out}})\big); \quad \upsilon(B) := \lambda - \frac{\zeta^2 n_{\mathrm{c}}^0(\boldsymbol{z})}{B}. \tag{4.5.7d}$$

All in all, when the building blocks of Jet evolution are re-parametrized in terms of the building blocks of CGC evolution,

$$\begin{aligned}\frac{d^4k}{2\pi}&\delta(k^2)\tilde{W}_{pq}(k)\Theta(E \geq \omega_k \geq E_{\mathrm{out}})\\ &= \frac{d^4z}{2\pi}\delta\big(z^+\big)\tilde{K}_{xy}\big(z\big)\bigg[\frac{\Omega_{\mathrm{c}}(z^-)}{\zeta}\bigg]\Theta\big(\upsilon(E) \geq z^- \geq \upsilon(E_{\mathrm{out}})\big).\end{aligned} \tag{4.5.8}$$

A remarkable feature of re-parametrization scheme highlighted in eq. (4.5.8) is the fact that 4 powers of conformal factors arising from the measure are reduced by 1 power arising from the constraint and 2 powers arising from the kernel, ultimately, leaving 1 power of the conformal factor $\Omega(z^-)$ which carries all z^- dependence. Integrating the z^- dependent parts of eq. (4.5.8),

$$\int_{\upsilon(E_{\rm out})}^{\upsilon(E)} dz^- \left[\frac{\Omega_{\rm c}(z^-)}{\zeta}\right] = \int_{\lambda-\zeta^2 n_{\rm c}^0(\boldsymbol{z})/E_{\rm out}}^{\lambda-\zeta^2 n_{\rm c}^0(\boldsymbol{z})/E} \frac{dz^-}{\lambda - z^-} = \int_{\zeta^2 n_{\rm c}^0(\boldsymbol{z})/E_{\rm out}}^{\zeta^2 n_{\rm c}^0(\boldsymbol{z})/E} \frac{-dz^-}{z^-} = \Delta, \tag{4.5.9}$$

reveals a regulator λ, scale ζ, and transverse position $\boldsymbol{z}$ independent logarithm in terms of the lightcone coordinate z^-. Moreover, due to the bounds imposed by re-parametrizing $\omega_k = \zeta\Omega_{\rm c} n_{\rm c}^0(\boldsymbol{z})$, that is $\{E, E_{\rm out}\} \mapsto \{\upsilon(E), \upsilon(E_{\rm out})\}$, the non-global logarithm encountered in Jet evolution resurfaces $\Delta := \ln E/E_{\rm out}$. Moreover, it should be noted that the differential logarithms $d\omega_k/\omega_k$ and dz^-/z^- - which arise from the Minkowskian extension to Hatta's Euclidean correspondence - are also scaleless. There may be recourse to interpret the dz^-/z^- logarithm as rapidity differences dk^-/k^- - however, more research is required to establish the degree to which the correspondence of logarithms (and consequently the correspondence of resummation structures in Jet and CGC evolution) may be concretized through conformal transformations.

When on-shell momenta $p, q, k \in \mathrm{L}$ and planar constrained coordinates $x, y, z \in \mathrm{T}$ are considered - the covariantized dipole kernels featured in eqs (4.5.4) and (4.5.5) reduce to $w_{pq}(k)$ and $\tilde{\mathcal{K}}_{\boldsymbol{xzy}}$, respectively. The relation in eq. (4.5.8), admits the following extension to the Euclidean correspondence proposed by Hatta through a stereographic projection,

$$\begin{aligned}\Big\{\frac{d\omega_k}{\omega_k}\Theta(E \geq \omega_k \geq E_{\rm out})\Big\} \times \frac{d^2\hat{\underline{k}}}{4\pi}\frac{(1-\hat{\underline{p}}\cdot\hat{\underline{q}})}{(1-\hat{\underline{p}}\cdot\hat{\underline{k}})(1-\hat{\underline{k}}\cdot\hat{\underline{q}})} \\ = \frac{d^2\boldsymbol{z}}{2\pi}\frac{(\boldsymbol{x}-\boldsymbol{y})^2}{(\boldsymbol{x}-\boldsymbol{z})^2(\boldsymbol{y}-\boldsymbol{z})^2} \times \Big\{\frac{-dz^-}{z^-}\Theta\Big(\frac{\zeta^2 n_{\rm c}^0(\boldsymbol{z})}{E} \geq z^- \geq \frac{\zeta^2 n_{\rm c}^0(\boldsymbol{z})}{E_{\rm out}}\Big)\Big\}.\end{aligned} \tag{4.5.10}$$

In eq. (4.5.10), the Jet kernel and measure along with the CGC kernel and measure are overall scaleless as pointed out earlier. Moreover, both ω_k and z^- logarithms (which are overall scaleless) are equal to $\Delta := \ln E/E_{\rm out}$.

Chapter 5

Conclusion

5.1 Summary

This study aims to bridge, with the use of conformal transformations, two distinct applications of QCD which are encapsulated by evolution equations for associated observables. Superficially, interjet energy flow multiplicity [9–12] and DIS at small-$x_{\rm bj}$ [13–20] describe entirely different physical phenomena. Jet evolution equations describe how soft gluons enter the final state of e^+e^- annihilation events and, accordingly, drive the energy dependence of s-channel multiplicities — see Chapter 3. On the other hand, Color Glass Condensate (CGC) evolution equations describe the change of dynamic gluon saturation effects (characteristic of DIS events at small-$x_{\rm bj}$) in terms of the change in kinematic rapidity – and, accordingly, characterize the t-channel exchange between probe and target — see Chapter 2. Despite difference of applications, both Jet and CGC evolution respectively characterize how logarithmically enhanced quantum fluctuations induced by the QCD action drive the energy and rapidity dependence of their respective observables.

The structural similarity of Jet and CGC evolution, respectively, showcased by the independently established BMS [9] and BK [13–16] equations was originally observed by Weigert [10] in 2004. At the time, only the BK equation had a finite N_c generalization (namely, the JIMWLK equation [17–20]) – which motivated Weigert to derive the BMS-W equation (a finite N_c generalization of BMS equation). In parallel, a surge of $\mathcal{N} = 4$ SYM interest in relating small-$x_{\rm bj}$ DIS and interjet energy flow [24, 26] – based on the AdS/CFT Correspondence – provided new perspectives on associated QCD descriptions. All these developments culminated in a search for tools to understand the origin and limitations of the correspondence of Jet/CGC physics – and have exposed conformal transformations as useful tools with which to formalize the correspondence [24–27].

On a foundational level, the structural similarities are geometric in origin: Wilson lines and the product of integration kernels and measures are tagged by transverse coordinates in the CGC case and by a sphere of directions on the Jet side. Hatta [24] provided the first link for the product of integration kernels and measures via a two dimensional stereographic projection. Later Vladimirov [36, 37] used a four dimensional conformal map originally devised by Hofman and Maldacena (HM) [26] to relate UV singularities of Wilson lines in Drell-Yan processes

to those in particle production cross sections. It is this map (called the HM map), properly adapted to the present purpose that is used in this study to provide a map between virtually all ingredients of the two evolution equations. In particular, re-parametrization of independently established mathematical objects encountered in both Jet and CGC evolution is used to furnish a four dimensional relationship of Wilson line geometry, logarithm structure, and integration kernels.

The main results of this study, discussed in Chapter 4, are summarized below:

1. The HM map relates the spacetime pictures of CGC and Jet events by mapping the past lightsheet – the subset of Minkowski space that features in the JIMWLK equation – onto the future lightcone – the subset of Minkowski space that features in the BMS-W equation. Quite remarkably, this map preserves path-ordering of trajectories and consequently preserves the order in which soft emissions, summarized by Wilson lines, occur in the respective processes.

2. The Wilson lines of the CGC case obtain their non-trivial contributions on the past lightsheet, and depend on the fixed transverse position where the represented parton pierces a boost enhanced background field. The HM map takes them onto the future lightcone with angular directions that are directly determined by the transverse position of their pre-image. The stereographic projection employed by Hatta emerges as part of the full four dimensional map at work in this case. There is no direct analogue of the CGC background field on the Jet side. The HM map takes the CGC background field out to infinite time, suggesting that the dominant contributions to the Jet cross section are indeed formed at late times.

3. The products of phase space measures and emission kernels can be covariantized in both cases. This unavoidably includes energy integrals on both sides. Again the HM map (followed by an arbitrary unit rescaling that takes length units into mass units, see item 4) takes these covariantized expressions onto each other if one restricts the evolution to color singlet correlators[1]. The energy logarithms are now automatically included in the procedure.

4. It is worth emphasizing that the HM map strictly is a map either from space-time to space-time, or from energy-momentum space to energy-momentum space. The leading order kernels together with the energy logarithms are, however, scale invariant. This is what, in the first instance, renders the procedure insensitive to all scales included in the HM map and removes all units from the final expressions.

All comparisons in this study were strictly done on the level of the well established leading logarithmic equations. As such, it only provides a firm basis and tools required for future work on NLO contributions.

[1] These are the only ones relevant for physically measureable quantities.

5.2 Outlook

Beyond the leading logarithmic equations [27–30, 68–73], scale carrying features like running couplings necessarily enter the picture. If additional resummations become necessary, these might also carry their own scales and may well force an adaptation to the procedures outlined in this study. Beyond LO, Jet and CGC observables are known to acquire additional contributions beyond the single logarithmic contributions:

- On the Jet side: Forshaw et al [68] have identified what they call super leading logarithms (SLL) that appear only at finite N_c. Specifically, SLL manifest at higher order $\mathcal{O}(\alpha_s^4)$ in perturbative expansions in processes involving at least four external particles. SLL corrections have not been fully integrated into the parton shower treatment of Becher et al [69]. Presently these contributions have only been included as a single insertion into an otherwise systematic NLO resummation at leading N_c. Since both JIMWLK and BMS-W equations contain no large N_c approximations, they offer an intriguing route towards a systematic inclusion of such contributions.

- On the CGC side: higher order perturbative corrections to CGC evolution are known to demonstrate sensitivity to collinear logarithms which arise from single or double transverse logarithms [70]. These logarithmically enhanced contributions manifest in the large N_c limit and are not included in the original work of Caron-Hout [27] or Kovner et al [28–30]. Resummation of the collinear enhancements in the JIMWLK framework, which arise from single or double transverse logarithms, is imperative to address the lack of convergence demonstrated by the CGC evolution equations at NLO [70–72].

Additionally – unlike their BMS-W counterpart, derivations of Jet evolution using Statistical Field Theory (SFT) or Soft Collinear Effective Thery (SCET) explicitly involve a factorization of hard and soft parts, with the latter comprised of Wilson line correlators [73]. Establishing a firmer match between the Effective Field Theory (EFT) approach and the methods used to derive BMS-W should open the door to explicitly map the standard factorization approach over to CGC cross sections. One might then devise a systematic factorization between impact factors (like the photon wave function in eq. (2.1.17)) and the Wilson correlators that can be used to view the JIMWLK equation, and its associated Balitsky hierarchies, in a new light.

This foray into future research is certainly incomplete and many hurdles remain to be overcome. Nevertheless, one would hope that this study provides a solid basis for what is to come...

Appendices

Appendix A

Conventions

A.1 Lightcone Coordinate System in the Kogut-Soper Convention

The Minkowski vector $x \in \mathbb{R}^{1,3}$, expanded as linear combination of **instant form** or standard spatio-temporal basis vectors take the form,

$$x^\mu = x^0 e_0^\mu + x^1 e_1^\mu + x^2 e_2^\mu + x^1 e_3^\mu. \tag{A.1.1}$$

The metric in instant form coordinate system gives rise to the inner product,

$$[\eta_{\circ\circ}] := \begin{bmatrix} +1 & 0 & 0 & 0 \\ 0 & -1 & 0 & 0 \\ 0 & 0 & -1 & 0 \\ 0 & 0 & 0 & -1 \end{bmatrix} \implies x.y := x^\mu \eta_{\mu\nu} y^\nu = x^0 y^0 - \sum_{i=1}^{3} x^i y^i. \tag{A.1.2}$$

Similarly, the Minkowski vector $x \in \mathbb{R}^{1,3}$, expanded as linear combination of **front form** or lightcone basis vectors take the form,

$$x^\mu = x^+ \bar{n}^\mu + x^1 e_1^\mu + x^2 e_2^\mu + x^- n^\mu. \tag{A.1.3}$$

The metric in front form coordinate system gives rise to the inner product,

$$(\eta_{\circ\circ}) := \begin{pmatrix} 0 & 0 & 0 & 1 \\ 0 & -1 & 0 & 0 \\ 0 & 0 & -1 & 0 \\ 1 & 0 & 0 & 0 \end{pmatrix} \implies x.y := x^\mu \eta_{\mu\nu} y^\nu = x^+ y^- + x^- y^+ - \sum_{i=1}^{2} x^i y^i. \tag{A.1.4}$$

Note that the lightlike vectors n and $\bar{n}$ are mutually reciprocal $\bar{n}.n = 1$ in the Kogut-Soper convention [46].

In matrix notation, instant and front form tensors will be denoted by square and round brackets, respectively. Coordinate transformations between the instant and front form vectors

are,

$$x = \begin{pmatrix} x^+ \\ x^1 \\ x^2 \\ x^- \end{pmatrix} = \begin{bmatrix} +\frac{1}{\sqrt{2}} & 0 & 0 & +\frac{1}{\sqrt{2}} \\ 0 & 1 & 0 & 0 \\ 0 & 0 & 1 & 0 \\ +\frac{1}{\sqrt{2}} & 1 & 1 & -\frac{1}{\sqrt{2}} \end{bmatrix} \begin{bmatrix} x^0 \\ x^1 \\ x^2 \\ x^3 \end{bmatrix}, \tag{A.1.5}$$

$$x = \begin{bmatrix} x^0 \\ x^1 \\ x^2 \\ x^3 \end{bmatrix} = \begin{pmatrix} +\frac{1}{\sqrt{2}} & 0 & 0 & +\frac{1}{\sqrt{2}} \\ 0 & 1 & 0 & 0 \\ 0 & 0 & 1 & 0 \\ +\frac{1}{\sqrt{2}} & 1 & 1 & -\frac{1}{\sqrt{2}} \end{pmatrix} \begin{pmatrix} x^+ \\ x^1 \\ x^2 \\ x^- \end{pmatrix}. \tag{A.1.6}$$

A.2 A Note on Euclidean Vectors

A Euclidean vector in standard Cartesian coordinates is denoted by an underline,

$$\underline{x} = x^1 \underline{e}_1 + x^2 \underline{e}_2 + x^1 \underline{e}_3. \tag{A.2.1}$$

The transverse part of Euclidean vector $\underline{x}$ is denoted by a boldface script,

$$\boldsymbol{x} = x^1 \underline{e}_1 + x^2 \underline{e}_2. \tag{A.2.2}$$

A Euclidean vector, additionally, may be written in terms of a norm $|\underline{x}|$ and a unit vector $\hat{\underline{x}}$ such that $\hat{\underline{x}}^2 = 1$,

$$\underline{x} = |\underline{x}|\hat{\underline{x}}. \tag{A.2.3}$$

A.3 A Note on Minkowskian Vectors

A Minkowski vector in standard Cartesian or instant form coordinates is denoted,

$$y = y^0 e_0 + y^1 e_1 + y^2 e_2 + y^1 e_3. \tag{A.3.1}$$

The transverse part of the Minkowski vector y is denoted by the subscript $_\perp$,

$$y_\perp = y^1 e_1 + y^2 e_2, \tag{A.3.2}$$

where it is to be noted that,

$$y_\perp^2 = -\boldsymbol{y}^2. \tag{A.3.3}$$

In addition, *lightlike* vectors y may be written in terms of a temporal coordinate y^0 and a lightlike vector $\underline{y}$ such that $\hat{y}^2 = 0$ and $\hat{y}^0 = 1$,

$$y = y^0 \hat{y} \tag{A.3.4}$$

Appendix B

Key Results

B.1 Leading Logarithmic Cross Section

This section is taken from a back-of-the-envelope explanation provided by Matt Sievert during a CTMP summer school seminar.

The perturbative expansion of a differential cross section in terms of the coupling constant α_s organizes a power series in terms of loop order n of cross section,

$$d\sigma = \sum_{n=0}^{\infty} \alpha_s^n d\sigma^{(n)} = d\sigma^{(0)} + \alpha_s d\sigma^{(1)} + \alpha_s^2 d\sigma^{(2)} + \mathcal{O}(\alpha_s^3). \tag{B.1.1}$$

Assuming that, at each loop order, logarithmic enhancement of the cross section is limited to single logarithmic contributions from a kinematic variable V - one may define a convention where $d\sigma^{(n,m)}$ which denotes the part of of the n-loop cross section which is logarithmically enhanced by $\ln V^m$,

$$d\sigma = d\sigma^{(0)} + \alpha_s \big[\ln V d\sigma^{(1,1)} + d\sigma^{(1,0)} \big] + \alpha_s^2 \big[\ln^2 V d\sigma^{(2,2)} + \ln V d\sigma^{(2,1)} + d\sigma^{(2,0)} \big] + \mathcal{O}(\alpha_s^3). \tag{B.1.2}$$

The differential cross section, may be re-organized in terms of single logarithmic and sub-leading logarithmic contributions,

$$\begin{aligned} d\sigma =& \big[d\sigma^{(0)} + \alpha_s \ln V d\sigma^{(1,1)} + \alpha_s^2 \ln^2 V d\sigma^{(2,2)} + \mathcal{O}(\alpha_s^3) \big] \\ &+ \alpha_s \big[d\sigma^{(1,0)} + \alpha_s \ln V d\sigma^{(2,1)} + \mathcal{O}(\alpha_s^2) \big] \\ &+ \alpha_s^2 \big[d\sigma^{(2,0)} + \mathcal{O}(\alpha_s) \big] \\ =:& d\sigma^{\mathrm{LLA}} + \alpha_s d\sigma^{\mathrm{NLL}} + \alpha_s^2 d\sigma^{\mathrm{NNLL}}. \end{aligned} \tag{B.1.3}$$

B.2 Rapidity and the Bjorken-x

This section is adapted from [34]

Consider the experimental setup of a DIS event where, without loss of generality, the leptonic projectile and hadronic target traverse trajectories in the $-\hat{\boldsymbol{e}}_3$ and $+\hat{\boldsymbol{e}}_3$ respectively. The four momenta of the lepton and the hadron are:

$$l = \left[l^0, \mathbf{0}, l^3\right]^T; \qquad l.l = m_l^2, \qquad l^3 \leq 0. \tag{B.2.1}$$

$$P = \left[P^0, \mathbf{0}, P^3\right]^T; \qquad P.P = m_P^2, \qquad P^3 \geq 0. \tag{B.2.2}$$

Note that since l and P are both timelike momenta, they are related through a Lorentz boost. Only temporal and longitudinal parts of the Lorentz boost are shown,

$$\frac{1}{m_P}\begin{bmatrix} P^0 \\ P^3 \end{bmatrix} = \begin{bmatrix} \cosh(Y) & \sinh(Y) \\ \sinh(Y) & \cosh(Y) \end{bmatrix} \frac{1}{m_l}\begin{bmatrix} l^0 \\ l^3 \end{bmatrix}, \tag{B.2.3}$$

where Y is the rapidity separation between the lepton and hadron. It is convenient to compute Y in the rest frame of the lepton where $l^3 = 0$,

$$\frac{P^0}{m_P} = \cosh(Y). \tag{B.2.4}$$

P^0 may be expressed in terms of x_{bj} and y,

$$x_{\mathrm{bj}} = \frac{Q^2}{2P.q} = \frac{Q^2}{2y(P.l)} = \frac{Q^2}{2yP^0 m_l} \Longleftrightarrow P^0 = \frac{Q^2}{2x_{\mathrm{bj}} m_e y}. \tag{B.2.5}$$

Note that for small-x_{bj} the leading contribution to the rapidity separation arises from the Bjorken-x variable,

$$Y = \cosh^{-1}\left(\frac{Q^2}{2x_{\mathrm{bj}} m_l m_P y}\right) \overset{x_{\mathrm{bj}}\to 0}{=} \ln\left(1/x_{\mathrm{bj}}\right) + \ln\left(\frac{Q^2}{2m_l m_P y}\right) + \mathcal{O}\left(x_{\mathrm{bj}}^2\right). \tag{B.2.6}$$

B.3 Large Background Field Formalism

Recall the Lagrangian provided in section 2.2 which is characteristically described as a sum of the Yang-Mills term, a gauge-fixing term, and a source term,

$$\begin{aligned}\mathcal{L}_{\text{gluons}}[A,j](x) := &-\frac{1}{4}F^{a}_{\mu\nu}[A](x)F^{a\mu\nu}[A](x) - \frac{1}{2\xi}\left(\bar{n}_\mu A^{a\mu}(x)\right)\left(\bar{n}_\nu A^{a\nu}(x)\right)\\ &- A^{a\mu}(x)j_{a\mu}(x).\end{aligned} \tag{2.2.2}$$

In the Large Background Field (LBF) formalism, quantum fluctuations α in the presence of a large background field b are considered,

$$A = b + \alpha. \tag{B.3.1}$$

Accordingly, the gluon field strength tensor in the LBF formalism may be expressed as,

$$\begin{aligned}F^{\mu\nu}[b+\alpha](x) &= \frac{i}{g}\big[D^\mu_x[b] - ig\alpha^\mu(x), D^\nu_x[b] - ig\alpha^\nu(x)\big]\\ &= F^{\mu\nu}[b](x) + \Big(\big[D^\mu_x[b],\alpha^\nu(x)\big] - \big[D^\nu_x[b],\alpha^\mu(x)\big]\Big) - (ig)\big[\alpha^\mu(x),\alpha^\nu(x)\big].\end{aligned} \tag{B.3.2}$$

Note that the gauge covariant derivative, through which the gluon field strength tensor is defined, in the LBF formalism may be expressed as,

$$D^\mu_x[b+\alpha] := \partial^\mu_x + ig(b+\alpha)^\mu(x) = D^\mu_x + ig\alpha^\mu(x). \tag{B.3.3}$$

Note that the commutators employed in eq. (B.3.2) may be re-expressed (using a test function),

$$\begin{aligned}\big[D^\mu_x[b],\alpha^\nu(x)\big]f(x) &= \big[\partial^\mu_x,\alpha^\nu(x)\big]f(x) - ig\big[b^\mu(x),\alpha^\nu(x)\big]f(x)\\ &= \Big(\partial^\mu_x\alpha^\mu(x)\big) - igb^{\mu b}(x)\alpha^{\nu c}(x)[T^a,T^b]\Big)f(x)\\ &= \Big(\big(\partial^\mu_x\delta^{ac} + gf^{abc}b^{\mu b}(x)\big)\alpha^{\nu c}(x)\Big)f(x)\\ &=: \Big(D^{\mu ac}_x\alpha^{\nu c}(x)\Big)f(x),\end{aligned} \tag{B.3.4}$$

such that the gauge covariant derivative in the adjoint representation only acts on $\alpha^{\nu c}(x)$.

Explicitly, in accordance with the LBF formalism, $\mathcal{L}_{\text{gluons}}[A=b+\alpha,j]$ is expanded in terms of the fluctuation field where $\mathcal{L}^{(n)}_{\text{gluons}}[b+\alpha,j]$ denotes the n-th order in α so that $n\in\{0,1,2,3,4\}$. The zeroth, first, and second order in α,

$$\begin{aligned}\mathcal{L}^{(0)}_{\text{gluons}}[b+\alpha,j](x) := &-\frac{1}{4}F^{a}_{\mu\nu}[b](x)F^{a\mu\nu}[b](x) - \frac{1}{2\xi}\left(\bar{n}_\mu b^{a\mu}(x)\right)\left(\bar{n}_\nu b^{a\nu}(x)\right)\\ &- b^{a\mu}(x)j_{a\mu}(x),\end{aligned} \tag{B.3.5}$$

$$\mathcal{L}^{(1)}_{\text{gluons}}[b+\alpha,j](x) := +\left\{D^{xca}_\mu F^{a\mu\rho}[b](x) + \frac{1}{\xi}\bar{n}^\mu b^c_\mu\bar{n}^\rho - j^{c\rho}(x)\right\}\alpha^c_\rho(x), \tag{B.3.6}$$

$$\mathcal{L}^{(2)}_{\text{gluons}}[b+\alpha,j](x) := +\frac{1}{2}\alpha^a_\mu(x)\Big\{D^2_x[b]^{ab}g^{\mu\nu} - (D^\mu_x[b]D^\nu_x[b])^{ab} \\ - 2gF^{c\mu\nu}[b](x)f^{cab} + \frac{1}{\xi}\bar{n}^\mu\bar{n}^\nu\delta^{ab}\Big\}\alpha^b_\nu(x). \tag{B.3.7}$$

Total derivatives are taken to be zero - since all fields are assumed to fall off to zero at infinity. The higher order terms in the Lagrangian in eq. (2.2.2) are not required to compute a Leading Log JIMWLK equation. The axial gauge-fixing prescription $\bar{n}.(b+\alpha) = (b+\alpha)^- = 0$ is enacted in a path integral by taking the limit $\xi \to 0$.

The term in the Lagrangian at linear order in α,

$$\left[D^x_\mu, F^{\mu\nu}[b](x)\right] = j^\nu(x),, \tag{2.2.4}$$

give rise to to Classical Yang-Mills (CYM) equation (as shown in [55]) in $\mathcal{L}^{(1)}_{\text{gluons}}[b+\alpha,j]$ which is the Euler-Lagrange equation of motion of the non-abelian background gauge field. The CYM equation is used to define the background field $b^{\mu a}(x)$ in terms of the color current $j^{\mu a}(x)$.

The axial gauge condition, $\alpha^-(x) = 0$ allows the expression of $\mathcal{L}^{(2)}_{\text{gluons}}[b+\alpha,j](x)$ in canonical matrix multiplication,

$$\mathcal{L}^{(2)}_{\text{gluons}}[b+\alpha,j](x) = \frac{1}{2}\begin{bmatrix} \alpha^{a+}_x & \alpha^{ai}_x \end{bmatrix}\begin{bmatrix} -(\partial^-_x)^2\delta^{ab} & +\partial^-_x\partial^j_x\delta^{ab} \\ +\partial^i_x\partial^-_x\delta^{ab} & -D^2_x[b]^{ab}\delta^{ij} - \partial^i_x\partial^j_x\delta^{ab} \end{bmatrix}\begin{bmatrix} \alpha^{b+}_x \\ \alpha^{bj}_x \end{bmatrix}, \tag{B.3.8}$$

to diagonalize the block matrix in eq. (B.3.8) new modes $\tilde{\alpha}$ of the fluctuation field are specified,

$$\tilde{\alpha}^{a+}(x) := \alpha^{a+}(x) + \int_y \left[\frac{1}{-(\partial^-)^2}\right](x,y)(\partial^-_y\partial^i_y)\alpha^{ai}(y), \tag{B.3.9}$$

$$\tilde{\alpha}^{ai}(x) := \alpha^{ai}(x). \tag{B.3.10}$$

where it is understood that $-(\partial^-)^2[-1/(\partial^-)^2](x,y) = \delta^{(4)}(x-y)$.

$$\mathcal{L}^{(2)}_{\text{gluons}}[b+\alpha,j](x) = \frac{1}{2}\begin{bmatrix} \tilde{\alpha}^{a+}_x & \tilde{\alpha}^{ai}_x \end{bmatrix}\begin{bmatrix} -(\partial^-_x)^2\delta^{ab} & 0 \\ 0 & -D^2_x[b]^{ab}\delta^{ij} \end{bmatrix}\begin{bmatrix} \tilde{\alpha}^{b+}_x \\ \tilde{\alpha}^{bj}_x \end{bmatrix}, \tag{B.3.11}$$

so that,

$$\left\langle \tilde{\alpha}^{a+}_x\tilde{\alpha}^{b+}_y\right\rangle_\alpha := \delta^{ab}\left[\frac{1}{-[\partial^-]^2}\right](x,y), \tag{B.3.12}$$

$$\left\langle \tilde{\alpha}^{ai}_x\tilde{\alpha}^{bj}_y\right\rangle_\alpha[b] := \delta^{ij}\left[\frac{1}{-D^2[b]}\right]^{ab}(x,y). \tag{B.3.13}$$

The fluctuation gluon propagator that features in the JIMWLK derivation:

$$\left\langle \alpha^{a+}_u\alpha^{b+}_v\right\rangle_\alpha[b] = \left\langle \tilde{\alpha}^{a+}_x\tilde{\alpha}^{b+}_y\right\rangle_\alpha \\ - \int_{u'v'}\left(i\partial^-_u\right)\left[\frac{i}{-\left(\partial^-\right)^2}\right](u,u')\left(i\partial^-_v\right)\left[\frac{i}{-\left(\partial^-\right)^2}\right](v,v') \\ \times\left(i\partial^i_{u'}\right)\left(i\partial^i_{v'}\right)\left\langle \tilde{\alpha}^{ai}_{u'}\tilde{\alpha}^{bj}_{v'}\right\rangle_\alpha[b]. \tag{B.3.14}$$

B.4 JIMWLK Derivation

B.4.1 Background Field Derivative of CGC Wilson Lines

All dependence of the quantity $S[b]$ on the background field $b(x)$ is encapsulated by the Wilson lines $U_x^\dagger[b]$,

$$\frac{\delta S[b]}{\delta b_u^{+a}} = \int_{\boldsymbol{x}} \big[J_{\boldsymbol{x}}^\dagger\big]_{ij} \frac{\delta}{\delta b_u^{+a}} \big[U_{\boldsymbol{x}}[b]\big]_{ij} + \big[J_{\boldsymbol{x}}\big]_{kl} \frac{\delta}{\delta b_u^{+a}} \big[U_{\boldsymbol{x}}^\dagger[b]\big]_{kl}. \tag{B.4.1}$$

Taking the background field derivative of the Wilson line $U_{\boldsymbol{x}}^{(\dagger)} = U_{\boldsymbol{x};+\infty,-\infty}^{(\dagger)}[b]$ requires taking the path ordering into account,

$$\frac{\delta}{\delta b_v^{+b}} U_{\boldsymbol{x};+\infty,-\infty}[b] = (-ig)\delta_{0,v^+}\delta^{(2)}_{\boldsymbol{x},\boldsymbol{v}} U_{\boldsymbol{x};+\infty,v^-} t^b U_{\boldsymbol{x};v^-,-\infty} \tag{B.4.2a}$$

$$\frac{\delta}{\delta b_v^{+b}} U^\dagger_{\boldsymbol{x};+\infty,-\infty}[b] = (+ig)\delta_{0,v^+}\delta^{(2)}_{\boldsymbol{x},\boldsymbol{v}} U^\dagger_{\boldsymbol{x},v^-,-\infty} t^b U^\dagger_{\boldsymbol{x},+\infty,v^-} \tag{B.4.2b}$$

The highly localized form of the background field $b^{+a}(x) = \delta(x^-)\beta^a(\boldsymbol{x})$ admits the following simplifications of the background field derivative of the (anti)fundamental Wilson lines,

$$\frac{\delta}{\delta b_v^{+b}} U_x = (-ig)\delta_{0,v^+}\delta^{(2)}_{\boldsymbol{x},\boldsymbol{v}} \left(\theta_{v^-,0} t^b U_x + \theta_{0,v^-} U_x t^b\right), \tag{B.4.3a}$$

$$\frac{\delta}{\delta b_v^{+b}} U^\dagger_{\boldsymbol{x}} = (+ig)\delta_{0,v^+}\delta^{(2)}_{\boldsymbol{x},\boldsymbol{v}} \left(\theta_{v^-,0} U^\dagger_{\boldsymbol{x}} t^b + \theta_{0,v^-} t^b U^\dagger_{\boldsymbol{x}}\right). \tag{B.4.3b}$$

The gluon exchange background field derivatives,

$$\begin{aligned}\frac{\delta S[b]}{\delta b_u^{+a}} \frac{\delta S[b]}{\delta b_v^{+b}} = (-ig)^2\delta_{u^+0}\delta_{v^+0}\Big\{ &+ \big[J^\dagger_{\boldsymbol{u}}\big]_{ij}\big[J^\dagger_{\boldsymbol{v}}\big]_{kl}\big[U^{qq}_{\boldsymbol{u},\boldsymbol{v},u^-,v^-}\big]^{ab}_{ijkl} \\ &- \big[J^\dagger_{\boldsymbol{u}}\big]_{ij}\big[J_{\boldsymbol{v}}\big]_{kl}\big[U^{\bar{q}q}_{\boldsymbol{u},\boldsymbol{v},u^-,v^-}\big]^{ab}_{ijkl} \\ &- \big[J_{\boldsymbol{u}}\big]_{ij}\big[J^\dagger_{\boldsymbol{v}}\big]_{kl}\big[U^{q\bar{q}}_{\boldsymbol{u},\boldsymbol{v},u^-,v^-}\big]^{ab}_{ijkl} \\ &+ \big[J_{\boldsymbol{u}}\big]_{ij}\big[J_{\boldsymbol{v}}\big]_{kl}\big[U^{\bar{q}\bar{q}}_{\boldsymbol{u},\boldsymbol{v},u^-,v^-}\big]^{ab}_{ijkl}\Big\},\end{aligned} \tag{B.4.4}$$

where,

$$\begin{aligned}\big[U^{qq}_{\boldsymbol{u},\boldsymbol{v},u^-,v^-}\big]^{ab}_{ijkl} = \Big(&+ \theta_{u^-,0}\theta_{v^-,0}\big[t^a U_{\boldsymbol{u}}\big]_{ij}\big[t^b U_{\boldsymbol{v}}\big]_{kl} + \theta_{u^-,0}\theta_{0,v^-}\big[t^a U_{\boldsymbol{u}}\big]_{ij}\big[U_{\boldsymbol{v}} t^b\big]_{kl} \\ &+ \theta_{0,u^-}\theta_{v^-,0}\big[U_{\boldsymbol{u}} t^a\big]_{ij}\big[t^b U_{\boldsymbol{v}}\big]_{kl} + \theta_{0,u^-}\theta_{0,v^-}\big[U_{\boldsymbol{u}} t^a\big]_{ij}\big[U_{\boldsymbol{v}} t^b\big]_{kl}\Big)\end{aligned} \tag{B.4.5a}$$

$$\begin{aligned}\big[U^{\bar{q}q}_{\boldsymbol{u},\boldsymbol{v},u^-,v^-}\big]^{ab}_{ijkl} = \Big(&+ \theta_{u^-,0}\theta_{v^-,0}\big[t^a U_{\boldsymbol{u}}\big]_{ij}\big[U^\dagger_{\boldsymbol{v}} t^b\big]_{kl} + \theta_{u^-,0}\theta_{0,v^-}\big[t^a U_{\boldsymbol{u}}\big]_{ij}\big[t^b U^\dagger_{\boldsymbol{v}}\big]_{kl} \\ &+ \theta_{0,u^-}\theta_{v^-,0}\big[U_{\boldsymbol{u}} t^a\big]_{ij}\big[U^\dagger_{\boldsymbol{v}} t^b\big]_{kl} + \theta_{0,u^-}\theta_{0,v^-}\big[U_{\boldsymbol{u}} t^a\big]_{ij}\big[t^b U^\dagger_{\boldsymbol{v}}\big]_{kl}\Big)\end{aligned} \tag{B.4.5b}$$

$$\big[U^{q\bar{q}}_{\boldsymbol{u},\boldsymbol{v},u^-,v^-}\big]^{ab}_{ijkl} = \Big(+ \theta_{u^-,0}\theta_{v^-,0}\big[U^\dagger_{\boldsymbol{u}}t^a\big]_{ij}\big[t^bU_{\boldsymbol{v}}\big]_{kl} + \theta_{u^-,0}\theta_{0,v^-}\big[U^\dagger_{\boldsymbol{u}}t^a\big]_{ij}\big[U_{\boldsymbol{v}}t^b\big]_{kl} + \theta_{0,u^-}\theta_{v^-,0}\big[t^aU^\dagger_{\boldsymbol{u}}\big]_{ij}\big[t^bU_{\boldsymbol{v}}\big]_{kl} + \theta_{0,u^-}\theta_{0,v^-}\big[t^aU^\dagger_{\boldsymbol{u}}\big]_{ij}\big[U_{\boldsymbol{v}}t^b\big]_{kl}\Big), \tag{B.4.5c}$$

$$\big[U^{\bar{q}\bar{q}}_{\boldsymbol{u},\boldsymbol{v},u^-,v^-}\big]^{ab}_{ijkl} = \Big(+ \theta_{u^-,0}\theta_{v^-,0}\big[U^\dagger_{\boldsymbol{u}}t^a\big]_{ij}\big[U^\dagger_{\boldsymbol{v}}t^b\big]_{kl} + \theta_{u^-,0}\theta_{0,v^-}\big[U^\dagger_{\boldsymbol{u}}t^a\big]_{ij}\big[t^bU^\dagger_{\boldsymbol{v}}\big]_{kl} + \theta_{0,u^-}\theta_{v^-,0}\big[t^aU^\dagger_{\boldsymbol{u}}\big]_{ij}\big[U^\dagger_{\boldsymbol{v}}t^b\big]_{kl} + \theta_{0,u^-}\theta_{0,v^-}\big[t^aU^\dagger_{\boldsymbol{u}}\big]_{ij}\big[t^bU^\dagger_{\boldsymbol{v}}\big]_{kl}\Big). \tag{B.4.5d}$$

The gluon self-energy background field derivatives,

$$\frac{\delta^2 S[b]}{\delta b^{+a}_u \delta b^{+b}_v} =: (-ig)^2\delta^{(2)}_{\boldsymbol{u},\boldsymbol{v}}\delta_{u+0}\delta_{v+0}\Big\{ + \big[J^\dagger_{\boldsymbol{u}}\big]_{ij}\big[U^q_{\boldsymbol{u},\boldsymbol{u}^-,\boldsymbol{v}^-}\big]^{ab}_{ij} + \big[J_{\boldsymbol{u}}\big]_{ij}\big[U^{\bar{q}}_{\boldsymbol{u},u^-,v^-}\big]^{ab}_{ij}\Big\} \tag{B.4.6}$$

where,

$$\begin{aligned}\big[U^q_{\boldsymbol{u},u^-,v^-}\big]^{ab}_{ij} = \\ \big[&+ \theta_{u^-,v^-}(\theta_{u^-,0}\theta_{v^-,0}t^at^bU_{\boldsymbol{u}} + \theta_{u^-,0}\theta_{0,v^-}t^aU_{\boldsymbol{u}}t^b + \theta_{0,u^-}\theta_{0,v^-}U_{\boldsymbol{u}}t^at^b) \\ &+\theta_{v^-,u^-}(\theta_{u^-,0}\theta_{v^-,0}t^bt^aU_{\boldsymbol{u}} + \theta_{0,u^-}\theta_{v^-,0}t^bU_{\boldsymbol{u}}t^a + \theta_{0,u^-}\theta_{0,v^-}U_{\boldsymbol{u}}t^bt^a)\big]_{ij}\end{aligned} \tag{B.4.7a}$$

$$\begin{aligned}\big[U^{\bar{q}}_{\boldsymbol{u},u^-,v^-}\big]^{ab}_{ij} = \\ \big[&+ \theta_{u^-,v^-}(\theta_{u^-,0}\theta_{v^-,0}U^\dagger_{\boldsymbol{u}}t^bt^a + \theta_{u^-,0}\theta_{0,v^-}t^bU^\dagger_{\boldsymbol{u}}t^a + \theta_{0,u^-}\theta_{0,v^-}t^bt^aU^\dagger_{\boldsymbol{u}}) \\ &+\theta_{v^-,u^-}(\theta_{u^-,0}\theta_{v^-,0}U^\dagger_{\boldsymbol{u}}t^at^b + \theta_{0,u^-}\theta_{v^-,0}t^aU^\dagger_{\boldsymbol{u}}t^b + \theta_{0,u^-}\theta_{0,v^-}t^at^bU^\dagger_{\boldsymbol{u}})\big]_{ij}\end{aligned} \tag{B.4.7b}$$

B.4.2 Two-point Fluctuation in the Leading Log JIMWLK Derivation

The one-point fluctuation correlator $\langle\alpha\rangle$ is considered to be zero. While the two-point fluctuation correlator,

$$\begin{aligned}\left\langle \alpha_u^{+a}\alpha_v^{+b}\right\rangle_\alpha[b] &= \delta^{ab}\left[\frac{i}{-(\partial^-)^2}\right]_{uv} \\ &- \int_{u'v'}(i\partial_u^-)\left[\frac{i}{-(\partial^-)^2}\right]_{uu'}(i\partial_v^-)\left[\frac{i}{-(\partial^-)^2}\right]_{vv'}(i\partial^i_{u'})(i\partial^i_{v'})\left[\frac{i}{-D[b]^2}\right]^{ab}_{u'v'}\end{aligned} \tag{B.4.8}$$

The first term of the fluctuation gluon propagator $\left\langle \alpha_u^{+a}\alpha_v^{+b}\right\rangle_\alpha[b]$ is a divergent term that needs to be regulated at the level of the Lagrangian through counter terms. Furthermore, the derivative in the second term pull down relevant momentum factors which yields the form of the fluctuation gluon propagator[1],

$$\left\langle \alpha_u^{+a}\alpha_v^{+b}\right\rangle_\alpha[b] = \int_{u'v'}\left[\frac{ik_1^-}{-(\partial^-)^2}\right]_{uu'}\left[\frac{ik_2^-}{-(\partial^-)^2}\right]_{vv'}\left[\frac{ip^iq^i}{-D^2[b]}\right]^{ab}_{u'v'}, \tag{B.4.9}$$

where the propagators in the Feynman prescription [34], relevant for this section, are:

$$\left[\frac{i}{-(\partial^-)^2}\right]_{uv} = \delta_{u^-,v^-}\delta^{(2)}_{\boldsymbol{u},\boldsymbol{v}}\int\frac{dk^-}{2\pi}\frac{i}{(k^-)^2+i\varepsilon}e^{-ik^-(u^+-v^+)}, \tag{B.4.10}$$

$$\begin{aligned}\left[\frac{i}{-D^2[b]}\right]^{ab}_{uv} &= \int\frac{dk^-}{(2\pi)^3\,(2k^-)}\left[\theta_{u^-,v^-}\theta_{k^-,0}-\theta_{v^-,u^-}\theta_{0,k^-}\right] \\ &\times\int d^2\boldsymbol{p}d^2\boldsymbol{q}\;e^{-i(p.u-q\cdot v)}\Big|_{k^2=q^2=p^2,k^-=p^-=q^-} \\ &\times\int\frac{d^2\boldsymbol{z}}{(2\pi)^2}e^{-i(\boldsymbol{p}-\boldsymbol{q})\cdot\boldsymbol{z}}\left[\tilde{U}_{\boldsymbol{z};u^-,v^-}\right]^{ab}.\end{aligned} \tag{B.4.11}$$

An elegant simplification of the finite difference equation entails accounting for the common parts of gluon exchange and gluon self-energy terms,

$$\begin{aligned}&\frac{1}{2}\int_{uv}\left\langle \alpha_u^{+a}\alpha_v^{+b}\right\rangle_\alpha[b](ig)^2\delta_{u^+,0}\delta_{v^+,0} \\ &\quad=\frac{(ig)^2}{2}\int_{uv}\int_{u'v'}\delta_{u^+,0}\left[\frac{ik_1^-}{-(\partial^-)^2}\right]_{uu'}\delta_{v^+,0}\left[\frac{ik_2^-}{-(\partial^-)^2}\right]_{vv'}\left[\frac{ip^iq^i}{-D^2[b]}\right]^{ab}_{u'v'}.\end{aligned} \tag{B.4.12}$$

Firstly, note that all u^+ and v^+ dependence is eliminated by the Dirac deltas. Secondly, there is a $e^{-ik^-(u'^+-v'^+)}$ which is to be evaluated with the $u'+$ and v'^+ dependent parts of $[\frac{1}{-(\partial^-)^2}]$,

$$(i)^2\int\frac{dk_1^-dk_2^-}{k_1^-k_2^-}\int\frac{du'^+}{2\pi}\frac{dv'^+}{2\pi}e^{-iu'^+\left(k^--k_1^-\right)}e^{+iv'^+\left(k^-+k_2^-\right)} = \frac{1}{(k^-)^2}, \tag{B.4.13}$$

[1]Note the abuse of notation for simplification purposes; momenta displayed within propagators are assumed to be integrated over.

which along with the Dirac deltas in $[\frac{1}{-(\partial^-)^2}]$ eliminate all u' and v' dependence,

$$\begin{aligned}
&\frac{1}{2}\int_{uv}\left\langle \alpha_u^{+a}\alpha_v^{+b}\right\rangle_\alpha [b](ig)^2\delta_{u^+,0}\delta_{v^+,0}\\
&\quad=\frac{1}{4}\frac{(ig)^2}{(2\pi)^2}\int_{\boldsymbol{uzv}}\int d^2\boldsymbol{p}d^2\boldsymbol{q}e^{i(\boldsymbol{p}\cdot\boldsymbol{u}-\boldsymbol{q}\cdot\boldsymbol{v})}e^{-i(\boldsymbol{p}-\boldsymbol{q})\cdot\boldsymbol{z}}p^iq^i\\
&\qquad\times\int\frac{dk^-du^-dv^-}{(2\pi k^-)^3}\left[\theta_{u^-,v^-}\theta_{k^-,0}-\theta_{v^-,u^-}\theta_{0,k^-}\right]e^{-i(\boldsymbol{p}^2u^-\boldsymbol{q}^2v^-)/2k^-}\left[\tilde{U}_{\boldsymbol{z},u^-,v^-}\right]^{ab}.
\end{aligned}\tag{B.4.14}$$

The Wilson line is non-trivial if and only if it contains the background field,

$$U_{\boldsymbol{z};u^-,v^-}=\left[\theta_{u^-,0}\theta_{v^-,0}\mathbb{1}+\theta_{u^-,0}\theta_{0,v^-}\tilde{U}_{\boldsymbol{z}}+\theta_{0,u^-}\theta_{v^-,0}\tilde{U}^\dagger_{\boldsymbol{z}}+\theta_{0,u^-}\theta_{0,v^-}\mathbb{1}\right].\tag{B.4.15}$$

All of the u^- and v^- dependence may be written as $\theta_{s_uu^-,0}$ and $\theta_{s_vv^-,0}$ where $s_u,s_v=\pm1$. Evaluating the k^- and u^- and v^- dependent parts of the fluctuation propagator yields,

$$\begin{aligned}
&\int\frac{dk^-}{(2\pi k^-)^3}\int du^-dv^-\theta_{s_uu^-,0}\theta_{s_vv^-,0}\left[\theta_{u^-,v^-}\theta_{k^-,0}-\theta_{v^-,u^-}\theta_{0,k^-}\right]\\
&\qquad\qquad\times\exp\Big[-i\Big(\frac{\boldsymbol{p}^2}{2k^-}u^--\frac{\boldsymbol{q}^2v^-}{2k^-}\Big)\Big]\\
&=\frac{s_us_v}{(2\pi)^3}\int\frac{dk^-}{(k^-)^3}\left\{\theta_{k^-,0}\int_0^\infty dv^-\exp\Big[-i(\boldsymbol{p}^2-\boldsymbol{q}^2)\frac{v^-}{2k^-}\Big]\Big(-\frac{i2k^-}{\boldsymbol{p}^2}\Big)\right.\\
&\qquad\qquad\left.-\theta_{0,k^-}\int_0^\infty du^-\exp\Big[-i(\boldsymbol{p}^2-\boldsymbol{q}^2)\frac{u^-}{2k^-}\Big]\Big(+\frac{i2k^-}{\boldsymbol{q}^2}\Big)\right\}\\
&=-s_us_v\frac{4}{(2\pi)^3}\frac{1}{\boldsymbol{p}^2-\boldsymbol{q}^2}\int_{-\infty}^{+\infty}\frac{dk^-}{k^-}\left[\frac{\theta_{k^-,0}}{\boldsymbol{p}^2}+\frac{\theta_{0,k^-}}{\boldsymbol{q}^2}\right]\\
&=+s_us_v\frac{4}{(2\pi)^3}\frac{1}{\boldsymbol{p}^2\boldsymbol{q}^2}\int_0^\infty\frac{dk^-}{k^-}.
\end{aligned}\tag{B.4.16}$$

The transverse momentum integrals reveal the **gluon emission kernel** for CGC evolution,

$$\mathcal{K}_{\boldsymbol{uzv}}:=\frac{(\boldsymbol{u}-\boldsymbol{z})^i(\boldsymbol{z}-\boldsymbol{v})^i}{(\boldsymbol{u}-\boldsymbol{z})^2(\boldsymbol{z}-\boldsymbol{v})^2}=-\int\frac{d^2\boldsymbol{p}d^2\boldsymbol{q}}{(2\pi)^2}\frac{p^iq^i}{\boldsymbol{p}^2\boldsymbol{q}^2}e^{i\boldsymbol{p}(\boldsymbol{u}-\boldsymbol{z})}e^{i\boldsymbol{q}(\boldsymbol{z}-\boldsymbol{v})}.\tag{B.4.17}$$

The momentum integral, which is logarithmically both infrared and ultraviolet divergent, must be regulated,

$$\int_0^\infty\frac{dk^-}{k^-}\mapsto\int_{\lambda_0}^\lambda\frac{dk^-}{k^-}=\ln\frac{\lambda}{\lambda_0}=\ln\lambda-\ln\lambda_0.\tag{B.4.18}$$

The logarithmic difference $\ln\lambda-\ln\lambda_0$ lends itself to interpretation as rapidity difference through,

$$Y:=\frac{1}{2}\ln\frac{k^+}{k^-}\implies\int_Y^{Y+\delta Y}dY=-\int_{\lambda_0}^\lambda\frac{dk^-}{k^-}\implies\ln\lambda-\ln\lambda_0=-\delta Y.\tag{B.4.19}$$

All in all, simplifying the eq. (B.4.12) yields a rapidity difference δY, a gluon emission kernel $\mathcal{K}_{\boldsymbol{uzv}}$, and a Wilson line in the adjoint representation $\tilde{U}_{\boldsymbol{z}}$ which is decomposed base on u^-,v^-

ordering,

$$\begin{aligned}\frac{1}{2}\int_{uv}\left\langle\alpha_u^{+a}\alpha_v^{+b}\right\rangle_\alpha[b](ig)^2\delta_{u^+,0}\delta_{v^+,0}\\ &= +\delta Y\cdot\frac{\alpha_s}{2\pi^2}\int_{\boldsymbol{uzv}}\mathcal{K}_{\boldsymbol{uzv}}\\ &\qquad\times\left[\theta_{u^-,0}\theta_{v^-,0}\mathbb{1}-\theta_{u^-,0}\theta_{0,v^-}\tilde{U}_{\boldsymbol{z}}-\theta_{0,u^-}\theta_{v^-,0}\tilde{U}^\dagger_{\boldsymbol{z}}+\theta_{0,u^-}\theta_{0,v^-}\mathbb{1}\right]^{ab},\end{aligned}\tag{B.4.20}$$

where $\alpha_s = g^2/4\pi$

B.4.3 Gluon Exchange and Gluon Self-Energy Diagrams

The product of the fluctuation gluon propagator and the gluon exchange background field derivatives generate,

$$+\frac{1}{2}\int_{uv}\left\langle \alpha_u^{+a}\alpha_v^{+b}\right\rangle_\alpha[b]\frac{\delta S[b]}{\delta b_u^{+a}}\frac{\delta S[b]}{\delta b_v^{+b}} = \delta Y\cdot\int_{\boldsymbol{u},\boldsymbol{v}}\frac{1}{2}J^\alpha_{\boldsymbol{u}}J^\beta_{\boldsymbol{v}}\chi^{\alpha\beta}_{\boldsymbol{u},\boldsymbol{v}}. \tag{B.4.21}$$

The terms below demonstrate all possible combinations for gluon exchange diagrams to manifest in an arbitrary Wilson line correlator,

$$\begin{aligned}\left[\bar{\chi}^{qq}_{\boldsymbol{u},\boldsymbol{v}}\right]_{ijkl} :=& -\frac{\alpha_s}{\pi}\int\frac{d^2\boldsymbol{z}}{2\pi}\mathcal{K}_{\boldsymbol{uzv}}\Big(+\left[U_{\boldsymbol{z}}\right]_{il}\left[U_{\boldsymbol{v}}U^\dagger_{\boldsymbol{z}}U_{\boldsymbol{u}}\right]_{kj}+\left[U_{\boldsymbol{u}}U^\dagger_{\boldsymbol{z}}U_{\boldsymbol{v}}\right]_{il}\left[U_{\boldsymbol{z}}\right]_{kj}\\ &-\left[U_{\boldsymbol{u}}\right]_{il}\left[U_{\boldsymbol{v}}\right]_{kj}-\left[U_{\boldsymbol{v}}\right]_{il}\left[U_{\boldsymbol{u}}\right]_{kj}\Big),\end{aligned} \tag{B.4.22a}$$

$$\begin{aligned}\left[\bar{\chi}^{q\bar{q}}_{\boldsymbol{u},\boldsymbol{v}}\right]_{ijkl} :=& +\frac{\alpha_s}{\pi}\int\frac{d^2\boldsymbol{z}}{2\pi}\mathcal{K}_{\boldsymbol{uzv}}\Big(+\left[U_{\boldsymbol{z}}U^\dagger_{\boldsymbol{v}}\right]_{il}\left[U^\dagger_{\boldsymbol{z}}U_{\boldsymbol{u}}\right]_{kj}+\left[U_{\boldsymbol{u}}U^\dagger_{\boldsymbol{z}}\right]_{il}\left[U^\dagger_{\boldsymbol{v}}U_{\boldsymbol{z}}\right]_{kj}\\ &-\left[U_{\boldsymbol{u}}U^\dagger_{\boldsymbol{v}}\right]_{il}\delta_{kj}-\delta_{il}\left[U^\dagger_{\boldsymbol{v}}U_{\boldsymbol{u}}\right]_{kj}\Big),\end{aligned} \tag{B.4.22b}$$

$$\begin{aligned}\left[\bar{\chi}^{\bar{q}q}_{\boldsymbol{u},\boldsymbol{v}}\right]_{ijkl} :=& +\frac{\alpha_s}{\pi}\int\frac{d^2\boldsymbol{z}}{2\pi}\mathcal{K}_{\boldsymbol{uzv}}\Big(+\left[U^\dagger_{\boldsymbol{z}}U_{\boldsymbol{v}}\right]_{il}U_{\boldsymbol{z}}U^\dagger_{\boldsymbol{u}}\right]_{kj}+\left[U^\dagger_{\boldsymbol{u}}U_{\boldsymbol{z}}\right]_{il}\left[U_{\boldsymbol{v}}U^\dagger_{\boldsymbol{z}}\right]_{kj}\\ &-\delta_{il}\left[U_{\boldsymbol{v}}U^\dagger_{\boldsymbol{u}}\right]_{kj}-\left[U^\dagger_{\boldsymbol{u}}U_{\boldsymbol{v}}\right]_{il}\delta_{kj}\Big),\end{aligned} \tag{B.4.22c}$$

$$\begin{aligned}\left[\bar{\chi}^{\bar{q}\bar{q}}_{\boldsymbol{u},\boldsymbol{v}}\right]_{ijkl} :=& -\frac{\alpha_s}{\pi}\int\frac{d^2\boldsymbol{z}}{2\pi}\mathcal{K}_{\boldsymbol{uzv}}\Big(+\left[U^\dagger_{\boldsymbol{z}}\right]_{il}\left[U^\dagger_{\boldsymbol{v}}U_{\boldsymbol{z}}U^\dagger_{\boldsymbol{u}}\right]_{kj}+\left[U^\dagger_{\boldsymbol{u}}U_{\boldsymbol{z}}U^\dagger_{\boldsymbol{v}}\right]_{il}\left[U^\dagger_{\boldsymbol{z}}\right]_{kj}\\ &-\left[U^\dagger_{\boldsymbol{u}}\right]_{il}\left[U^\dagger_{\boldsymbol{v}}\right]_{kj}-\left[U^\dagger_{\boldsymbol{v}}\right]_{il}\left[U^\dagger_{\boldsymbol{u}}\right]_{kj}\Big).\end{aligned} \tag{B.4.22d}$$

The $\chi^{q\bar{q}}$ term gives rise to the following diagrams,

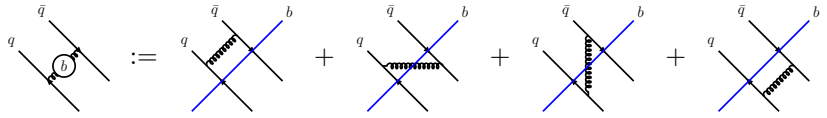

(2.2.10)

The product of the fluctuation gluon propagator and the gluon self-energy background field derivatives generate,

$$+\frac{1}{2}\int_{uv}\left\langle \alpha_u^{+a}\alpha_v^{+b}\right\rangle_\alpha[b]\frac{\delta^2 S[b]}{\delta b_u^{+a}\delta b_v^{+b}} = \delta Y\cdot\int_{\boldsymbol{u}}J^\alpha_{\boldsymbol{u}}\sigma^\alpha_{\boldsymbol{u}}. \tag{B.4.23}$$

The terms below demonstrate all possible combinations for gluon self-energy diagrams to manifest in an arbitrary Wilson line correlator,

$$\left[\bar{\sigma}^{q}_{\boldsymbol{u}}\right]_{ij} := -\frac{\alpha_s}{\pi}\int\frac{d^2\boldsymbol{z}}{2\pi}\mathcal{K}_{\boldsymbol{uzu}}\Big(\left[U_{\boldsymbol{z}}\right]_{ij}\mathrm{tr}\left(U_{\boldsymbol{u}}U^\dagger_{\boldsymbol{z}}\right)-N_c\left[U_{\boldsymbol{u}}\right]_{ij}\Big) \tag{B.4.24a}$$

$$\left[\bar{\sigma}^{\bar{q}}_{\boldsymbol{u}}\right]_{ij} := -\frac{\alpha_s}{\pi}\int\frac{d^2\boldsymbol{z}}{2\pi}\mathcal{K}_{\boldsymbol{uzu}}\Big(\left[U^\dagger_{\boldsymbol{z}}\right]_{ij}\mathrm{tr}\left(U^\dagger_{\boldsymbol{u}}U_{\boldsymbol{z}}\right)-N_c\left[U^\dagger_{\boldsymbol{u}}\right]_{ij}\Big). \tag{B.4.24b}$$

The σ^q term gives rise to the following diagrams,

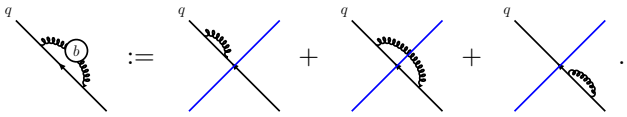

(2.2.12)

B.5 Color Singlets

(Anti)quarks are fermions which carry color. The spinor structure of (anti)quarks therefore admits the following structure,

$$\psi : \mathbb{R}^{1,3} \to \mathbb{C}^4_{\text{spin}} \otimes \mathbb{C}^{N_c}_{\text{color}}; \quad x \mapsto \psi(x) = \psi_{ai}(x)\, e_a \otimes e_i. \tag{B.5.1}$$

The vector space $\mathbb{C}^{N_c}_{\text{color}}$ referred to as the color part of the quark and antiquark spinor. The **Color Fock space** (for quarks and antiquarks) is the following direct sum of vector spaces [74],

$$\mathfrak{C} := \bigoplus_{m,\bar{m}=0}^{\infty} \big[F^{\otimes m} \otimes \bar{F}^{\otimes \bar{m}}\big], \tag{B.5.2}$$

where F and $\bar{F}$ are complex vector spaces of dimension N_c which carry the fundamental and anti-fundamental representation of the gauge group $\mathsf{SU}(N_c)$. Both F and $\bar{F}$ may be considered isomorphic to $\mathbb{C}^{N_c}_{\text{color}}$. An element of the Color Fock space may be expressed as a linear combination,

$$|\lambda\rangle := \lambda^{i_1 \cdots i_m}{}_{j_1 \cdots j_{\bar{m}}} e_{i_1} \otimes \cdots \otimes e_{i_m} \otimes e^{j_1} \otimes \cdots \otimes e^{j_{\bar{m}}} \in \mathfrak{C}. \tag{B.5.3}$$

By definition, color singlets, a subset of elements of $\mathfrak{C}$, remain invariant under global color rotations (position independent Wilson line products), that is, in component form

$$\prod_{l=1}^{m} \big[U(s)\big]^{i_l}{}_{j_l} \prod_{k=1}^{\bar{m}} \big[U^\dagger(s)\big]^{\bar{j}_k}{}_{\bar{i}_k} \sigma^{j_1 \cdots j_m}{}_{\bar{j}_1 \cdots \bar{j}_{\bar{m}}} = \sigma^{i_1 \cdots i_m}{}_{\bar{i}_1 \cdots \bar{i}_{\bar{m}}}, \tag{B.5.4}$$

For global color rotations,

$$U(s) := \exp\big[+ist^a\big]; \quad U^\dagger(s) := \exp\big[-ist^a\big]. \tag{B.5.5}$$

A graphical notation called birdtracks [56] will be used to simplify color algebra calculations. To this end, unit matrices are denoted as:

$$\delta^i{}_j = \quad i \longleftarrow j \ , \qquad \delta_i{}^j = \quad i \longrightarrow j \ , \tag{B.5.6a}$$

and analogously, the Hermitian generators are in the fundamental and anti-fundamental representation are denoted as:

$$[t^a]^i{}_j = \quad \overset{i}{\underset{a}{\overset{\longleftarrow}{\vdots}}} j \ , \qquad [t^{a*}]^i{}_j = \quad \overset{i}{\underset{a}{\overset{\longrightarrow}{\vdots}}} j \ = [t^a]_j{}^i. \tag{B.5.6b}$$

Note that 'left-down-right-up' indices are ill-defined unless unit matrices δ_{ij} and δ^{ij} are considered. A birdtrack notation (see appendix (B.5)) for position dependent (anti)fundamentally

represented Wilson lines may also be adopted,

$$[U_{\boldsymbol{x}}]^{i}{}_{j} =: \; i \longleftarrow j \; ; \qquad [U^{\dagger}_{\boldsymbol{y}}]^{j}{}_{i} =: \; i \longrightarrow j \; = [U^{*}_{\boldsymbol{y}}]_{i}{}^{j} \tag{B.5.7}$$

so that, a product of m fundamental and $\bar{m}$ antifundamental Wilson lines (in component form) is depicted as a tower of Wilson lines,

$$\begin{array}{l} i_1 \longleftarrow j_1 \\ \vdots \\ i_m \longleftarrow j_m \\ \bar{i}_1 \longrightarrow \bar{j}_1 \\ \vdots \\ \bar{i}_{\bar{m}} \longrightarrow \bar{j}_{\bar{m}} \end{array} = \prod_{l=1}^{m} [U_{\boldsymbol{x}_l}]^{i_l}{}_{j_l} \prod_{k=1}^{\bar{m}} [U^{\dagger}_{\boldsymbol{y}_k}]^{\bar{j}_k}{}_{\bar{i}_k} \tag{B.5.8}$$

Evaluating the action of the right and left invariant vector field in accordance with their operational definition eq. (2.2.15), and integrating thereafter in accordance with eq. (2.3.8) on a tower of m fundamentally and $\bar{m}$ anti-fundamentally represented Wilson lines in birdtrack notation,

$$\int_{\boldsymbol{u}} i\bar{\nabla}^{a}_{\boldsymbol{u}} \; \vdots \; = \left[+ \; \overset{a}{\vdots} \; + \cdots + \; \overset{a}{\vdots} \; - \; \underset{a}{\vdots} \; - \cdots - \; \underset{a}{\vdots} \right] \times \; \vdots \tag{B.5.9a}$$

$$\int_{\boldsymbol{u}} i\nabla^{a}_{\boldsymbol{u}} \; \vdots \; = \; \vdots \; \times \left[- \; \overset{a}{\vdots} \; - \cdots - \; \overset{a}{\vdots} \; + \; \underset{a}{\vdots} \; + \cdots + \; \underset{a}{\vdots} \right] \tag{B.5.9b}$$

is seen to demonstrate infinitesimal color global (coordinate independent) rotations which will annihilate color singlet states. To demonstrate, consider the $\frac{d}{ds}|_{s=0}$ of eq. (B.5.4),

$$\left.\frac{d}{ds}\right|_{s=0} \text{eq. } (B.5.4) = \left[+ \; \overset{a}{\vdots} \; + \cdots + \; \overset{a}{\vdots} \; - \; \underset{a}{\vdots} \; - \cdots - \; \underset{a}{\vdots} \right] \sigma = 0 \tag{B.5.10}$$

where the right-hand-side of the equation is zero. Note that the graphical notation used to denote the color singlet σ above is defined in [33].

B.6 Stereographic Projection

Stereographic projections stand as the quintessential examples of conformal transformations and are a natural way to relate the transverse plane to the sphere of directions.

B.6.1 Construction

The construction of a pair of stereographic projections and their inverses will be implemented in an $(n+1)$-dimensional Euclidean space $\mathbb{R}^{n+1}$. To this end, the surface which is defined as the n-**sphere** of radius r,

$$\mathrm{S}^n(r) := \Big\{ \underline{s} \in \mathbb{R}^{n+1} : \underline{s} \cdot \underline{s} = \sum_{i=1}^{n+1} (s^i)^2 \stackrel{!}{=} r^2 \text{ where } r \in \mathbb{R} \Big\}, \tag{B.6.1}$$

and the surface which is defined to be the n-**plane** at height h,

$$\mathrm{P}^n(h) := \Big\{ \underline{p} \in \mathbb{R}^{n+1} : \underline{p} = \big[p^1, p^2, \ldots, p^n, p^{n+1} \stackrel{!}{=} h\big] \text{ where } h \in \mathbb{R} \Big\}. \tag{B.6.2}$$

Stereographic projections are defined as non-global, bijective maps from open, connected subsets of the sphere onto the plane $\underline{\pi}_\pm : \mathrm{S}^n(r) \backslash \{\underline{s}_\pm\} \to \mathrm{P}^n(h)$. The north pole $\underline{s}_+ := (0, \cdots, 0, +r)$ and south pole $\underline{s}_- := (0, \cdots, 0, -r)$ are chosen to be the *projection points* from which the north pole $\underline{\pi}_+$ and south pole $\underline{\pi}_-$ stereographic projections are defined. Stereographic projections $\underline{\pi}_\pm$ are constructed by specifying a line $\underline{s}_\pm t + (1-t)\underline{s} = \underline{p}$ and subsequently solving for t such that plane constraint is enacted, that is, $p^{n+1} \stackrel{!}{=} h$. Component-wise, the north and south pole stereographic projections manifest as,

$$\pi^i_\pm(\underline{s}) = p^i = (r \mp h) \frac{s^i/r}{1 \pm s^{n+1}/r} \text{ for } i \in \{1, 2, \ldots, n\}, \tag{B.6.3a}$$

$$\pi^{n+1}_\pm(\underline{s}) = p^{n+1} = h. \tag{B.6.3b}$$

The vector form of the north and south pole stereographic projections demonstrate a relation between the scaleless direction vector $\hat{\underline{s}} = \underline{s}/r$ and the scale dependent transverse coordinate vector $\boldsymbol{p}$

$$\underline{\pi}_\pm(\underline{s}) = \boldsymbol{p} + \underline{p}_\parallel = \sum_{i=1}^{n} (r \mp h) \frac{\hat{s}^i}{1 \pm \hat{s}^{n+1}} \underline{e}_i + h \underline{e}_{n+1} \tag{B.6.4}$$

Analogously, inverse stereographic projections $\underline{\sigma}_\pm : \mathrm{P}^n(h) \to \mathrm{S}^n(r)$ are constructed by specifying a line $\underline{s}_\pm t + (1-t)\underline{p} = \underline{s}$ and subsequently solving for t such that the sphere constraint is enacted, that is, $\underline{s} \cdot \underline{s} \stackrel{!}{=} r^2$.

$$\sigma^i_\pm(\underline{p}) = s^i = r \frac{2p^i/(r \mp p^{n+1})}{1 + \sum_{j=1}^{n} p^j p^j / (r \mp p^{n+1})^2} \text{ for } i \in \{1, 2, \ldots, n\}, \tag{B.6.5a}$$

$$\sigma^{n+1}_\pm(\underline{p}) = s^{n+1} = \mp r \frac{1 - \sum_{j=1}^{n} p^j p^j / (r \mp p^{n+1})^2}{1 + \sum_{j=1}^{n} p^j p^j / (r \mp p^{n+1})^2}. \tag{B.6.5b}$$

The vector form of the inverse north pole and south pole stereographic projections demonstrate a relation between the scale dependent transverse coordinate vector $\boldsymbol{p}$ and the scaleless direction vector $\underline{\hat{s}}$.

$$\frac{\underline{\sigma}_{\pm}(\underline{p})}{r} = \underline{\hat{s}} = \sum_{i=1}^{n} \frac{2p^i/(r \mp h)}{1 + \boldsymbol{p}^2/(r \mp h)^2} \underline{e}_i \mp \frac{1 - \boldsymbol{p}^2/(r \mp h)^2}{1 + \boldsymbol{p}^2/(r \mp h)^2} \underline{e}_{n+1}. \tag{B.6.6}$$

B.6.2 Spherical Coordinate Trigonometric Ratios in terms of Cartesian Coordinates

The stereographic projection from 2-sphere of radius r onto a 2-plane at height h: $\underline{\pi}_{\pm} : \mathrm{S}^2(r) \to \mathrm{P}^2(h)$ where $\underline{x} = \underline{\pi}_{\pm}(\underline{y})$. Note that the $\pm$ subscript denotes that both north pole and south pole stereographic projections are to be simultaneously considered. Assuming that the 2-sphere is parametrized by the usual spherical coordinate system with inclination angle θ, azimuthal angle ϕ, and radius r, that is $\underline{y} = r(\sin\theta\cos\phi\underline{e}_1 + \sin\theta\sin\phi\underline{e}_2 + \cos\theta\underline{e}_3)$, one invents an avenue to relate Cartesian coordinates (native on the 2-plane) to spherical coordinates (native on the 2-sphere).

$$\frac{\pi^1_{\pm}(\underline{y})}{(r \mp h)} = \frac{x^1}{(r \mp h)} = \frac{\sin\theta\cos\phi}{1 \pm \cos\theta}, \quad \frac{\pi^2_{\pm}(\underline{y})}{(r \mp h)} = \frac{x^2}{(r \mp h)} = \frac{\sin\theta\sin\phi}{1 \pm \cos\theta}, \quad \pi^3_{\pm}(\underline{y}) = x^3 = h. \tag{B.6.7}$$

The trigonometric ratios featuring the inclination and azimuthal angle may be also be expressed, solely, in terms of the transverse part $\boldsymbol{x} = x^1\underline{e}_1 + x^2\underline{e}_2$ since the longitudinal component has no spherical coordinate dependence $x^3 = h$. The expression of the aforementioned trigonometric relies on a trigonometric identity - to this end one defines $t^{\pm 1} := (\tan(\theta/2))^{\pm} = (\sin\theta)/(1 \pm \cos\theta)$ to show that $\cos\theta = (1 - t^2)/(1 + t^2)$ and that $\sin\theta = 2t/(1 + t^2)$. As a result the inclination trigonometric ratios may be expressed, solely, in terms of t defined above (trick is known as the Weierstrass' substitution , for the interested reader). Note that since $\boldsymbol{x} = (r \mp h)t\cos\phi\underline{e}_1 + (r \mp h)t\sin\phi\underline{e}_2$, the various inclination and azimuthal trigonometric ratios encountered in eq. (B.6.7) may be re-expressed,

$$\cos\theta = \hat{y}^3 = \mp\frac{1 - \boldsymbol{x}^2/(r \mp h)^2}{1 + \boldsymbol{x}^2/(r \mp h)^2}, \qquad \sin\theta = \frac{2|\boldsymbol{x}|/(r \mp h)}{1 + \boldsymbol{x}^2/(r \mp h)^2}. \tag{B.6.8a}$$

$$\cos\phi = \frac{\hat{y}^1}{\sin\theta} = \frac{x^1}{|\boldsymbol{x}|}, \qquad \sin\phi = \frac{\hat{y}^2}{\sin\theta} = \frac{x^2}{|\boldsymbol{x}|}. \tag{B.6.8b}$$

B.7 Conformal Geometry

B.7.1 Definition and Properties

This subsection is adapted from the textbook [31]

A **semi-Riemannian manifold** is a double (M, g) - where M is a smooth manifold of dimension $m+n=d$ and g is a metric tensor field,

$$g(x) : T_x\mathrm{M} \times T_x\mathrm{M} \to \mathbb{R} \tag{B.7.1}$$

which assigns to each point $x \in \mathrm{M}$ a symmetric, non-degenerate, semi-definite bilinear form on the tangent space $T_x\mathrm{M}$. The double $\mathbb{R}^{m,n} := (\mathbb{R}^{m+n}, g^{m,n})$, where the matrix structure of the metric $g^{m,n}$,

$$(g^{m,n}(x))_{\mu\nu} = \mathrm{diag}(\underbrace{+1,\ldots,+1}_{m \text{ times}},\underbrace{-1,\ldots,-+1}_{n \text{ times}})_{\mu\nu} \tag{B.7.2}$$

is diagonal with m positive components and n negative components is an example of a semi-Riemannian manifold. A Riemannian manifold is a special case of the semi-Riemannian definition where the semi-definiteness condition of the metric tensor is tightened to a definiteness of the metric tensor. In particular, Euclidean space $\mathbb{R}^{3,0}$ is an example of a Riemannian manifold.

Let (M, g) and (N, g') be two semi-Riemannian manifolds of the same dimension $d = m+n$. Let $U \in \mathrm{M}$ and $U' \in \mathrm{N}$ be open neighbourhoods. A smooth map $\varphi : U \to U'$ is called a **conformal transformation** if there exists a smooth function $\Omega : U \to \mathbb{R}$ such that,

$$g'_{\mu'\nu'}(y)\frac{\partial y^{\mu'}}{\partial x^{\mu}}\frac{\partial y^{\nu'}}{\partial x^{\nu}} \overset{!}{=} \Omega^2(x)\cdot g_{\mu\nu}(x). \tag{B.7.3}$$

The function $\Omega(x)$ is called the associated **conformal factor** of the map φ. For a conformal factor $\Omega(x) \equiv 1$, the conformal condition - highlighted in eq.(B.7.3) - becomes a condition for local isometries.

The differentials featured in eq. (B.7.3) admit the following factorization,

$$\frac{\partial y^{\mu}(x)}{\partial x^{v}} = \Omega(x)R(x)^{\mu}{}_{\nu}; \quad \Omega(x) := \det\left[\frac{\partial y(x)}{\partial x}\right]^{1/d} \iff \det\left[R(x)\right] := 1, \tag{B.7.4}$$

The tensor $R(x)^{\mu}{}_{\nu}$ is thus explicitly an isometry of the metric, that is an element of $\mathrm{O}(m,n)$ [32].

Theorem 1 *If $\varphi : \mathrm{M} \to \mathrm{N}$ is a bijective conformal transformation with conformal factor Ω then φ is a diffeomorphism (that is φ^{-1} is smooth) and, moreover, $\varphi^{-1} : \mathrm{N} \to \mathrm{M}$ is conformal with conformal factor $\frac{1}{\Omega}$ [31].*

As a caveat: alternative definitions of a conformal transformations, for example in [75], specify the conformal factor as a map $\Omega' : U' \to \mathbb{R}$,

$$g_{\mu\nu}(x)\frac{\partial x^{\mu}}{\partial y^{\mu'}}\frac{\partial x^{\nu}}{\partial y^{\nu'}} \overset{!}{=} \Omega'^2(y)\cdot g'_{\mu\nu}(y), \tag{B.7.5}$$

however, due to theorem (1) the definitions of conformal transformations provided in eq. (B.7.3) and eq. (B.7.5) are equivalent for bijective conformal transformations.

B.7.2 Conformal Symmetry of Spacetime

This subsection is adapted from lecture notes [32]

Minkowski space is defined as the semi-Riemannian manifold $\mathbb{R}^{1,3}$. The instant form metric considered in appendix (A.1) is, explicitly, a 'mostly minus' diagonal metric $g_{\mu\nu} = \text{diag}(+1, -1, -1, -1)_{\mu\nu}$. Moreover, like the instant form metric, the front form metric considered in appendix (A.1) is coordinate independent. Therefore, for considerations of conformal symmetry on Minkowski space in this thesis, only metrics which have no coordinate dependence will be considered. Resultantly, the conformal condition therefore becomes,

$$g_{\mu'\nu'} \frac{\partial y_s^{\mu'}(x)}{\partial x^\mu} \frac{\partial y_s^{\nu'}(x)}{\partial x^\nu} \stackrel{!}{=} \Omega_s^2(x) g_{\mu\nu}. \tag{B.7.6}$$

A full set of infinitesimal conformal transformations and the constraints that follow from eq. (B.7.6) will be identified through a one parameter family of coordinate transformations. The dimensionless parameter s will be used to keep track of terms constituting a power series. Note, additionally, that although Minkowski space is explicitly defined as $\mathbb{R}^{1,3}$, in this subsection the semi-Riemannian manifold $\mathbb{R}^{m,n}$, where $m + n = d$, will be considered to maintain generality. Drawing attention to the leading order in s, the coordinate transformation $x \mapsto y_s$

$$y_s(x) := x + s\epsilon(x) + \mathcal{O}(s^2), \tag{B.7.7}$$

with ϵ defined as the *leading order coordinate transformation* yields the following transformation for the metric,

$$\frac{\partial y_s^\alpha}{\partial x^\beta} = g^\alpha{}_\beta + s\partial_\beta \epsilon^\alpha + \mathcal{O}(s^2) \iff g_{\mu'\nu'} \frac{\partial y_s^{\mu'}}{\partial x^\mu} \frac{\partial y_s^{\nu'}}{\partial x^\nu} = g_{\mu\nu} + s\left(\partial_\mu \epsilon_\nu + \partial_\nu \epsilon_\mu\right) + \mathcal{O}(s^2). \tag{B.7.8}$$

The coordinate transformation in eq. (B.7.6) naturally induces deformations in the conformal factor which is also considered to constitute a power series. Moreover, a trivial conformal factor corresponding to $\Omega \equiv 1$, results in eq. (B.7.6) admitting all isometries associated with the semi-Riemannian manifold in question[2]. Once again emphasing leading order changes in s - the conformal factor is expressed as,

$$\Omega_s(x) = 1 + s\sigma(x) + \mathcal{O}(s^2), \tag{B.7.9}$$

with σ defined as the *leading order conformal factor.*

Enforcing the conformal transformation condition in eq. (B.7.6) at leading order yields,

$$\begin{aligned} \left.\frac{d}{ds}\right|_{s=0} g_{\mu'\nu'} \frac{\partial y_s^{\mu'}(x)}{\partial x^\mu} \frac{\partial y_s^{\nu'}(x)}{\partial x^\nu} &\stackrel{!}{=} \left.\frac{d}{ds}\right|_{s=0} \Omega_s^2(x) g_{\mu\nu} \\ \left(\partial_\mu \epsilon_\nu + \partial_\nu \epsilon_\mu\right) &\stackrel{!}{=} 2\sigma \cdot g_{\mu\nu} \xRightarrow{\text{trace}} \partial_\mu \epsilon^\mu = d \times \sigma, \end{aligned} \tag{B.7.10}$$

where the implication is gathered by contracting the preceding equality with the contravariant metric $g^{\mu\nu}$ yielding the trace $g^\mu{}_\mu = d$. Note that the constraint eq. (B.7.10) may further be

[2]The isometry group associated with Minkowski space $\mathbb{R}^{1,3}$ is the Poincaré group $\text{ISO}(1,3)$

simplified by evaluating second order derivatives of the leading order coordinate transformation, which reveals

$$\begin{aligned}\partial_\rho\partial_\nu\epsilon_\mu &= \frac{1}{2}\left(\partial_\rho\left(\partial_\mu\epsilon_\nu+\partial_\nu\epsilon_\mu\right)+\partial_\nu\left(\partial_\mu\epsilon_\rho+\partial_\rho\epsilon_\mu\right)-\partial_\mu\left(\partial_\rho\epsilon_\nu+\partial_\nu\epsilon_\rho\right)\right) \\ &= \partial_\rho\sigma g_{\mu\nu}+\partial_\nu\sigma g_{\mu\rho}-\partial_\mu\sigma g_{\rho\nu}.\end{aligned} \tag{B.7.11}$$

Contracting eq. (B.7.11) with ∂^μ and using the constraints expressed in eq. (B.7.10) yields the following constraint dependant on the dimensionality of the semi-Riemannian manifold in question,

$$(d-2)\partial_\rho\partial_\nu\sigma \overset{!}{=} -g_{\rho\nu}\partial^2\sigma. \tag{B.7.12}$$

Additionally, eq. (B.7.12) through its contraction with $g^{\rho\nu}$ yielding $(d-1)\partial^2\sigma \overset{!}{=} 0$ - which combined with eq. (B.7.12) yields,

$$(d-1)(d-2)\partial_\rho\partial_\nu\sigma \overset{!}{=} 0, \tag{B.7.13}$$

The constraint eq. (B.7.13) demonstrates that for $d>2$ second order derivatives of σ must vanish. As such, the leading order conformal factor is expressed in general terms,

$$\sigma(x) = \kappa + 2b\cdot x, \tag{B.7.14}$$

where $\kappa\in\mathbb{R}$ and $b\in\mathbb{R}^{m,n}$ and which in conjunction with eq. (B.7.10) yields that third order derivatives of ϵ must vanish. As such, the leading order coordinate transformation is expressed in general terms,

$$\epsilon_\mu(x) = a_\mu + B_{\mu\alpha}x^\alpha + C_{\mu\alpha\beta}x^\alpha x^\beta; \qquad C_{\mu\alpha\beta}\overset{!}{=}C_{\mu\beta\alpha}, \tag{B.7.15}$$

where $a_\mu, B_{\mu\alpha}, C_{\mu\alpha\beta}$ are arbitrary tensors. Note that the symmetry of tensor $C_{\mu(\alpha\beta)}$ in the last two indices is due to the factor $x^\alpha x^\beta$ being symmetric and through properties of the Hadamard product.

Nonetheless, using $(\partial_\mu\epsilon_\nu+\partial_\nu\epsilon_\mu)\overset{!}{=}2\sigma\cdot g_{\mu\nu}$ in eq. (B.7.10) one necessarily has,

$$B_{\nu\mu}+B_{\mu\nu}+2C_{\nu\mu\alpha}x^\alpha+2C_{\mu\nu\alpha}x^\alpha \overset{!}{=} 2(\kappa+2b\cdot x)g_{\mu\nu}. \tag{B.7.16}$$

Note that since x is arbitrary, one may equate terms in powers of x. Resultantly, it should be noted that $B_{\mu\nu}$ is composed of symmetric and anti-symmetric parts which are respectively constrained and unconstrained in accordance with eq. (B.7.16),

$$B_{\nu\mu}+B_{\mu\nu}\overset{!}{=}2\kappa g_{\mu\nu} \iff B_{\mu\nu}=\kappa g_{\mu\nu}+\omega_{\mu\nu}; \qquad +\omega_{\mu\nu}\overset{!}{=}-\omega_{\nu\mu}. \tag{B.7.17}$$

Moreover, from eq. (B.7.11) and the ansatz for ϵ and σ through eqs (B.7.14-B.7.15);

$$\partial_\rho\partial_\nu\epsilon_\mu = C_{\mu\nu\rho}+C_{\mu\rho\nu}\overset{!}{=}2b_\rho g_{\mu\nu}+2b_\nu g_{\mu\rho}-2b_\mu g_{\rho\nu}=\partial_\rho\sigma g_{\mu\nu}+\partial_\nu\sigma g_{\mu\rho}-\partial_\mu\sigma g_{\rho\nu} \tag{B.7.18}$$

$$\implies C_{\mu\nu\rho}x^\nu x^\rho = 2x_\mu b\cdot x - b_\mu x^2.$$

All of which amounts to encapsulating all coordinate transformations which respect the conformal transformation condition at leading order:

$$\left.\frac{dy_s^\mu(x)}{ds}\right|_{s=0} = \epsilon^\mu(x) = a^\mu - \omega^\mu{}_\nu x^\nu + \kappa x^\mu + \left(2x^\mu b\cdot x - b^\mu x^2\right) \tag{B.7.19}$$

where the total number of parameters defining conformal transformations $\frac{1}{2}(d+1)(d+2)$ - provided that $d \neq 2$ [32]. Moving from left to right: a^μ characterizes d degrees of freedom (d.o.f) for *translations*, (due to antisymmetry $\omega_{\mu\nu} = -\omega_{\nu\mu}$) $\omega^\mu{}_\nu x^\nu$ characterizes $\frac{1}{2}d(d-1)$ d.o.f for *Lorentz transformations*, κx^μ characterizes 1 d.o.f for *scale transformations*, and $\left(2x^\mu b\cdot x - b^\mu x^2\right)$ characterizes d d.o.f for *special conformal transformations*.

B.7.3 Finite Conformal Transformations on Manifolds

For the one-parameter group of transformations y_s^μ, there exists a unique vector field obtained through,

$$\left.\frac{dy_s^\mu(x)}{ds}\right|_{s=0} = \epsilon^\mu(x). \tag{B.7.20}$$

Eq. (B.7.20), demonstrates the leading order coordinate transformation as a vector field. Resultantly, the coordinate transformation y_s^μ, being an integral curve to the vector field ϵ^μ yields the following differential equation,

$$\frac{dy_s^\mu(x)}{ds} = \epsilon^\mu \circ y_s(x) = a^\mu - \omega^\mu{}_\nu y_s^\nu + \kappa y_s^\mu + \left(2y_s^\mu b\cdot y_s - b^\mu y_s^2\right). \tag{B.7.21}$$

On the manifold $\mathbb{R}^{m,n}$, solving the differential equation set up eq. (B.7.21), with the initial condition $y_0(x) = x$, for each generator class separately yields finite translations $T_a(x)$, Lorentz transformations $\Lambda_\omega(x)$, dilations $D_\kappa(x)$, special conformal transformations $\Sigma_{-b}(x)$

$$T_a^\mu(x) := x^\mu + a^\mu. \tag{B.7.22a}$$
$$\Lambda_\omega^\mu(x) := P\exp\left\{-\left[\omega^\circ{}_\circ\right]\right\}^\mu{}_\nu\, x^\nu \tag{B.7.22b}$$
$$D_\kappa^\mu(x) := e^\kappa x^\mu \tag{B.7.22c}$$
$$\Sigma_{-b}^\mu(x) = \frac{x^\mu - b^\mu x^2}{1 - 2b.x + b^2x^2} \tag{B.7.22d}$$

Note that special conformal transformations may be defined through the successive composition of an inversion, a translation, and a subsequent inversion, that is,

$$x^\mu \overset{I_\varrho}{\mapsto} \frac{x^\mu}{x^2/\varrho^2} \overset{T_a}{\mapsto} \frac{x^\mu}{x^2/\varrho^2} - a^\mu \overset{I_\varrho}{\mapsto} \frac{x^\mu + x^2(a^\mu/\varrho^2)}{1 + 2x.(a/\varrho^2) + x^2(a/\varrho^2)^2} = \Sigma_{a/\varrho^2}^\mu(x), \tag{B.7.23}$$

or equivalently,

$$\Sigma_{a/\varrho^2}^\mu(x) := (I_\varrho \circ T_a \circ I_\varrho)^\mu(x) = \frac{x^\mu + x^2(a^\mu/\varrho^2)}{1 + 2x.(a/\varrho^2) + x^2(a/\varrho^2)^2} \tag{B.7.24}$$

In comparing eq. (B.7.22d) to eq. (B.7.24), $-b^\mu = a^\mu/\varrho^2$. Eq. (B.7.24) will be considered the definition of special conformal transformations due to its explicit use of a scale parameter ϱ is employed in the definition of the inversion,

$$I_\varrho^\mu(x) := \frac{x^\mu}{x^2/\varrho^2}. \tag{B.7.25}$$

Note that employing the use the scale parameter in the inversion showcased in eq. (B.7.25), is aimed to remove ambiguity regarding the translation involved in the definition of the special conformal transformation in eq. (B.7.24). More specifically, if x carries a unit of length $[\ell]$, then the inversion with the scale made explicit also carries a unit of length $[\ell]$. Therefore, translations used to define special conformal transformations remain well-defined as maps $T_a : \mathbb{R}^{m,n} \to \mathbb{R}^{m,n}$. Note additionally, that the inversion map is ill-defined for lightlike vectors. To the best of the

authors' knowledge, this problem has not been adequately tackled within the physics literature and all relevant calculations will commence with the aforementioned caveat in mind. A useful text on compactification of Minkowski space is [76].

B.7.4 Differential Conformal Transformations on Tangent Spaces

For the one-parameter group of transformations y_s, the differential may be written as,

$$\frac{\partial y_s^\mu(x)}{\partial x^v} = \Omega_s(x) R_s(x)^\mu{}_\nu; \quad \Omega_s(x) := \det\left[\frac{\partial y_s(x)}{\partial x}\right]^{1/d} \iff \det\left[R_s(x)\right] := 1, \tag{B.7.26}$$

While coordinate transformations on the manifold are characterized by the eq. (B.7.21), the transformations of the tangent space space element are characterized by the differential,

$$\begin{aligned}\frac{\partial}{\partial x^v}\frac{dy_s^\mu}{ds} = \frac{\partial \epsilon^\mu(y_s)}{\partial x^v} &= \left[(\kappa + 2b\cdot y_s)\, g^\mu_\alpha - (\omega^\mu{}_\alpha + 2\left(b^\mu y_{s\alpha} - y_s^\mu b_\alpha\right))\right]\frac{\partial y_s^\alpha}{\partial x^\nu} \\ &=: \left[\sigma_{\kappa,b}(y_s) g^\mu{}_\alpha - \rho_{\omega,b}(y_s)^\mu{}_\alpha\right]\frac{\partial y_s^\alpha}{\partial x^\nu}.\end{aligned} \tag{B.7.27}$$

Notice that $\sigma_{\kappa,b}(y_s)$ is the leading order conformal factor and is symmetric. Additionally, note that the tensor $\rho_{\omega,b}(y_s)$ is antisymmetric $\rho_{\omega,b}(y_s)_{\mu\nu} = -\rho_{\omega,b}(y_s)_{\nu\mu}$.

B.7.5 Conformal Invariants

Now let $\phi : \{x, y\} \mapsto \{x_s, y_s\}$ be a conformal transformation. Taking the derivative $\frac{d}{ds}$ of the squared distance,

$$\begin{aligned}\frac{d}{ds}(x_s - y_s)^2 &= 2\left(\epsilon(x_s) - \epsilon(y_s)\right)^\mu (x_s - y_s)_\mu \\ &= -2\omega^\mu{}_\nu (x_s - y_s)^\nu (x_s - y_s)_\mu + 2\big[\kappa + b.(x_s + y_s)\big](x_s - y_s)^2 \\ &= \left(\sigma_{\kappa,b}(x_s) + \sigma_{\kappa,b}(y_s)\right)(x_s - y_s)^2\end{aligned} \tag{B.7.28}$$

where the first term is zero due to the antisymmetry of $\omega_{\mu\nu}$. Quite notably, eq. (B.7.28) implies that the squared distance between two points under a conformal transformation,

$$(x_s - y_s)^2 = \Omega_s(x)\Omega_s(y)\,(x - y)^2 \tag{B.7.29}$$

To form conformal invariants, it is necessary to have at least four points such that all conformal factors cancel,

$$C_{ijkl} = \frac{x_{ij}^2 x_{kl}^2}{x_{ik}^2 x_{jl}^2}; \qquad i \neq j \neq k \neq l,\ x_{ij} := x_i - x_j. \tag{B.7.30}$$

Bibliography

[1] J. A. Bohra and Heribert Weigert. "The Jet/CGC Correspondence: A Conformal Perspective". In: *Acta Physica Polonica B*. [Presented at Excited QCD 2022, Sicily, Italy, 27 October, 2022. Proceedings in preparation]. 2023 (cit. on p. iii).

[2] Abu Bakr ibn Tufail. *The History of Hayy ibn Yaqzan*. Ed. by Simon Ockley and A. S. Fulton. (Authored by Abu Bakr ibn Tufail in Al-Andalus circa 12th century. Translated from the Arabic by Ockley in 1708. Revised, with an Introduction, by Fulton in 1929.) Frederick A. Stokes Company Publishers, 1929. URL: https://web.archive.org/web/20051210130856/http://umcc.ais.org/~maftab/ip/pdf/bktxt/hayy.pdf (cit. on p. ix).

[3] Murray Gell-Mann and Yuval Ne'eman. "The Eightfold way: a review with a collection of reprints". In: (Sept. 1964) (cit. on p. 1).

[4] Murray Gell-Mann. "A Schematic Model of Baryons and Mesons". In: *Phys. Lett.* 8.3 (Feb. 1964), pp. 214–215. DOI: 10.1016/S0031-9163(64)92001-3 (cit. on p. 1).

[5] H. Fritzsch, Murray Gell-Mann, and H. Leutwyler. "Advantages of the Color Octet Gluon Picture". In: *Phys. Lett. B* 47.4 (Nov. 1973), pp. 365–368. DOI: 10.1016/0370-2693(73)90625-4 (cit. on p. 1).

[6] David J. Gross and Frank Wilczek. "Ultraviolet Behavior of Non-Abelian Gauge Theories". In: *Physical Review Letters* 30.26 (June 1973), pp. 1343–1346. DOI: https://doi.org/10.1103%2FPhysRevLett.30.1343 (cit. on p. 1).

[7] H. David Politzer. "Reliable Perturbative Results for Strong Interactions?" In: *Phys. Rev. Lett.* 30 (1973). Ed. by J. C. Taylor, pp. 1346–1349. DOI: 10.1103/PhysRevLett.30.1346 (cit. on p. 1).

[8] Gerard 't Hooft. "A Planar Diagram Theory for Strong Interactions". In: *Nucl. Phys. B* 72.3 (Apr. 1974). Ed. by J. C. Taylor, p. 461. DOI: 10.1016/0550-3213(74)90154-0 (cit. on p. 2).

[9] A. Banfi, G. Marchesini, and G. Smye. "Away from Jet Energy Flow". In: *JHEP* 08.08 (June 2002), p. 006. DOI: 10.1088/1126-6708/2002/08/006. arXiv: hep-ph/0206076 [hep-ph] (cit. on pp. 2, 5, 27–29, 40, 51).

[10] Heribert Weigert. "Non-global Jet Evolution at Finite N_c". In: *Nucl. Phys. B* 685.1-3 (Dec. 2004), pp. 321–350. DOI: 10.1016/j.nuclphysb.2004.03.002. arXiv: hep-ph/0312050 [hep-ph] (cit. on pp. 2, 5, 31, 32, 40, 51).

[11] Yoshitaka Hatta and Takahiro Ueda. "Resummation of Non-Global Logarithms at Finite N_c". In: *Nucl. Phys. B* 874.3 (Apr. 2013), pp. 808–820. DOI: 10.1016/j.nuclphysb.2013.06.021. arXiv: 1304.6930 [hep-ph] (cit. on pp. 2, 35, 51).

[12] René Ángeles Martínez et al. "Soft Gluon Evolution and Non-global Logarithms". In: (Feb. 2018). arXiv: 1802.08531 [hep-ph] (cit. on pp. 2, 51).

[13] Ian Balitsky. "Operator Expansion for Diffractive High-Energy Scattering". In: *AIP Conf. Proc.* 407.1 (June 1997). Ed. by José Repond and Daniel Krakauer, p. 953. DOI: 10.1063/1.53693. arXiv: hep-ph/9706411 [hep-ph] (cit. on pp. 2, 22, 27, 51).

[14] I. Balitsky. "Operator expansion for high-energy scattering". In: *Nucl. Phys. B* 463.1 (Sept. 1996), pp. 99–160. DOI: 10.1016/0550-3213(95)00638-9. arXiv: hep-ph/9509348 [hep-ph] (cit. on pp. 2, 22, 27, 51).

[15] Yuri V. Kovchegov. "Small-x F_2 Structure Function of a Nucleus including Multiple Pomeron Exchanges". In: *Phys. Rev. D* 60.3 (June 1999), p. 034008. DOI: 10.1103/PhysRevD.60.034008. arXiv: hep-ph/9901281 [hep-ph] (cit. on pp. 2, 22, 27, 51).

[16] Yuri V. Kovchegov. "Unitarization of the BFKL pomeron on a nucleus". In: *Phys. Rev. D* 61.7 (May 2000), p. 074018. DOI: 10.1103/PhysRevD.61.074018. arXiv: hep-ph/9905214 [hep-ph] (cit. on pp. 2, 22, 27, 51).

[17] Edmond Iancu, Andrei Leonidov, and Larry D. McLerran. "Nonlinear Gluon Evolution in the Color Glass Condensate. 1." In: *Nucl. Phys. A* 692.3-4 (Nov. 2001), pp. 583–645. DOI: 10.1016/S0375-9474(01)00642-X. arXiv: hep-ph/0011241 [hep-ph] (cit. on pp. 2, 13, 16, 51).

[18] Alfred H. Mueller. "A Simple derivation of the JIMWLK equation". In: *Phys. Lett. B* 523 (Oct. 2001), pp. 243–248. DOI: 10.1016/S0370-2693(01)01343-0. arXiv: hep-ph/0110169 [hep-ph] (cit. on pp. 2, 51).

[19] Heribert Weigert. "Unitarity at Small Bjorken x". In: *Nucl. Phys. A* 703 (Apr. 2002), pp. 823–860. DOI: 10.1016/S0375-9474(01)01668-2. arXiv: hep-ph/0004044 [hep-ph] (cit. on pp. 2, 22, 51).

[20] Heribert Weigert. "Evolution at small x_{bj}: The Color Glass Condensate". In: *Prog. Part. Nucl. Phys. 55:461-565, 2005* (Jan. 2005). DOI: 10.1016/j.ppnp.2005.01.029. arXiv: hep-ph/0501087 [hep-ph] (cit. on pp. 2, 14, 31, 51).

[21] N. Seiberg and Edward Witten. "Electric - magnetic duality, monopole condensation, and confinement in N=2 supersymmetric Yang-Mills theory". In: *Nucl. Phys. B* 426 (July 1994). [Erratum: Nucl.Phys.B 430, 485–486 (1994)], pp. 19–52. DOI: 10.1016/0550-3213(94)90124-4. arXiv: hep-th/9407087 [hep-th] (cit. on p. 2).

[22] S. S. Gubser, Igor R. Klebanov, and Alexander M. Polyakov. "Gauge theory correlators from noncritical string theory". In: *Phys. Lett. B* 428.1-2 (Feb. 1998), pp. 105–114. DOI: 10.1016/S0370-2693(98)00377-3. arXiv: hep-th/9802109 [hep-th] (cit. on p. 2).

[23] Juan Martin Maldacena. "The Large N Limit of Superconformal Field Theories and Supergravity". In: *Adv. Theor. Math. Phys.* 2 (Nov. 1998), pp. 231–252. DOI: 10.1023/A:1026654312961. arXiv: hep-th/9711200 [hep-th] (cit. on pp. 2, 36).

[24] Yoshitaka Hatta. "Relating $e + e-$ Annihilation to High Energy Scattering at Weak and Strong Coupling". In: *JHEP* 11.11 (Oct. 2008), p. 057. DOI: 10.1088/1126-6708/2008/11/057. arXiv: 0810.0889 [hep-ph] (cit. on pp. 2, 4, 5, 25, 35, 36, 40, 43, 51).

[25] Giuseppe Marchesini and A. H. Mueller. "The BMS equation and $c\bar{c}$ production; a comparison of the BMS and BK equations". In: *JHEP* 02 (2016), p. 010. DOI: 10.1007/JHEP02(2016)010. arXiv: 1510.08763 [hep-ph] (cit. on pp. 2, 51).

[26] Diego M. Hofman and Juan Maldacena. "Conformal Collider Physics: Energy and Charge Correlations". In: *JHEP* 05.05 (Mar. 2008), p. 012. DOI: 10.1088/1126-6708/2008/05/012. arXiv: 0803.1467 [hep-th] (cit. on pp. 2, 5, 35, 36, 51).

[27] Simon Caron-Huot. "Resummation of Non-Global Logarithms and the BFKL Equation". In: *JHEP* 03.3 (Jan. 2018), p. 036. DOI: 10.1007/JHEP03(2018)036. arXiv: 1501.03754 [hep-ph] (cit. on pp. 2, 4, 5, 36, 51, 53).

[28] Alex Kovner, Michael Lublinsky, and Yair Mulian. "Jalilian-Marian, Iancu, McLerran, Weigert, Leonidov, Kovner Evolution at Next to Leading Order". In: *Physical Review D* 89.6 (Mar. 2014), p. 061704. DOI: 10.1103/physrevd.89.061704 (cit. on pp. 2, 53).

[29] Alex Kovner, Michael Lublinsky, and Yair Mulian. "Conformal Symmetry of JIMWLK Evolution at NLO". In: *JHEP* 04.4 (Apr. 2014), p. 030. DOI: 10.1007/JHEP04(2014)030. arXiv: 1401.0374 [hep-th] (cit. on pp. 2, 53).

[30] Alex Kovner, Michael Lublinsky, and Yair Mulian. "NLO JIMWLK Evolution Unabridged". In: *JHEP* 08.8 (May 2014), p. 114. DOI: 10.1007/JHEP08(2014)114. arXiv: 1405.0418 [hep-ph] (cit. on pp. 2, 53).

[31] Martin Schottenloher. *A Mathematical Introduction to Conformal Field Theory*. Springer-Verlag GmbH, Sept. 2008. ISBN: 978-3540686255. URL: https://www.ebook.de/de/product/7512094/martin_schottenloher_a_mathematical_introduction_to_conformal_field_theory.html (cit. on pp. 3, 76).

[32] Hugh Osborn. *Lectures on Conformal Field Theories in more than two dimensions*. https://www.damtp.cam.ac.uk/user/ho/CFTNotes.pdf. [Online; last accessed 13/03/2022]. Department of Applied Mathematics and Theoretical Physics, Wilberforce Road,Cambridge CB3 0WA, England, 2019 (cit. on pp. 3, 76, 78, 80).

[33] Judith Magdalena Alcock-Zeilinger. "Symmetry Implications for Wilson Line Correlators in QCD at High Energies". [Supervised by Prof. Weigert]. PhD thesis. Faculty of Science, Department of Physics: University of Cape Town, Nov. 2017 (cit. on pp. 4, 17, 73).

[34] Robert Moerman. "A Gauge-Invariant, Symmetry-Preserving Truncation of JIMWLK". [Supervised by Prof. Weigert]. MA thesis. Faculty of Science, Department of Physics: University of Cape Town, 2018. URL: http://hdl.handle.net/11427/27998 (cit. on pp. 4, 62, 67).

[35] Jonathan Rayner. "Reps for JIMWLK: Applications of Representation Theory to a Novel Approach to the JIMWLK Equation". [Supervised by Prof. Weigert]. MA thesis. Faculty of Science, Department of Physics: University of Cape Town, 2018. URL: http://hdl.handle.net/11427/29532 (cit. on p. 4).

[36] Alexey A. Vladimirov. "Correspondence between Soft and Rapidity Anomalous Dimensions". In: *Phys. Rev. Lett.* 118.6 (Oct. 2017), p. 062001. DOI: 10.1103/PhysRevLett.118.062001. arXiv: 1610.05791 [hep-ph] (cit. on pp. 5, 35, 36, 38, 51).

[37] Alexey Vladimirov. "Structure of Rapidity Divergences in Multi-Parton Scattering Soft Factors". In: *JHEP* 04 (July 2018), p. 045. DOI: 10.1007/JHEP04(2018)045. arXiv: 1707.07606 [hep-ph] (cit. on pp. 5, 35, 36, 38, 51).

[38] E. Rutherford. "The Scattering of α and β Particles by Matter and the Structure of the Atom". In: *The London, Edinburgh, and Dublin Philosophical Magazine and Journal of Science* 21.125 (May 1911), pp. 669–688. DOI: https://doi.org/10.1080%2F14786440508637080 (cit. on p. 7).

[39] Bureau International des Poids et Mesures. *The International System of Units*. Tech. rep. 2022. URL: https://www.bipm.org/en/publications/si-brochure (cit. on p. 7).

[40] Steven R. Jefferts. *February 2016 Evaluation of NIST-F1*. [Online; last accessed 02/02/2023]. 2016. URL: %5Curl%7Bhttps://webtai.bipm.org/ftp/pub/tai//data/PSFS_reports/nist-f1_57419-57439.pdf%7D (cit. on p. 7).

[41] D. Hanneke, S. Fogwell, and G. Gabrielse. "New Measurement of the Electron Magnetic Moment and the Fine Structure Constant". In: *Phys. Rev. Lett.* 100.12 (Mar. 2008), p. 120801. DOI: 10.1103/PhysRevLett.100.120801. arXiv: 0801.1134 [physics.atom-ph] (cit. on p. 7).

[42] X. Fan et al. "Measurement of the Electron Magnetic Moment". In: *Physical Review Letters* 130.7 (Feb. 2023), p. 071801. DOI: https://doi.org/10.1103/PhysRevLett.130.071801. eprint: https://arxiv.org/pdf/2209.13084.pdf (cit. on p. 7).

[43] Stefano Laporta. "High-Precision Calculation of the 4-loop Contribution to the Electron g-2 in QED". In: *Phys. Lett. B* 772 (Apr. 2017), pp. 232–238. DOI: 10.1016/j.physletb.2017.06.056. arXiv: 1704.06996 [hep-ph] (cit. on p. 8).

[44] A. Accardi et al. "Electron Ion Collider: The Next QCD Frontier - Understanding the glue that binds us all". In: (Dec. 2012). arXiv: https://arxiv.org/abs/1212.1701 [nucl-ex] (cit. on p. 9).

[45] Francois Gelis et al. "The Color Glass Condensate". In: *Ann. Rev. Nucl. Part. Sci.* 60 (Feb. 2010), pp. 463–489. DOI: 10.1146/annurev.nucl.010909.083629. arXiv: 1002.0333 [hep-ph] (cit. on p. 9).

[46] Stanley J. Brodsky. "QCD technology: Light Cone Quantization and Commensurate Scale Relations". In: *AIP Conf. Proc.* 494.1 (Sept. 1999). Ed. by C. R. Ji and D. P. Min, pp. 3–44. DOI: 10.1063/1.1301659. arXiv: hep-ph/9909234 [hep-ph] (cit. on pp. 10, 57).

[47] Richard P. Feynman. "Very High-Energy Collisions of Hadrons". In: *Phys. Rev. Lett.* 23.24 (Dec. 1969). Ed. by L. M. Brown, pp. 1415–1417. DOI: 10.1103/PhysRevLett.23.1415 (cit. on p. 10).

[48] Matthew D. Schwartz. *Quantum Field Theory and the Standard Model*. Cambridge University Press, Mar. 2019. 870 pp. ISBN: 978-1107034730. URL: https://www.ebook.de/de/product/21354919/matthew_d_schwartz_quantum_field_theory_and_the_standard_model.html (cit. on pp. 10, 23, 25).

[49] J. D. Bjorken. "Asymptotic Sum Rules at Infinite Momentum". In: *Phys. Rev.* 179.5 (Mar. 1969), pp. 1547–1553. DOI: 10.1103/PhysRev.179.1547 (cit. on p. 11).

[50] Ringaile Placakyte. "Parton Distribution Functions". In: (Nov. 2011). arXiv: http://arxiv.org/abs/1111.5452v4 [hep-ph] (cit. on p. 11).

[51] Larry D. McLerran and Raju Venugopalan. "Gluon Distribution Functions for Very Large Nuclei at Small Transverse Momentum". In: *Phys. Rev. D* 49.7 (Nov. 1994), pp. 3352–3355. DOI: 10.1103/PhysRevD.49.3352. arXiv: hep-ph/9311205 [hep-ph] (cit. on p. 12).

[52] Chen-Ning Yang and Robert L. Mills. "Conservation of Isotopic Spin and Isotopic Gauge Invariance". In: *Phys. Rev.* 96.1 (Oct. 1954). Ed. by Jong-Ping Hsu and D. Fine, pp. 191–195. DOI: 10.1103/PhysRev.96.191 (cit. on p. 12).

[53] Heribert Weigert. *Personal Communication*. 2022 (cit. on pp. 13, 32).

[54] Igor Olegovich Cherednikov, Tom Mertens, and Frederik F. Van der Veken. *Wilson Lines in Quantum Field Theory*. Vol. 24. De Gruyter Studies in Mathematical Physics. De Gruyter, Sept. 2014. ISBN: 978-3-11-030921-8. DOI: 10.1515/9783110309218 (cit. on p. 14).

[55] K. Kajantie, Larry D. McLerran, and Risto Paatelainen. "Gluon Radiation from a Classical Point Particle II: Dense Gluon Fields". In: *Phys. Rev. D* 101.5 (Nov. 2020), p. 054012. DOI: 10.1103/PhysRevD.101.054012. arXiv: 1911.12738 [hep-ph] (cit. on pp. 17, 64).

[56] Predrag Cvitanović. *Group Theory: Birdtracks, Lie's, and Exceptional Groups*. Princeton University Press, 2008. ISBN: 0691118361 (cit. on pp. 20, 72).

[57] Cyrille Marquet and Heribert Weigert. "New Observables to Test the Color Glass Condensate Beyond the Large- N_c limit". In: *Nucl. Phys. A* 843 (Mar. 2010), pp. 68–97. DOI: 10.1016/j.nuclphysa.2010.05.056. arXiv: 1003.0813 [hep-ph] (cit. on p. 20).

[58] G. P. Salam and D. Wicke. "Hadron Masses and Power Corrections to Event Shapes". In: *JHEP* 05 (Feb. 2001), p. 061. DOI: 10.1088/1126-6708/2001/05/061. arXiv: hep-ph/0102343 [hep-ph] (cit. on p. 23).

[59] S. Catani et al. "Resummation of Large Logarithms in e+ e- Event Shape Distributions". In: *Nucl. Phys. B* 407.1 (Oct. 1993), pp. 3–42. DOI: 10.1016/0550-3213(93)90271-P (cit. on p. 24).

[60] Guglielmo Coloretti, Aude Gehrmann-De Ridder, and Christian T. Preuss. "QCD Predictions for Event-Shape Distributions in Hadronic Higgs Decays". In: *JHEP* 06.6 (June 2022), p. 009. DOI: 10.1007/JHEP06(2022)009. arXiv: 2202.07333 [hep-ph] (cit. on p. 24).

[61] Jun Gao et al. "Thrust Distribution in Higgs Decays at the Next-to-Leading Order and Beyond". In: *JHEP* 03.3 (Mar. 2019), p. 030. DOI: 10.1007/JHEP03(2019)030. arXiv: 1901.02253 [hep-ph] (cit. on p. 24).

[62] Thomas Becher and Matthew D. Schwartz. "A Precise Determination of α_s from LEP Thrust Data Using Effective Field Theory". In: *JHEP* 07 (Mar. 2008), p. 034. DOI: 10.1088/1126-6708/2008/07/034. arXiv: 0803.0342 [hep-ph] (cit. on p. 24).

[63] A. Banfi, G. P. Salam, and G. Zanderighi. "Semi-Numerical Resummation of Event Shapes". In: *JHEP* 01.01 (Dec. 2002), p. 018. DOI: 10.1088/1126-6708/2002/01/018. arXiv: hep-ph/0112156 [hep-ph] (cit. on p. 25).

[64] Michael E. Peskin. *An Introduction To Quantum Field Theory*. Taylor and Francis Ltd, Sept. 2019. 868 pp. ISBN: 978-0367320560. URL: https://www.ebook.de/de/product/37889945/michael_e_peskin_an_introduction_to_quantum_field_theory.html (cit. on p. 25).

[65] M. Dasgupta and G. P. Salam. "Resummation of Nonglobal QCD Observables". In: *Phys. Lett. B* 512.3-4 (Apr. 2001), pp. 323–330. DOI: 10.1016/S0370-2693(01)00725-0. arXiv: hep-ph/0104277 [hep-ph] (cit. on p. 25).

[66] A. Bassetto, M. Ciafaloni, and G. Marchesini. "Jet Structure and Infrared Sensitive Quantities in Perturbative QCD". In: *Phys. Rept.* 100.4 (Nov. 1983), pp. 201–272. DOI: 10.1016/0370-1573(83)90083-2 (cit. on p. 28).

[67] F. Fiorani, G. Marchesini, and L. Reina. "Soft Gluon Factorization and Multi-Gluon Amplitude". In: *Nucl. Phys. B* 309.3 (Nov. 1988), pp. 439–460. DOI: 10.1016/0550-3213(88)90452-X (cit. on p. 28).

[68] Jeffrey R. Forshaw, A. Kyrieleis, and M. H. Seymour. "Super-Leading Logarithms in Non-Global Observables in QCD". In: *JHEP* 08.08 (Aug. 2006), p. 059. DOI: 10.1088/1126-6708/2006/08/059. arXiv: hep-ph/0604094 [hep-ph] (cit. on p. 53).

[69] Thomas Becher et al. "Factorization and Resummation for Jet Processes". In: *Journal of High Energy Physics* 2016.11 (Nov. 2016). DOI: https://doi.org/10.1007/JHEP11(2016)019 (cit. on p. 53).

[70] E. Iancu et al. "Resumming Double Logarithms in the QCD Evolution of Color Dipoles". In: *Phys. Lett. B* 744 (Feb. 2015), pp. 293–302. DOI: 10.1016/j.physletb.2015.03.068. arXiv: 1502.05642 [hep-ph] (cit. on p. 53).

[71] E. Iancu, A. H. Mueller, and D. N. Triantafyllopoulos. "CGC Factorization for Forward Particle Production in Proton-Nucleus Collisions at Next-to-Leading Order". In: *JHEP* 12.12 (Aug. 2016), p. 041. DOI: 10.1007/JHEP12(2016)041. arXiv: 1608.05293 [hep-ph] (cit. on p. 53).

[72] Guillaume Beuf et al. "Dipole model at Next-to-Leading Order meets HERA data". In: *PoS* HardProbes2020 (Aug. 2021), p. 101. DOI: 10.22323/1.387.0101. arXiv: 2008.05233 [hep-ph] (cit. on p. 53).

[73] Andrew J. Larkoski, Ian Moult, and Duff Neill. "Non-Global Logarithms, Factorization, and the Soft Substructure of Jets". In: *JHEP* 09.9 (Sept. 2015), p. 143. DOI: 10.1007/JHEP09(2015)143. arXiv: 1501.04596 [hep-ph] (cit. on p. 53).

[74] Stefan Keppeler and Malin Sjodahl. "Orthogonal Multiplet Bases in $\mathsf{SU}(N_c)$ Color Space". In: *JHEP* 09.9 (July 2012), p. 124. DOI: 10.1007/JHEP09(2012)124. arXiv: 1207.0609 [hep-ph] (cit. on p. 72).

[75] A. Zee. *Einstein Gravity in a Nutshell*. New Jersey: Princeton University Press, May 2013. 888 pp. ISBN: 978-0-691-14558-7. URL: https://www.ebook.de/de/product/20003940/a_zee_einstein_gravity_in_a_nutshell.html (cit. on p. 76).

[76] Arkadiusz Jadczyk. "On Conformal Infinity and Compactifications of the Minkowski Space". In: *Advances in Applied Clifford Algebras* 21.4 (Mar. 2011), pp. 721–756. DOI: https://doi.org/10.1007/s00006-011-0285-5 (cit. on p. 82).